Physics – Uspekhi **59** (8) 727 – 772 (2016)

REVIEWS OF TOPICAL PROBLEMS

PACS numbers: 42.25.Bs, 42.79.Wc, **61.46. – w**, 71.20.Nr, 71.20.Rv, **72.40. + w**, 72.80.Cw, 84.60.Jt

Solar photovoltaics: current state and trends

V A Milichko, A S Shalin, I S Mukhin, A E Kovrov,
A A Krasilin, A V Vinogradov, P A Belov, C R Simovski

DOI: 10.3367/UFNe.2016.02.037703

Contents

V A Milichko, A S Shalin, A E Kovrov, A A Krasilin, A V Vinogradov, P A Belov St. Petersburg National Research University of Information Technologies, Mechanics and Optics,
Kronverksky prosp. 49, 197101 St. Petersburg, Russian Federation
Tel. + 7 (931) 356 91 41. E-mail: ariesval@mail.ru
I S Mukhin St. Petersburg Academic University,
Russian Academy of Sciences
ul. Khlopina 8/3 lit. A, 194021 St. Petersburg, Russian Federation;
St. Petersburg National Research University of Information Technologies, Mechanics and Optics,
Kronverksky prosp. 49, 197101 St. Petersburg, Russian Federation
C R Simovski St. Petersburg National Research University of Information Technologies, Mechanics and Optics,
Kronverksky prosp. 49, 197101 St. Petersburg, Russian Federation;
Aalto University, Department of Radio Science and Engineering,
Otakaari 5A, Espoo, Finland
Tel. + 7 (358) 504 20 58 56
E-mail: konstantin.simovski@aalto.fi

Received 27 January 2016
Uspekhi Fizicheskikh Nauk **186** (8) 801 – 852 (2016)
DOI: 10.3367/UFNr.2016.02.037703
Translated by E N Ragozin, Yu V Morozov, A L Chekhov, A A Krasilin; edited by A Radzig

Abstract. Basic aspects of current solar photovoltaics (PVs) are reviewed, starting from the recently developed already-on-the-market first-generation solar cells and ending with promising but not yet commercialized third-generation cells and materials possibly leading to new cell designs. The emphasis is on the physical principles of operation of various solar cells, which are divided into several groups according to our classification scheme. To make the picture complete, some technological and economic aspects of the field are discussed. A separate chapter considers antireflection coatings and light-trapping textures — structures which, while not having appeared yet in the PV review literature, are an integral part of the solar cells.

Keywords: solar energy, photovoltaics, solar cells of three generations, organic and inorganic solar cells, commercial photovoltaics, perovskites, light-trapping structure

1. Introduction

Solar energy may be converted into electricity in various ways. In this review, we analyze the so-called photoelectric, or photovoltaic, light conversion to electric current. It is common knowledge that the French physicist A-E Becquerel (the father of the pioneer of radioactivity) discovered in 1839

the emergence of electric current in an electrolyte under light illumination. Forty-four years later, the American engineer C Fritts made the first photoelectric solar cell (SC) of selenium with a submicrometer gold coating. He reached an absorbed-light-to-electric energy conversion efficiency of 1%, which persisted for more than half a century. That is why the year 1883 is commonly considered to be the onset of the era of solar power engineering.

However, making a photoelectric SC a practically useful source of electric energy would have been impossible without understanding the occurring processes at a level of a quantitative theory. Mention should therefore be made of the role of physicists who examined the photoeffect at the turn of the 20th century, A Stoletov in the first place, who formulated the empirical law relating the photocurrent to the light flux [1]. But the path to progress in solar photoelectric power engineering was seriously opened by Albert Einstein, who laid the foundation for the general theory of the photoeffect [2] (it is precisely for this theory that he was awarded the Nobel Prize in Physics 1921). The level of understanding of the photoeffect reached in Einstein's work was sufficient for the purposeful development of efficient photoelectric SCs and, in the long run, for the advent of solar power engineering, or in other words solar photovoltaics.

Renewable energy sources are vitally required for modern civilization. Carbon energy sources (gas, oil, and coal, which currently account for 87% of the world's total energy supply) have vast, though limited, reserves. In addition, they are highly nonuniformly distributed over the Earth. Atomic power plants (4% of the world's energy market) and hydropowered generators (7%) are rigidly bound to sites and population density. Furthermore, they imply lengthy, bulky, and insufficiently safe power transmission lines. At the same time, solar-powered electric energy may be produced directly in the houses of consumers, which is becoming more and more available every year due to technology development. It comes as no surprise that a wealth of investigations is devoted to solar photovoltaics. The contemporary state of this realm of science has been reflected not only in papers but also in scientific monographs. Among these, early in the 21st century, Refs [3–5] stood out for their completeness and topicality.

Energy production does not lag behind science. Beginning in 2000, the power of the world's solar electric stations has doubled every three years [6]. At the end of the 20th century, the leadership in the production of solar cells — panels — consisting of photoelectric SCs connected in parallel or in series was seized by China. In one way or another, this branch of energy production also exists in other technologically developed countries. On the other hand, Russia, though a technologically developed country, has so far remained on the sidelines, despite the fact that, for instance, the development of cascade (multijunction) SCs at the Ioffe Physical-Technical Institute of the Russian Academy of Sciences [6] is of obvious interest for the space industry (see Section 5).

The lack of domestic demand for developments in the area of solar photovoltaics has an inevitable adverse effect on the financing of this area of science in Russia and, hence, on the scale of research and amount of scientific literature. Is this not the reason why we failed to find in the literature anything except for quite brief reviews like Ref. [6], written more than 10 years ago? Even earlier studies published in the USSR [7–10] do not reflect the modern state of solar power engineering. Although the physics of modern thin-film SCs is discussed at length in the recent book [11] by domestic authors, the book itself is concerned with only one aspect of solar photovoltaics and does not pretend to cover the broad field in this realm of knowledge.

However, despite the obvious scientific and industrial progress, in the recent international literature there is also a dearth of books like (in its time) Refs [3, 4], i.e., of books of a reference nature, covering the latest achievements in solar photovoltaics (and not only in photoelectric materials like Ref. [5]). In much the same way, all review papers in English published after 2011 that are available to us are rather highly specialized like, for instance, Refs [12–15]. That is why the aim of our review is to cover as broadly as possible the physical, technological, and systematic aspects of contemporary solar photovoltaics.

1.1 Solar cells of three generations

The development of solar photovoltaics has embarked on the path of improving the efficiency of SCs, with the simultaneous solution to problems like their cost reduction, extension of their service life, and improvement of operation stability in a varying environment (humidity, cloudiness, temperature drops). Historically, the first photoelectric SCs (hereinafter, simply SCs) with efficiencies well above 1% (namely, 6%) were crystal silicon cells (c-Si) [16]. These cells (along with germanium SCs) are referred to as first-generation cells, which presently account for 90% of the commercial SC market and exhibit, on the average, an efficiency of about 20% [5]. These cells have several drawbacks: a high fabrication cost, toxicity in production, a large amount of toxic waste, etc. [3–5].

Attempts to eliminate these disadvantages led to the development of alternative SCs, including thin-film ones [15, 17], which are now referred to as second-generation cells. These SCs are made of amorphous (a-Si), microcrystalline (μc-Si) or polycrystalline (multi-cSi) silicon, multicomponent A_3B_5 (GaP, InP, GaAs) and A_3B_6 (CdTe) semiconductors, as well as multicomponent CIS ($CuInS_2$) [18], CIGS (Cu(In, Ga)(Se, S)$_2$) [19], and CZTS ($Cu_2ZnSn(S, Se)_4$) type semiconductors [20]. Several disadvantages inherent in the first-generation SCs were eliminated in the second-generation SCs. Their fabrication requires less raw materials and consumes less energy, and they are easier to produce than crystal silicon SCs. Many solar batteries utilizing such SCs are flexible or plastic thin films and may be accommodated on nonplanar surfaces. These merits led to the rapid development of second-generation SCs utilizing both silicon and multicomponent semiconductors.

The leaders in the production and installation of second-generation SCs utilizing amorphous and microcrystalline silicon (with efficiencies of about 7–10%) are the Sunlight Corp. (USA) and Anwell Technologies Ltd. (Hong Kong). The leaders in the production and installation of second-generation SCs utilizing multicomponent semiconductors (with efficiencies above 15%) are the First Solar Ltd. and General Electric Ltd. companies (both of the USA). The average market price of 1 kW·h of electricity produced by second-generation SCs amounts to 0.6–0.9 US dollars (see, for instance, https://en.wikipedia.org/wiki/Cadmium_telluride_photovoltaics). This is already a reasonable price, which is of interest for the world market.

However, the change to second-generation SCs turned out not to be entirely successful. Beginning in the 1980s, commercial second-generation SCs with an average effi-

ciency of 15% occupied only 10% of the market, and no serious growth is presently observed. The reasons for this relative failure are numerous. Among them are the high production toxicity of multicomponent semiconductors and several starting materials (see Section 4.2), the dependence of operation on the ambient conditions (the need to clean off snow and dirt, the lowering of output power under illumination by scattered light), the instability of amorphous silicon SCs, and, lastly, ambiguity as to what materials a large investor is to rely on.

For high-efficiency and relatively expensive SC multicomponent semiconductors, this choice is not obvious, because the cost and volume of production depend on the level of raw material extraction. The level of starting material extraction in the world is unpredictable: so far, the production of second-generation SCs is insufficiently large in scale to foster the extraction itself. As a result, second-generation SCs have not revolutionized solar photovoltaics. However, as shown below, second-generation SCs do have industrial potential.

The next improvement stage of solar photovoltaics comprised the development of organic SCs — third-generation cells. In the development of these cells, there has been an endeavor to solve the known problems: to lower the toxicity of production and waste, the cost of manufacture, and material and energy expenses, and to raise the rate of manufacture and simplify this process, as well as to maximize the operation stability of a solar cell in various weather conditions.

Third-generation SCs make up a relatively broad class of cells utilizing conducting polymers, pigments (organic dyes), and organic–inorganic semiconductors, quantum dots, and hot electron SCs, and, lastly, SCs with a solar spectrum splitting. Among the last are so-called cascade, or multijunction SCs, in which the photoelectric material is formed by a multilayer structure 1–5 μm in overall thickness containing several (from 2 to 4 in practice) semiconductor junctions. Such a structure is nothing more than a series connection of optically thin SCs, each of which is optimized for its relatively narrow subrange of solar radiation. These are precisely the SCs which exhibited the highest efficiencies of 45–46% (see, for instance, Ref. [21]). These cells are made of the highest quality materials. Their production cost is very high, and therefore they are primarily applied for supplying energy to spacecraft and cannot compete with other SCs when used for civilian, and event more so for residential, purposes.

SCs with so-called parallel splitting of the solar spectrum consist of several narrow-band solar subcells, which are not integrated into the common multilayer structure but are spaced in a plane, with current-collecting lines common for all cells. These subcells are significantly cheaper than layered multijunction SCs but approach them in efficiency (their record efficiency amounts to 43% [22]). Nonetheless, these solar subcells require special optics — phase holograms — for achieving the desired quality of solar light splitting into the spectral subranges. Cheap optical dispersive devices — prisms or conventional periodic phase diffraction gratings — possess insufficiently high dispersion and significant losses due to reflection and scattering. So far, there is no way to do without phase holograms, which are expensive due to the large area requirement. As a result, the cost of such a solar battery in combination with optics is estimated to be only slightly lower than the cost of a multijunction SC battery without optics [23].

As for SCs exploiting quantum dots, conducting polymers, dyes, organic–inorganic semiconductors, and hot electrons, these third-generation cells cannot thus far drive out their predecessors from the market due to insufficient efficiency and service life and/or insufficient operation stability under real ambient conditions (see Section 6.6). However, the development of third-generation SCs continues with undiminishing intensity, new technical solutions are being found, and new materials not yet mastered by the industry but showing great promise are emerging. This is reflected in the scientific literature (see, for instance, Ref. [24]). Therefore, the potential of third-generation SCs is far from exhausted.

All SCs, with the exception of those with spectrum splitting just discussed above, have a fundamental efficiency limitation, which amounts to about 30% in terrestrial conditions. This is the so-called Shockley–Queisser limit [3–5, 9, 10, 17], which emerges due to the breadth of the frequency range of solar light. As a result, an appreciable fraction of solar light photons has a higher energy than required for producing free charge carriers in a given photoelectric material, and this excess energy converts to the kinetic energy of the carriers. Since the material has a finite conductivity, this energy converts to heat. Overcoming the 30% barrier for SC efficiency is possible, as is clear from the aforesaid, by splitting the solar spectrum (in parallel or in series) into subranges.

Another way to overcome this barrier involves the utilization of nonlinear processes that might prevent the dissipation of kinetic energy of the charge carriers induced by high-frequency photons. Most promising among the known proposals, in our view, is the idea of using dielectrics with a strong correlation, i.e., media in which the carriers are fermions and may move while remaining coupled. Among such dielectrics are so-called Mott media (see, for instance, Ref. [25]). When such a medium absorbs one photon with a frequency much higher than the bandgap energy, not one but two or more electron–hole pairs are generated, because the first pair of moving charges induces another one. In doing so, the first pair of moving charges gets rid of excess kinetic energy (sufficient for phonon excitation) and the dissipation turns out to be much smaller than in a semiconductor. According to the theory developed by Coulter et al. [26], the deposition of a micrometer-thick layer of a Mott medium (for instance, vanadium dioxide) as a photon absorber above crystal silicon would permit this single-junction SC to exceed the Shockley–Queisser limit by a factor of about two.

Of course, the idea expressed by the authors of Ref. [26] is not the sole one of its kind. The hot-electron SCs considered in Section 9 of our review also permit, in principle, overcoming the 30% Shockley–Queisser limit for single-junction SCs. In the literature, one may find other ideas on how to achieve this. Therefore, a new round in the development of solar photovoltaics would be expected: the advent of fourth-generation SCs without spectrum splitting and yet with as high an efficiency as that of multijunction SCs.

1.2 Classification of solar cells according to operation principle

As regards the method of solar radiation energy conversion to electricity, SCs may be divided into four types: diode, photoelectrochemical, excitonic, and thermophotovoltaic [3–9, 10, 27]. Diode SCs, which are the concern of the major part of our review, utilize a wide range of materials:

semiconductors (Si, Ge), multicomponent A_3B_5 and A_2B_6 semiconducting compounds, and organic materials in which the photoeffect is similar to that in semiconductors. In this type of SCs, the charge separation produced under external illumination takes place at the interface of two media with p- and n-type conductivity.

Depending on the thickness of the active region, diode SCs are subdivided into systems utilizing bulk crystal substrates (like Si, Ge, GaAs) and thin films of a different structure (crystalline, microcrystalline, amorphous). SCs exploiting bulk crystal materials possess a relatively high efficiency and exhibit stable operation, but are characterized by a high cost of manufacture. SCs utilizing multicomponent A_3B_5 and A_2B_6 semiconducting compounds possess high efficiencies, are characterized by a high parameter stability, and are immune to environmental effects. However, they are most costly and demanding from the technological standpoint. SCs built around thin films with a high absorption coefficient (a-Si:H, CIGS, CdTe) exhibit a lower efficiency and a relatively lower stability of parameters. However, the amount of input material expended in the course of their production is considerably smaller, with a consequential decrease in their cost [3–5, 9].

Photoelectrochemical type SCs, for instance, so-called Grätzel cells, which are the concern of Section 6 in our review, are void of a p–n semiconductor junction. As a rule (see, for instance, Refs [3, 4]), Grätzel's SCs comprise a micrometer-thick layer of a wide-band porous or structured semiconductor with a developed surface (usually titanium dioxide) deposited onto the glass substrate coated with a solar-transparent conducting layer of submicrometer thickness, which plays the role of the anode. The opposite surface of TiO_2, including the inner surface of the pores, is covered with an ultrathin dye layer (usually a monomolecular layer). The dye (a natural pigment, as a rule) exhibits a photoeffect but, unlike the semiconductor, cannot sustain a photocurrent. The light absorbed by the pigment molecules induces excitons which rapidly dissociate, with the photoelectrons tunneling into the TiO_2 and diffusing through this well-conductive material towards the metal which covers the glass substrate. The cathode on the pigment side is formed of a submicrometer platinum layer separated from the pigment by an electrolyte. The electrolyte provides electron transport from the platinum cathode to the pigment to make up the deficiency of negative charges in the dye and close the electric circuit. The semiconducting material layer (TiO_2) in such SCs is employed only for the transport of the carriers generated in the photoelectric layer.

An alternative SC design reduces to a structure consisting of an organic polymer layer (donor) coated with a solar-transparent material with electron type conductivity (acceptor). The solar radiation generates excitons in the photoelectric layer; the excitons are split apart into free electrons and holes when they reach the donor–acceptor interface to produce a photocurrent [3, 4, 17]. In the literature, SCs of this kind are termed excitonic.

Apart from planar heterojunction organic SCs there are SCs (with a higher efficiency) utilizing bulk heterojunctions and metal-organic perovskite SCs, which are discussed in Sections 6 and 7 of our review. Usually, the excitonic SCs classed in the literature are also structures in which excitons exist for a relatively long time and travel an appreciable distance prior to their dissociation into two free charges. In our view, Grätzel's SCs should also be classed with excitonic SCs for two reasons. First, the photoeffect in dyes gives rise to excitons and, second, Grätzel's SCs, like other excitonic SCs, are thin-film cells.

We briefly consider thermophotovoltaic (TPV) converters as applied to their using in solar photovoltaics. The principle of operation of any TPV device relies on the conversion of the infrared (IR) radiation energy of a high-luminosity heated body, which is termed a thermal emitter, to electricity using a narrow-band semiconductor photocell. This conversion is possible when the photocell is not in contact with the thermal emitter for two reasons. First, a high temperature gives rise to the appearance of dark current in the diode, which is opposite to the photocurrent. Second, the generation of phonons (in view of the phonon heat conductivity of the semiconductor) results in a sharp decrease in its spectral response [27]. That is why a TPV converter structurally represents a TPV cavity [27]. Its side walls are made of thermally insulating materials, while the upper and lower walls, respectively, are the emitter and the photocell optimized for converting to a photocurrent a narrow band of the solar spectrum lying in the near- or medium-IR range.

As applied to solar photovoltaics, two kinds of TPV converters are exploited. The first kind is adequately represented in the scientific literature, although, as far as we know, it has never been adopted by the industry. This is a low-temperature TPV converter, which complements a thin diode type SC. This SC, which is, together with the substrate, no more than several micrometers thick and is made of germanium (a material in which the diode dark current remains low up to a temperature of 500 °C), forms the upper wall of the TPV cavity. The lower wall is an IR photocell covered with a layered dielectric structure, which fulfills the function of an optical filter. The photoelectric layer is usually made of indium antimonide or gallium antimonide — materials in which the bandgap energy corresponds to the medium-IR spectral range [27].

Under illumination by concentrated solar light, the entire cell volume (i.e., the upper wall of the TPV cavity) heats up to a temperature of about 400–500 °C, sufficient for producing IR radiation of the specified range inside of the TPV cavity. According to the Wien law, the major fraction of the radiation spectrum is concentrated in the long-wavelength (LW) part of the medium-IR range, where photoelectric conversion is impossible (to be more exact, it is possible, but only in the photodiodes that utilize some cryogenically cooled lead compounds [27]). An optical filter does not transmit this part of the spectrum to the photocell produced from indium antimonide or gallium antimonide.

Another part of the radiation spectrum produced by the heated SC in the TPV cavity lies above the forbidden band frequency of the lower cell. The optical filter plays the role of an antireflection coating (ARC) for this frequency domain. Since only a minor part of the SC thermal radiation may be converted to the photocurrent of the IR photocell and since this conversion efficiency is far from 100%, the gain in electric power due to the addition of the TPV system to the upper SC turns out to be small. The main virtue of this tandem is the SC radiative cooling [4, 27].

A separate field in the literature is made up of high-temperature TPV converters, which operate due to solar radiation and which are named solar TPV systems [27]. In these systems, the upper wall of the TPV cavity is not an SC but a specially developed emitter illuminated by concentrated solar light. The light energy is almost entirely spent to heat the

emitter; in this case, temperatures above 1000 °C are achieved, because the properties of the solar-illuminated upper side of the emitter are close to those of a blackbody throughout the spectral range of a solar light.

As before, the cavity lower wall is formed by a narrow-band IR photodiode. However, the upper cavity wall, i.e., the lower side of the emitter, is nanostructured in a special way. That is why it emits, apart from ordinary — broadband and incoherent — thermal radiation, narrow-band near-IR thermal radiation. This is possible due to the high temperature throughout the emitter volume and the frequency selectivity of its lower (structured) surface. This selectivity is achieved by accommodating either IR nanoantennas or IR metamaterials on this surface [27–29].

The resonance thermal near-IR radiation is converted to photocurrent with a high efficiency. An optical filter reflects the remaining broadband thermal radiation back onto the emitter. Ideally, this part of the energy is not lost and serves to maintain the high emitter temperature, and so these converters may exhibit efficiencies of about 40% [27] and even over [28]. However, the best practically achieved efficiency so far amounts to 3.2% [29]. This departure of experiment from theory is primarily due to the fact that the emitter in the experiment of Ref. [29] represents a planar layer and therefore freely emits thermal radiation from its upper side. This emission is responsible for the radiative emitter cooling to a temperature of about 1000 °C.

In the ideal case, the thermal emitter should be made in the form of a cylindrical shell for a cylindrical TPV cavity. The shell, in turn, should be enclosed in a cylindrical layered structure termed a photonic thermos [27–29]. The concentrated solar radiation will be injected into the photonic thermos through a narrow slit. In this case, 80–90% of the thermal radiation from the outer emitter side will be stopped, and the emitter temperature may be as high as 2000 °C [27–29].

Solar TPV systems like the SC tandems with a TPV converter have not been industrially produced so far. At the same time, they deserve a detailed review because of the interesting physical effects. For these two reasons, they are beyond the scope of our review and are not discussed below.

Finally, from the standpoint of the optical systems in use, all photoelectric converters may be divided into devices operating without and with the concentrated solar radiation by focusing systems (most often by lenses, less frequently by parabolic mirrors [3–5, 9, 10]). Optical light-focusing systems that are not parts of the SCs themselves are not within the scope of our review, either. The optimization of these systems was practically completed several years ago, so that the reader is referred to monograph [10]. Since no books have been written about optical systems for the parallel division of the solar spectrum, in Section 5 of our review we give an idea about the corresponding optical systems. In Section 8, we consider the optical systems which are integral parts of any SC, namely antireflection coatings for some SCs and so-called light-trapping structures.

2. Main characteristics of solar cells

The operation of all SCs, irrespective of the type of materials employed, is characterized by the following parameters: the open-circuit voltage V_{oc}, the short-circuit current I_{sc}, the fill factor FF, and the efficiency. Figure 1a gives a graphic illustration of these parameters. The initial data significant for calculating these parameters are the spectral characteristics of the SC, which define the quantum yield of its constituent structures, and the quantum efficiency in the first place [3–5, 9, 10, 11, 17]. The quantum efficiency (QE) is defined as the ratio of the number of charge carriers collected by the solar cell to the number of incident photons of specific energy (in the unit spectral interval). The QE of an ideal SC is independent of photons with energies higher than the bandgap energy and is equal to zero for photons with an energy lower than that. The departure of the QE curve from the ideal one in short-wavelength (SW) and low-wavelength (LW) domains of the absorption spectrum is affected by a multitude of factors responsible for a useful-energy loss (in silicon SCs, primarily the quality of silicon surface passivation). In the central region of the absorption spectrum, the decisive role is played by reflection losses and the short diffusion length of photoinduced carriers.

The second key SC characteristic is its photovoltaic spectral response (SR), i.e., the ratio of the photocurrent generated in the photoelectric layer to the power of radiation absorbed in this layer in a unit frequency interval. The dependence of the room-temperature SR on the radiation frequency ω for some materials (crystalline silicon, germanium, and main multicomponent semiconductors) may be approximately replaced with an idealized dependence: $SR = 0$ for photons with energies lower than the bandgap energy $E_g = \hbar\omega_g$, and $SR = e/\hbar\omega$ for higher-energy photons (here, e is the elementary charge, and $\hbar$ is the Planck constant). For many photoelectric materials, however, the functions $SR(\omega)$ have a different form and different tempera-

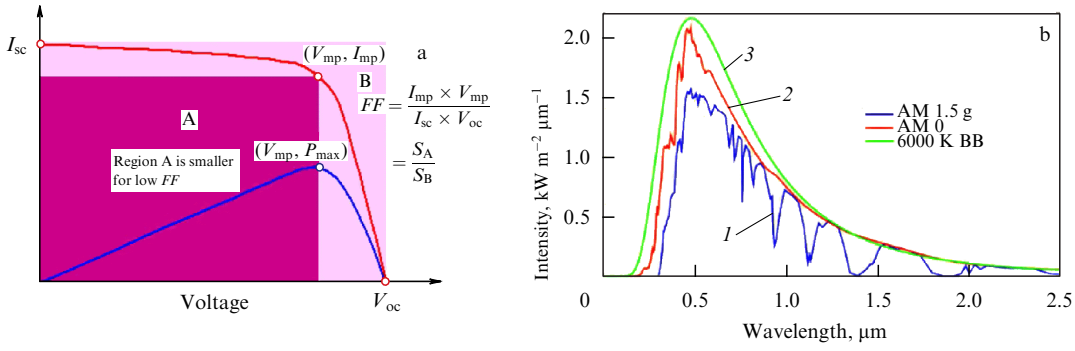

Figure 1. (a) Volt–ampere and watt–ampere characteristics of a solar cell. (b) Solar radiation spectra on the surface of Earth (AM — air mass, AM 1.5g — at a latitude of 50° (curve *1*) and AM 0 — in a circumterrestrial orbit (curve *2*). Shown for comparison is the blackbody (BB) spectrum with the temperature of the solar photosphere (curve *3*).

ture dependence. The quantum efficiency and the photovoltaic spectral response define the SC frequency operating range.

In a diode type SC, the magnitude of the photocurrent is determined by the number of excess charge carriers produced by light through the photoeffect and separated at the p–n junction or the interface of semiconductor materials. In this case, electrons find themselves in the n-region, while the holes in the p-region. In an ideal SC, the photocurrent I_{ph} is the highest current emerging under sunlight illumination, i.e., the short-circuit current I_{sc}, which is produced when the illuminated SC is short-circuited by the external circuit. The current I_{sc} depends on the cell area s, the number of incident photons with different energies (i.e., on the intensity of incident radiation and its spectrum), and the useful absorption coefficient of the SC, which is also referred to as optical efficiency. This coefficient is determined by the power loss of incident light, i.e., by a loss due to reflection, and in thin-film SCs also by a loss due to parasitic light transmission through the photoelectric layer.

The optical efficiency is made as close as possible to 100%; to this end, use is made of a broadband antireflection coating (ARC) and special light-trapping structures. When roughly evaluating the photocurrent ($J_{ph} = I_{sc}/s$) collected from a unit SC area, $SR(\omega)$ is multiplied by the spectral density $P_A(\omega)$ of absorbed radiation flux and integrated over the spectrum. $P_A(\omega)$ is the product of the spectral density of incident solar radiation flux, which is shown in Fig. 1b, by the useful absorption coefficient [3, 4]. This simplified calculation gives an optimistic estimate of the surface photocurrent density J_{ph} in a diode SC, which also depends on the carrier separation probability defined, in turn, by diode surface passivation and charge carrier lifetimes [3, 7, 9].

The current flowing in the external photodiode circuit consists of a dark diode current (direct bias current) I_d and a photocurrent I_{ph} (Fig. 2b). When the external circuit is broken, the separation of charge carriers results in an increase in the number of electrons in the n-region and of holes in the p-region and, therefore, in the emergence of a secondary electric field opposed to the intrinsic field of the p–n junction. In this case, a new equilibrium sets in and the carrier diffusion current rises to a value of I_d, with the total current through the diode becoming zero and the voltage across its disconnected terminals being equal to the open-circuit voltage V_{oc}. I_{sc} and V_{oc} are the highest current and voltage values obtainable from an SC, the power output being equal to zero in both modes at issue.

The fill factor FF is a parameter which determines, in combination with the photocurrent (short-circuit current) and the open-circuit voltage, the maximum power output of an SC. FF is defined as the ratio of the maximum SC power to the product $I_{sc}V_{oc}$ and is equal to the maximum area of the rectangle which may be inscribed under the volt–ampere curve of the SC (Fig. 1a).

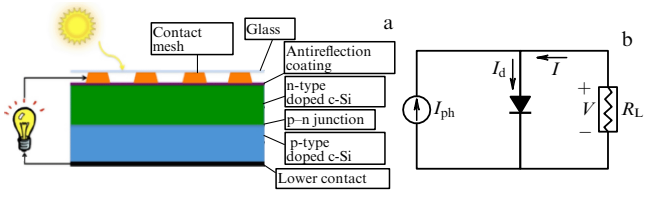

Figure 2. Silicon diode type SC: (a) simplest version with a mesh upper electrode, and (b) equivalent SC circuit. The current I through the load R_L consists of the dark diode current I_d and the photocurrent I_{ph}.

Efficiency is defined as the ratio of output SC power to the incident sunlight power and serves as a parameter for comparing different SCs. The efficiency may be represented as the product of the integral (over the spectrum) quantum efficiency by the following factors: the fill factor, the integral optical efficiency, and, lastly, the so-called ultimate conversion efficiency (*UCE*) [3, 4, 9, 27]. It should be noted that the integral optical efficiency of an SC sometimes depends not only on the design of the SC itself, but also on the optical system when it focuses light onto the SC. First, the concentration of light furthers heating, which may be beneficial in a certain temperature range for increasing the open-circuit voltage without a sacrifice in the photocurrent. Second, focused light is absorbed better than a plane wave [10].

For a given incident radiation spectrum, the ultimate conversion efficiency depends on the spectral response. It is precisely the *UCE* that imposes the so-called Shockly–Queisser limit, i.e., the highest attainable efficiency. Mathematically, this limit appears due to the lowering of SR in the high-frequency region of the solar spectrum. Should a semiconductor photocell whose SR is close to ideal be illuminated by radiation with a frequency of ω_g and a relative spectral width of no more than 20%, the *UCE* of this photocell would be higher than 80% [27]. Thus, the Shockly–Queisser limit does not apply to photocells operating under narrow-band light illumination, whereas the *UCE* turns out to be close to 30% for broadband SCs, as already noted.

It is possible to single out the main conditions for the efficient operation of an SC. First, the optical absorption coefficient of the photoelectric layer should be rather close to unity to provide absorption of essentially all the incident radiation energy. Second, photogenerated charge carriers should efficiently collect at the contact electrodes on either side of the photoelectric layer containing the p–n junction. Third, the p–n junction barrier height in an SC should be optimal: high enough for providing a high value of V_{oc} but not so high as to prevent the absorption of the solar spectrum photons. Fourth, the total resistance of the external circuit connected in series to the solar cell should meet the criterion of maximal power transfer to the load, i.e., be equal to the resistance of the SC itself.

3. Modern trends in silicon solar photovoltaics

To date, silicon has remained the main material for modern commercial photoelectric converters and solar cells. Such wide use of silicon in the manufacture of SCs is primarily due to the adequate development of silicon technology, large resources of silicon as a raw material, and the ecological safety of the material. On the solar cell market, the fraction of SCs made on the basis of crystalline silicon exceeds 90%, of which polycrystalline and single-crystalline silicon account for about 2/3 and 1/3, respectively [30]. Boron-doped p-type single-crystalline and polycrystalline plates 5 and 6 inches (127 and 152 mm) in diameter are the materials used most often for producing silicon SCs. Industrial polycrystalline silicon SCs exhibit efficiencies 2–3% lower than similar single-crystalline silicon structures [10, 30]. The lower efficiency is due to the higher recombination rate of minority carriers at the boundary of the photoelectric region, as well as

at crystal grain boundaries due to a high density of dislocations and impurities that are not subject to removal during purification.

The remaining part of the existing SC market is covered by thin-film cells that are fabricated from other materials, up to 5% of all the thin-film SCs utilizing the thin films of amorphous hydrogenized (hydrogen-doped) silicon [30].

3.1 Single- and polycrystalline silicon solar cells

Single-crystalline silicon SCs operating under unconcentrated solar irradiation have gained the widest acceptance under terrestrial conditions. In these SCs, the back contact is made in the form of a continuous metallic film, and the front one in the form of a contact mesh. Its period and width are a trade-off between the efficiency of carrier collection from the SC entire front surface, which is required for reaching a high fill factor, and the requirement to minimize the optical loss by reflection and scattering, which is necessary for obtaining a high optical efficiency. A mesh electrode produced, for instance, by a screen print, is soldered to current-carrying busses made of more massive wires. The simplest version of such an SC structure is depicted in Fig. 2a, where a lamp stands for the external circuit. Figure 2b is a simplified equivalent schematic of a photoelectric converter, which does not show the loss resistors in both branches modeling the current in the SC.

Figure 3 depicts the modern structure of a single-crystalline silicon SC borrowed from review [31] (the external circuit of the SC and the protective glass are not shown in this and the following drawings). The idea of this technical solution is to decrease the loss by electron–hole pair recombination. The recombination of charge carriers produced by photons from the SW part of the spectrum on the front surface lowers the SC quantum efficiency in this part of the spectrum. To reduce the surface carrier recombination, the front surface is coated with a passivative dielectric layer several nanometers in thickness (not shown in Fig. 3).

However, it is not enough. To minimize the recombination loss, the front part of the dielectric layer should be so thin that the majority of carriers would be produced in the base of the photodiode rather than in its upper part (emitter). In silicon SCs, this is achieved when the base region is made of perfectly purified single-crystalline silicon, which provides long diffusion lengths and lifetimes of minority charge carriers. To improve the separation efficiency for the charges generated in the base region, either a propelling electric field is imposed on the base region or (most often) an isotype potential barrier is created on the base back surface ($p-p^+$, as shown in Fig. 3, or $n-n^+$ [10]). The existence of a back surface field leads to the reflection of minority charge carriers from the SC rear surface. This not only lowers their surface recombination and improves the photocurrent collection efficiency, but also raises the open-circuit voltage without increasing the ohmic loss in the SC.

In the simplest version, the back potential barrier may be formed by fusing aluminum paste deposited on the back surface of an SC [31]. The ohmic contact between the upper mesh electrode and the heavily doped emitter region is also achieved by fusing, with the mesh metal (most often silver) penetrating through the submicrometer antireflection layer and the passivative layer. We note that a further increase in the SC spectral response in the SW part of the solar spectrum involves an enhancement in the static electric field in the front layer by introducing a doping gradient [17]. When the p–n junction resides at a sufficiently large depth (in practice, an n^+ layer thickness of about 1 μm is enough), a stepped dopant distribution in the front layer provides, on the one hand, a rather high spectral response of the SC in the SW spectral range and, on the other hand, a decrease in the spreading resistance in the front layer, which raises the fill factor and, accordingly, the photocurrent.

To improve SC efficiency, use is also made of textured surfaces. For instance, the teeth in Fig. 3 correspond to micrometer-sized pyramids. This modification of the front surface serves to lower the optical loss by reflection of the incident light, which is especially significant for oblique incidence [32–35]. The pyramidal texturing makes the SiN_x or TiO_x antireflection layers not only broader-band antireflection coatings, but also all-angle ones. The latter signifies that the SC coating suppresses the reflection of direct solar light at all angles of incidence that are practically possible for a solar cell. To further decrease the optical loss, use is made of simultaneous texturing of the front and back surfaces [34]. The natural surface roughness [36, 37] of deposited silicon and the existence of pores in porous silicon [38] also improve the surface antireflection properties. The physics of lowering the optical loss is discussed in Section 8 of our review.

Let us now discuss three alternative, but no less popular, realizations of single-crystalline and polycrystalline silicon SCs: the passivated emitter rear localized (PERL) cell, the heterojunction with intrinsic thin layer (HIT) structure, and, lastly, the back contact–back junction (BC–BJ) structure [39–42].

The SCs of a PERL design (Fig. 4a) are characterized by a thick base layer of single- or polycrystalline p-type silicon and a thin (0.2–0.3 μm) heavily doped n-type emitter layer of polycrystalline silicon, as well as by passivation of the front and back surfaces. In these structures, as in Fig. 3, there is a textured (with micrometer-sized pits of a pyramidal shape) antireflection coating and a back potential barrier; the contact on the rear surface is continuous, and the contact on the cell front surface is a mesh (Fig. 4a). An n-type layer is

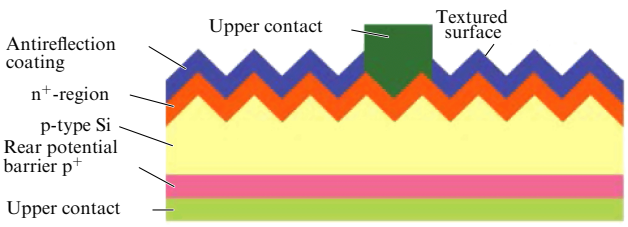

Figure 3. Schematic representation of a silicon SC. Modern version of the structure with a back potential barrier [31].

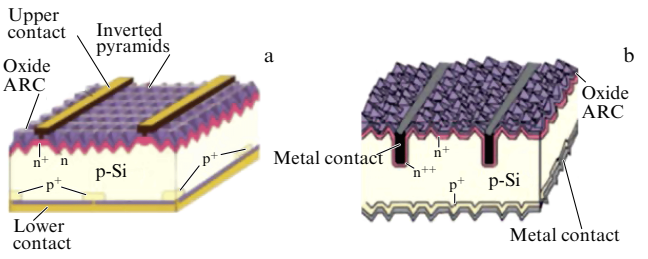

Figure 4. Schematic representations of silicon SCs: (a) with the PERL geometry [39], and (b) with a buried front contact [41].

obviously required to produce a diode, but heavy doping lowers the spectral response, so that virtually all the photocurrent is produced in the base — a layer with p-type conductivity — while the relatively small thickness of the n-layer permits minimizing the loss by light dissipation. In this case, the isotype $p-p^+$ barrier shown in Fig. 4 serves the same purpose as above (specifically, for suppressing recombination in the contact region by lowering the density of minority charge carriers). A bilayer antireflection coating made of oxide films minimizes the optical loss by reflection. The record efficiency for the structures of such a design utilizing single-crystalline silicon amounts to about 25% for ordinary, i.e., unconcentrated, light [39]. Taking advantage of a 92-fold sunlight concentration, the efficiency of these SCs amounts to 27.6%, because the absorption of concentrated light in a lossy medium is stronger than the damping of a plane wave in the same medium [40].

In the formation of a mesh electrode using a screen print on the cell front side, account is taken of two competing factors. On the one hand, the optical loss arising from the cell shading by the metal electrode and the scattering by the contact is optimized. On the other hand, the ohmic loss arising from the series resistance due to the insufficiently large contact area between the electrode and the emitter layer is also optimized [3]. An alternative to the method of forming the upper mesh electrode by a screen print of silver paste concerns the formation of a buried metal contact covered with a layer of nickel, copper, or silver, as shown in Fig. 4b [41]. This geometry ensures the employment of narrow contact strips and the consequential smallness of optical losses and permits attaining a low series resistance by increasing the contact surface between the upper electrode and the emitter layer.

The same objective — lowering the loss by recombination — is reached in SCs with the HIT structure by introducing an undoped silicon layer, i.e., by replacing the p–n junction with a p–i–n heterojunction. Instead of polycrystalline silicon, these SCs usually contain very thin p-, i-, and n-type conductive layers of amorphous silicon (a-Si) on either side of the single-crystalline (c-Si) silicon base with a bandgap energy of 1.1 eV [31]. The primary role of the doped a-Si layers lies with raising the open-circuit voltage, since amorphous silicon has a broad energy gap (1.7–1.8 eV). The amorphous silicon i-type layer plays an equally important role: it permits a high quality of the interfaces to be provided, since many defects would inevitably appear between the crystalline substrate and the doped amorphous layers [42]. Since the lifetimes of minority charge carriers in amorphous layers are very short [10], transparent conductive oxides, for instance, indium–titanium oxide (ITO) or aluminum–zinc oxide (AZO), are often employed for collecting the photocurrent in lieu of contact meshes in such SCs.

Figure 5a represents a schematic of an HIT structure, in which the photocurrent is generated in the weakly doped c-Si layer with an n-type conductivity. Thin layers of amorphous silicon are formed on either side of this single-crystalline layer. A transparent conductive oxide (TCO) layer collects the photocurrent. A mesh of submillimeter wires is made in this structure with a large period (about 1 cm) and serves to enhance contact with the external circuit. Such an SC may be operated under illumination on both sides [31].

The record efficiency of 25.6% for HIT type SCs was demonstrated by Panasonic Co. (Japan) [43] (under conventional, without concentration, illumination by solar light). In

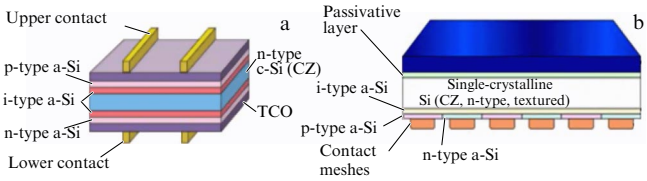

Figure 5. Schematic representations of SCs: (a) utilizing crystalline and amorphous Si with the HIT structure [31], and (b) with the HIT structure from Panasonic Co. (Japan) with a record efficiency [43].

this structure, the p–i–n heterojunction and the photocurrent-collecting metal contacts were located on the SC rear surface (Fig. 5b). This technical solution provided a lowering of the reflection of incident radiation, an increase in the useful light absorption in crystalline silicon, and a decrease in series resistance of the cell [44]. Structurally, positioning the contacts on one side of the SC makes easier the integration of cells in a module (a solar battery). A back potential barrier is formed in front of the p-type contact. The front side of the crystalline silicon layer is textured by randomly distributed roughness (asperities of average height 0.5–0.7 μm with the same average spacing between them), which serve to additionally lower the reflection. This reflection quenching is referred to as the *black silicon* effect and is discussed below in Section 8.1. To demonstrate the record efficiency, use was made of illumination by normally incident light, and therefore no texturing of this coating was required.

An alternative version of the HIT structure contains a single-crystalline p-type layer. The advantages and disadvantages of this technical solution presented in Fig. 6a are discussed in Ref. [44]. The main drawback is the lower spectral response of p-type single-crystalline silicon (3% lower than for n-type silicon), and the main virtue is a significantly lower cost of the doping procedure (injection of boron).

The so-called SCs with the BC–BJ structure (see Fig. 6b) have n- and p-doped regions, as well as point contacts on the cell rear surface [45]. The structure shown in Fig. 6b is characterized by passivation of both the cell front and rear surfaces, the existence of a broadband (as a rule, textured) antireflection coating, a front potential barrier due to a thin n^+ layer, n- and p-doped regions on the rear surface, and, as noted above, the location of contacts intended for the collection of both type carriers on the cell rear surface [45]. The low series resistance in these solar cells permits attaining high fill factors on volt–ampere characteristics. Evidently, the structure of Ref. [43] combines the features of the HIT and BC–BJ structures.

In BC–BJ-based solar cells, the photoelectric layer thickness should be decreased to about the diffusion length of minority carriers in silicon of the corresponding kind [41–44]. Specifically, in crystalline silicon, this length amounts to about 100 μm, whereas in amorphous silicon to only 150 nm. This thickness minimization lowers the SC ohmic loss resistance; in this case, the open-circuit voltage decreases only slightly, while the fill factor and, hence, the efficiency become higher.

Apart from the BC–BJ structure, to decrease the optical loss stemming from the cell shading by the upper mesh electrode and to facilitate the packing of solar cells in large area modules (panels), use is made of the following geometries with arrangement of both type contacts on the rear surface [45]: metal wrap through (MWT), and emitter

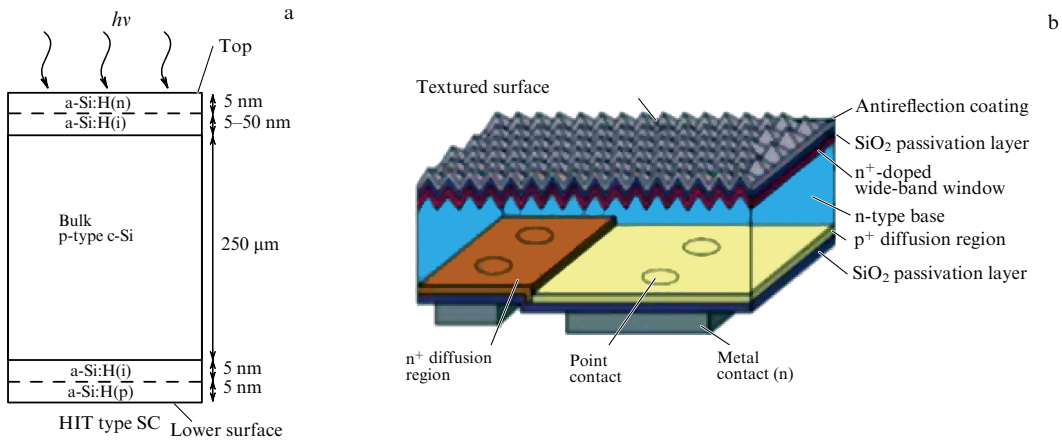

Figure 6. Schematic representations of silicon SCs: (a) HIT structure with a p-doped base photoelectric layer [44], and (b) BC–BJ structure [45].

wrap through (EWT) (Fig. 7). In these geometries, unlike the BC–BJ one, the emitter is located on the front surface of the cell, with the charge carrier transport to the rear surface being provided due to the formation of metallized through holes in the substrate with the aid of laser technologies. The holes are made either up to the upper metal contact, as for MWT, or up to the emitter layer, as in the case of EWT.

The proposed structure versions are also suited for making SCs on the base of polycrystalline silicon, where the lifetimes and carrier diffusion lengths are significantly shorter than those of single-crystalline substrates. The main difference between these structures lies in the fact that the metal mesh contact, though without current-carrying busses, is located on the front side in the MWT as before. In this case, the MWT cells call for the formation of a smaller number of through holes for the direct collection of photoinduced carriers. For the EWT geometry, there is no metal mesh on the cell front surface, and a larger number of through holes from the back contact to the emitter layer is required for the efficient collection of charge carriers. Using this approach, it has been possible to make an SC with an efficiency above 20% [46].

Generalizing different technical solutions for creating crystalline silicon solar cells, one may formulate the main approaches to efficiency improvement, which is the objective of all these solutions.

(1) Minimization of optical reflection loss by texturing the front side of an SC and depositing multilayer antireflection coatings. To minimize the loss due to shading by a contact mesh, all contacts are formed on the cell rear surface. Minimization of emitter thickness for SCs of the PERL design.

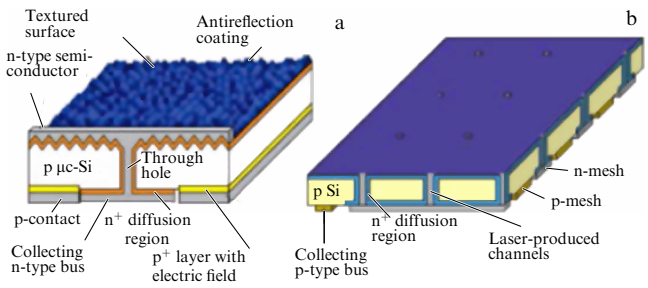

Figure 7. Schematic representations of solar cells with MWT (a) and EWT (b) geometries of contact arrangement on the cell rear surface.

(2) Minimization of surface recombination loss by passivating the cell front and rear surfaces and forming a back potential barrier.

(3) Minimization of electric loss by decreasing the series resistance between the contact mesh and the emitter; selection of the base thickness at about the diffusion length of minority carriers.

It is pertinent to note that the efficiency of large-area commercial cell modules is always somewhat lower than the efficiency of laboratory type solar cells and amounts to 17–19% for modules utilizing single-crystalline substrates, and to 16–18% for polycrystalline substrates [44].

3.2 Thin-film silicon solar cells

The cost of crystal substrate material accounts for the bulk of the cost of silicon SCs. A change to thin-film SCs with a total silicon layer thickness on the order of 1 μm or less permits not only a decrease in the amount of the semiconductor, but also a change to much cheaper functional flexible substrates. Not only is the cost of the produced energy thereby reduced, but also the possibilities for the deployment of SC panels are broadened: such solar batteries are conformal and may be produced in the form of rolls. Furthermore, the amount of production waste decreases many-fold — in direct proportion to the amount of silicon. Lastly, in the utilization of thin-film solar cells, the environmental damage proves to be smaller [3, 4, 11, 17, 47].

One way to make the active region of a silicon SC thinner is to use cheap substrates of low crystal quality (so-called grade-Si) as the base on which to form the active layers of epitaxial crystalline silicon of high quality [11, 17, 47]. Figure 8a represents a schematic of a solar cell utilizing thin (about 5–10 μm) epitaxial Si layers. This design has features in common with the classical design of a crystalline silicon SC. On the surface of a grade-Si substrate in such SCs, the microcrystalline silicon base and emitter regions are formed by epitaxial chemical vapor deposition (CVD) methods and liquid phase epitaxy (LPE) [47]. To lengthen the optical path for incident light, a high-reflectivity layer is introduced at the epitaxial layer–substrate interface, which increases the fraction of absorbed sunlight and the short-circuit current. The surface of the upper part of the silicon epitaxial layer is textured.

Currently, the maximal efficiency of an epitaxial thin-film silicon SC with a whole single-crystalline substrate amounts

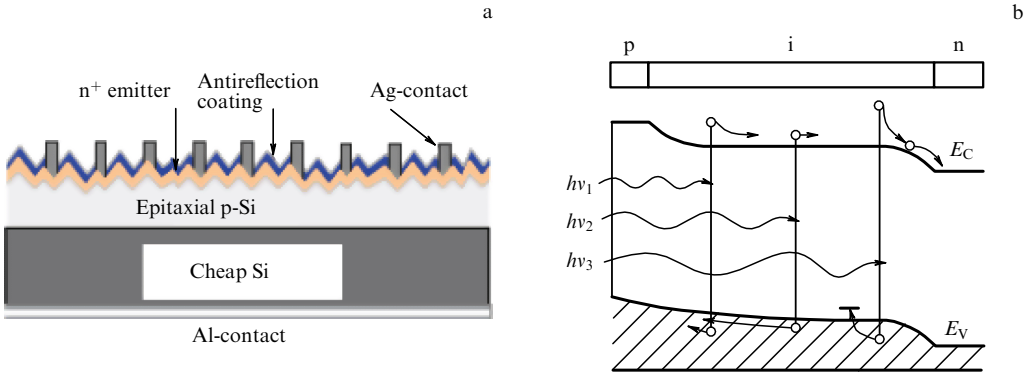

Figure 8. (a) Schematic of a thin-film SC utilizing epitaxial Si layers. (b) Energy band diagram of an amorphous silicon p–i–n structure.

to about 19%; the use of grade-Si substrates, which cost half as much, leads to a decrease in efficiency to 10–13% [47]. Thinning the epitaxial region to less than approximately 4–5 μm in these SCs results in a loss in optical efficiency, because not all light that enters the epitaxial layer is absorbed in it. These problems are solved with the use of light-trapping structures, which will be analyzed in Section 8.

Another approach to the development of thin-film silicon SCs involves the utilization of amorphous and microcrystalline silicon. Optical absorption in amorphous silicon, which exhibits only a short-range order, is 20 times higher than the absorption in single-crystalline silicon [11, 47], although the photoelectric spectral response is approximately one third as strong and the spectrum itself is one third the width. The latter signifies an order of magnitude lower photocurrent and, accordingly, efficiency, all other factors being the same. However, as follows from the aforesaid, the efficiency is affected by a variety of factors, and SCs utilizing amorphous silicon turn out to be a more gratifying object for optimization than those utilizing crystalline silicon and are therefore quite competitive.

First, the high optical absorption permits thinning the photoelectric layer to about 0.5–1 μm without concern about loss due to light transmission to the lower electrode, which possesses significant optical absorption in such SCs.

Second, the bandgap energy in amorphous silicon may be changed by introducing a hydrogen dopant (hydrogenization) in the range of 1.7–1.8 eV, while the position of the Fermi level is controlled by doping (P for the n-type substances, and B for the p-type). Therefore, it becomes possible to make SCs utilizing hydrogenized amorphous silicon (a-Si:H) with a thickness of about 0.5–1 μm. Simultaneously, the ohmic loss is minimized and the open-circuit voltage does not become lower. The fill factor turns out to be large enough and the efficiency of these SCs is only 2–3 times, but not an order of magnitude, smaller than that for crystalline silicon SCs. Furthermore, such SCs may be fabricated on a flexible substrate, for instance, on a polymer or foil substrate, in lieu of costly silicon substrates.

Among the methods of preparing silicon layers, mention should be made of vapor phase and liquid phase deposition techniques [11, 47]. The main technologies for the formation of thin silicon layers are CVD and LPE, as well as plasma chemical vapor deposition and magnetron sputtering. A virtue of these processes is the possibility of forming amorphous silicon layers at a relatively low substrate temperature ($\sim 200\,^{\circ}$C and lower). At low temperatures, the impurities can hardly migrate from the substrate to silicon crystal during its growth. The low-temperature deposition of amorphous silicon permits using as a substrate the cheap organic glasses, polymers with transparent conducting layers deposited on their surface to serve as electrodes [11], or metallic foil [47]. As a result, the change from crystalline silicon to the amorphous one may lead to about a ten-fold reduction in the cost of a unit area of a photovoltaic module, the module itself being flexible [47, 48].

For a working junction in amorphous silicon SC, use can be made of a Schottky barrier with a metallic contact or a metal–oxide–semiconductor structure. However, the highest solar cell efficiency has been obtained with exploiting the p–i–n structures [11, 17, 47], whose energy band is diagrammed in Fig. 8b. The thin heavily doped p- and n-type layers provide the existence of an internal field and, hence, an efficient separation of the charge carriers generated in the i-layer.

In thin-film amorphous silicon SCs, the i-layer thickness amounts to 250–900 nm and the p- and n-layer thicknesses range between 20 and 30 nm, so that the total thickness lies between approximately 0.3 and 1.0 μm. The charge carriers generated in the n- and p-type layers do not contribute to the photocurrent because of their short lifetime. That is why the cell sunlight absorption in these layers exhibits a parasitic effect responsible only for dissipation. Accordingly, it is desirable to thin these layers to values whereby the light absorption in them may be ignored. Furthermore, the diffusion length of minority carriers in a-Si:H lies in the 10–50 nm range [47], and making the doped layers thicker than 50 nm is inexpedient.

A p–i–n structure thickness of 0.3 μm evidently corresponds to lower losses than a 1-μm thickness, but it cannot be decreased further. This lower bound is related to the thickness of depletion regions of the p–i and n–i junctions. The latter is equal to about 150 nm and is primarily located in the i-layer. Evidently, the p–i–n structure, which contains two such junctions, should not be appreciably thinner than 300 nm, otherwise the photocurrent will be short of carriers and it will be significantly lower. The depletion region extends to the p- and n-conduction layers by 10–20 nm, and so these layers may not be thinner than these values. However, making the p–i–n structure thicker than approximately 350–400 nm is also inexpedient. Bearing in mind only the photocurrent generation and assuming the 100% absorption of incident light, a structure thickness of about 300 nm (for doped layer thicknesses of 20–30 nm) is indeed the optimum for thin-film amorphous silicon SCs.

Unfortunately, for so thin a structure and with total compensation for reflection, about half of the power of incident solar light is transmitted through the photoelectric layer. This results in a parasitic light absorption at the back electrode and, if the electrode is made of a conductive oxide, in the substrate as well. Of course, it would be desirable to employ a polished metal for the back electrode. This approach proves itself in microcrystalline silicon SCs. Substrates made of specially polished stainless steel exhibit surface irregularities of only tens of nanometers, form a good electrical contact with μc-Si, and work as a mirror. The solar light reflected from such an electrode back onto μc-Si is virtually completely absorbed when the μc-Si thickness exceeds approximately 2.5–3 μm [47].

The same effect is achieved when metallized polished optical glasses are employed as substrates. However, such substrates are not flexible and appropriate SCs cannot be produced in rolled form, which shows promise for especially low cost in the mass production of SCs utilizing amorphous silicon. Such SCs cannot have electrodes of polished steel. The electrodes of amorphous silicon SCs are either transparent to solar light — are made of conductive oxides or metal meshes — or absorb light. In the latter case, the SC has a heavily doped lower (with n-type conduction) silicon layer which maintains a good contact with aluminum foil.

It is vital to prevent in such structures the loss due to sunlight transmission through the photoelectric layer. However, no industrial solutions for the requisite *light-trapping structures* have been found to date (see Section 8). That is why the p–i–n amorphous silicon structure in SC-producing companies have been made approximately one micrometer thick [48]. For this thickness, it is sufficient to suppress the loss due to light reflection by depositing an antireflection coating.

However, hydrogenized amorphous silicon turned out to be subject to degradation, which lowers the SC efficiency by about one third after a half year of operation. This effect was mentioned above and is called the Staebler–Wronski effect [49]. It was discovered in 1977 but ignored by SC researchers and developers at that time. Along with other factors, this effect contributed to the bankruptcy of companies producing these SCs (see, for instance, Ref. [50]). The nature of the effect was not conclusively elucidated until 2014: the formation of large defects (caverns) around hydrogen atoms under light irradiation [51]. According to the theory [51], an approximately 300-nm thick CVD-produced amorphous silicon layer with doped regions much thinner than 100 nm must be far less subject to degradation (an efficiency lowering of about 10%) than amorphous silicon 1 μm and above in thickness (the efficiency lowering amounts to 30%).

In known 250–400-nm thick amorphous silicon SC samples, use is made of textured antireflection coatings, but the loss due to light transmission through the photolayer influences the efficiency, which does not exceed 7 % [11, 47]. The virtues are the cheapness of the photovoltaic module of such SCs with the use of roll technology, the possibility of placing the battery as well as individual SC on nonplanar surfaces, retention of the same solar energy conversion efficiency at temperatures of about 40–60 °C, and, lastly, an insignificant lowering of the output power under cloudy conditions. It turns out that the efficiency of an amorphous silicon SC is 20–30% lower under irradiation by scattered light arriving from random directions, while the decrease for a crystalline silicon SC is nearly twofold [11, 47].

The highest practically achieved efficiency of an amorphous silicon SC reached 10.2%, which corresponds to a rigid construction with a p–i–n structure approximately 310 nm in thickness (the i-layer thickness was equal to 220 nm) [52]. An efficiency improvement of 3.2% over SCs produced on flexible substrates was achieved due to a significant lowering of the optical loss in the lower electrode. In this SC, use was made of a reflecting lower electrode and a 'butterfly eye' textured antireflection coating with a gradient of the refractive index (see Section 8.1). After 1000 h of continuous illumination by a solar light simulator, the SC efficiency degradation amounted to 11% due to the Staebler–Wronski effect.

Thin-film SCs utilizing microcrystalline silicon (μc-Si) with a bandgap energy of 1.1 eV exhibit a higher efficiency than amorphous silicon SCs; however, as noted above, they do not ensure flexibility. The spectral photoelectric response of μc-Si is no better than that of amorphous silicon, but the diffusion length and the lifetime of minority carriers in the doped region are longer. In view of the significantly lower light absorption, such SCs are rated as thin-film ones for a photoelectric layer thickness of up to 5 μm, with the optimal thicknesses (providing the highest fill factor and quantum efficiency) lying in the 1–2 μm range. This is sufficient for the total sunlight absorption in the presence of an antireflection coating and a reflecting lower electrode. The record efficiency of such SCs, which is equal to 11.4%, was reached for an optical efficiency of 99%, i.e., for a nearly total absorption of the incident light in silicon [53].

Described in Ref. [53] is the fabrication procedure for a μc-Si SC on a glass substrate textured with a hexagonal grid of glass micropyramids coated with Ag and ZnO:Ga layers 200- and 100-nm thick, respectively. The lower layer (Ag) provided a high reflectivity, while the ZnO:Ga layer ensured a good ohmic contact between silver and silicon. This lower reflecting texture in combination with the upper antireflection one made up a light-trapping structure operating in the framework of geometrical optics (see Section 8.2). The 1-μm thick bulk μc-Si layer, the buffer layers, and the doped nanocrystalline SiO_x layers were formed by plasma-activated CVD method. The upper contact comprised an ITO layer and a silver mesh electrode. The buffer layer at the p- and i-layer interface was introduced to raise the open-circuit voltage. The structure is schematized in Fig. 9a.

To improve the efficiency of thin-film silicon SCs, photoelectric converters with two or three cascades were developed. Such hybrid SCs may also be termed multijunctional. Unlike truly multijunction SCs — those involving semiconductors of different types — their cost is relatively low, because they are made up of readily compatible kinds of silicon. In the development of two-cascade silicon SCs, the upper p–i–n type heterojunction is made of a-Si:H with an overall thickness of 350 nm (with a 250-nm thick i-layer having a bandgap energy of about 1.7 eV); the lower heterojunction, also of the p–i–n type, is composed of μc-Si:H with a total thickness of 3 μm (with a 2.50-μm thick i-layer and $E_g = 1.1$ eV) [54]. This type of SCs is hardly subject to light-induced degradation and is characterized by an efficiency of 12.2%, which is high for thin-film silicon SCs. The corresponding structure is depicted in Fig. 9b.

Also developed were thin-film SCs with three successive cascades comprising junctions on the base of a-Si:H, a-SiH with additions of germanium (a-SiGe:H), as well as μc-Si:H with a bandgap energy lying in the 1.1–1.8 eV range [55]. These materials may be prepared using plasma-activated

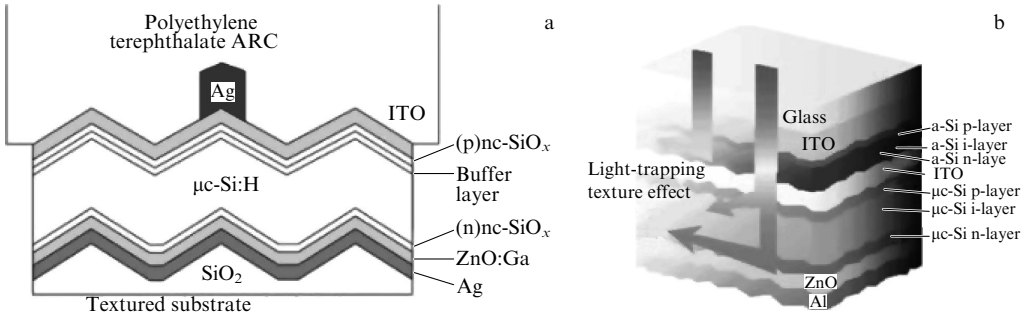

Figure 9. (a) Schematic representation of a μc-Si SC [53]. Texturing the metallic substrate with micropyramids results in the texturing of the entire structure grown on the substrate, which provides the light-trapping effect. (b) Schematic of a two-cascade SC with heterojunctions [54]. The ZnO layer improves the contact between metal and microcrystalline silicon. The indium–titanium oxide (ITO) interlayer, which divides the two SC cascades, improves the SC antireflection properties, maintains the total photocurrent, and does not prevent the passage of light to the lower cascade. The contact mesh (Ag) at the upper ITO electrode is not shown.

Table 1. Record efficiencies of silicon solar cells (borrowed from Ref. [56]).

SC type	Efficiency, %	Area, cm^2	V_{oc}, V	J_{sc}, mA cm^{-2}	*FF*, %	Manufacturer
c-Si	25.6	143.7	0.74	41.8	82.7	Panasonic (Japan)
Multi-c-Si	20.8	243.9	0.66	39.0	80.3	Trina Solar (China)
PERL Si	21.2	239.7	0.69	38.5	80.3	Solexel (USA)
a-Si	10.2	1.001	0.90	16.4	69.8	AIST (Japan)
μc-Si	11.4	1.046	0.54	29.7	73.1	AIST

CVD. The highest efficiency of such three-cascade cells reaches 16.3%, with its stabilized value being equal to 13.4%. Unfortunately, all attempts to obtain so high an efficiency for similar SCs on flexible substrates have not met with success. Furthermore, the rather complex structure (Fig. 9b) of cascade silicon SCs is responsible for their relatively high cost.

The highest achieved efficiencies (from 10.2 to 25.6%) of different types of silicon SCs (and, accordingly, with different costs) [56] produced by industrial companies as of January 2015 are collected in Table 1. Although second-generation SCs appear in this table, so far they have failed to conquer the market. The demand for flexible and thin solar batteries, which could be accommodated on nonplanar surfaces (on house corrugated roofs, as bracelets for SC wristwatches, etc.), turned out to be small. For instance, the surface of a solar panel for powering a house calls for regular cleaning. On the other hand, accommodation of SCs on a flexible substrate with the application of roll technology permits making large-area solar batteries, thereby compensating for the low efficiency. This dilemma generates the uncertainty of choice. Companies producing second-generation silicon SCs have not yet chosen between more efficient SCs on a rigid substrate and less efficient SCs on a flexible substrate. At present, second-generation thin-film silicon SCs are poorly represented on the market.

4. Commercial second-generation multicomponent semiconductor-based solar cells

Second-generation solar cells, namely, those consisting of a layer of a photoelectric material a few micrometers (or less) thick and based on multicomponent A_3B_5 (InP, GaP, GaAs) and A_2B_6 (CdTe) semiconductors, as well as multicomponent semiconducting compounds (CIGS, CZTS) hold the second-place position after first-generation SCs on the global market; they account for roughly 10% of the total SC production. Global electricity production exploiting second-generation SCs is growing annually; multijunction solar cells based on these cells are the main power sources in space missions.

Typical SC structures built around single-junction semiconductors are demonstrated in Fig. 10. The manufacture of such SCs requires less starting materials than that of crystalline silicon SC, but is usually associated with toxic waste generation (especially CdTe manufacture), while production costs depend on the level of raw material extraction; indeed, they may be so high that even a large producer will prove unable to withstand competition (see, for instance, Ref. [50]). These and some other factors explain why research and development of technologies for manufacturing such SCs either are not funded from State budgets or are supported by private investments. Naturally, private companies concentrate on the development of technologies rather than basic

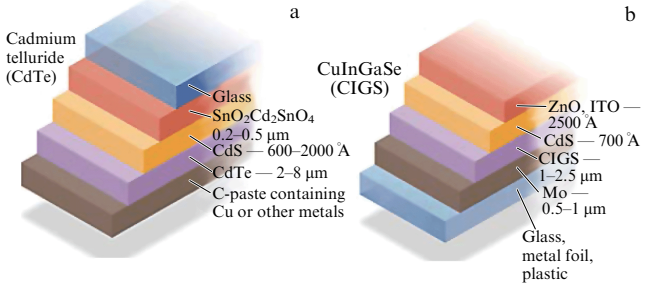

Figure 10. Typical CdTe (a) and CIGS (b)-based SCs with a diode structure (according to data from Refs [18, 59]).

research and physical effects. For this reason, the present section is concerned with an overview of technological advances in the field of interest and certain related practical issues.

4.1 CdTe-based solar cells

The formation of SC diode structures based on cadmium telluride (CdTe) dates back to the 1970s. Attention was focused on a direct gap semiconductor with a bandgap energy of 1.45 eV and a perfect ionic structure of the crystal, providing high chemical and thermal stabilities; it was justifiably regarded as a potential alternative to silicon (an indirect gap semiconductor) for solar photovoltaics. The high absorption coefficient of cadmium telluride (over 10^5 cm^{-1}) allowed absorbing layers as thick as a few micrometers and even thinner to be made without detriment to efficiency. This permitted reducing the cost of CdTe-based cells and increasing their efficiency by decreasing carrier recombination and ohmical losses.

The first thin-film CdTe-based SC was manufactured almost half a century ago at Ioffe Physical-Technical Institute under the guidance of E I Adirovich [57]. The conceptual structure of this SC has not changed since then. The challenges encountered by Adirovich's cells remain in force too, viz. the extreme difficulty of industrial deposition of a thin CdS layer possessing n-type conductivity on a CdTe surface layer with the p-type conductivity; the exceptionally high toxicity of the SC activation process using chlorine ions to form cadmium chloride without which the efficiency is unacceptably low (the causes behind the growth of cadmium telluride spectral sensitivity in the presence of its chloride remain debatable [58]); the unresolved problem of preventing metal ion migration into a photoelectric layer during creation of current-carrying contacts (the migration sharply decreases the SC spectral sensitivity).

Developments along these lines in photovoltaics were initiated by several European companies [58] in the 1980s with the participation of a few research groups and became almost totally commercialized in the course of time. The structure of a modern CdTe-based SC is shown in Fig. 10a. See Refs [59, 60] for a detailed description of its operational principles and the function of each constituent element. The main technologies for manufacturing such SCs (sublimation, chemical spraying, chemical vapor deposition, epitaxy, screen printing, etc.) were proposed by Monosolar, Ametec, Kodak, Photon Energy, Glass Tech Solar (all USA) and other companies. The highest efficiency of CdTe-based SC under laboratory conditions amounts to 20% [61], but the possibility of industrial application of this technology remains unclear.

4.2 Solar cells based on multicomponent semiconducting compounds $Cu(In, Ga)(Se, S)_2$ and $Cu_2ZnSn(S, Se)_4$

Direct gap semiconductors with a 1.1–1.5-eV bandgap energy, high absorption coefficients (10^4 cm^{-1} or higher), and a crystallographic structure of chalcopyrite or kesterite are also used as the materials for second-generation thin-film SCs [18–20]. The $Cu(In, Ga)(Se, S)_2$ type chalcopyrites and $Cu_2ZnSn(Se, S)_4$ type kesterites (marked as CIGS and CZTS, respectively) are semiconducting crystals readily synthesized in the laboratory conditions and differing in the substitution of Zn and Sn for In and Ga, respectively [18–20]. The substitution is needed because In and Ga are highly toxic elements. Utilization of SC containing these elements is very expensive, and their application was restricted by the Energy Directorate-General, European Commission and US Department of Energy at the beginning of this century [62]. The restriction also covered the use of Te in thin-film CdTe-based SCs [62]. Another undesirable aspect of manufacturing chalcopyrite-based SCs consists in the fact that all their components (In, Ga, and Te for CdTe) are side-products of mining Al, Zn and Cu-containing minerals [60–62]. Therefore, fluctuations in mining activity introduce uncertainty as regards prices of chalcopyrite-based SCs.

All chalcopyrite and kesterite-based SCs exhibit a diode structure (Fig. 10b). CIGS and CZTS take the part of p-type semiconductors deposited on a glass substrate coated with a thin Mo layer as the lower contact. The p–n structure is formed by depositing a thin (of order 50 nm) layer of the n-type doped broadband CdS semiconductor. The diode structure is completed by coating the CdS layer with thin layers of transparent zinc oxide and conducting ITOs that make up the upper contact (ITO is sometimes substituted by a metallic mesh contact). Figure 11 shows the typical structure of a thin-film CIGS-based SC [19].

The substitution of In and Ga by Zn and Sn, justified from an environmental health perspective, proved less than perfect from the quality standpoint of crystals, which were found to have quite a few crystallographic defects; moreover, such replacement does not allow crystals bigger than 1 μm in size to be grown. Simultaneously, the crystalline structure of chalcopyrites makes it possible to deposit additional layers more easily and is more convenient for creating ohmic contacts than the kesterite structure [61, 63]; also, it contains

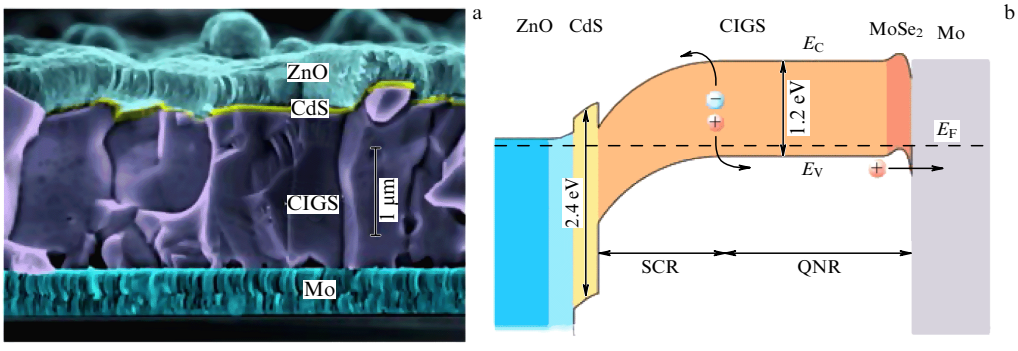

Figure 11. (a) Structural cross section of a CIGS-based SC obtained by scanning electron microscopy. (b) The structure of the p–n junction in an optimized thin-film CIGS-based SC [19], where SCR and QNR are space charge and quasineutral regions, respectively.

fewer defects. The mismatch between crystalline structures of CdS and kesterite also accounts for the impaired efficiency of solar cells based on these materials. Modern chalcopyrite-based SCs have an efficiency of roughly 20% [61], compared with the one half efficiency of the best kesterite-based SCs [20, 64].

A great deal of effort was taken to prepare flexible thin-film CIGS-based SCs having a high enough efficiency [18, 19, 62]. Nevertheless, their effectiveness remains slightly reduced due to addressing to low-temperature manufacturing technologies (flexible structures are grown on an aluminum foil or polymer film as a substrate sensitive to high temperatures). In this case, the energy structure of a p–n junction contains a local potential well in the CIGS region. Its idealized variant is shown in Fig. 11b. This parasitic effect leads to the photocurrent loss for an additional recombination of carriers in the well. As a result, a flexible thin-film SC has an efficiency of 18.7% instead of the expected 20% [19].

Methods for manufacturing CIGS and CZTS-based SCs may be divided into two main groups: with and without exposure to vacuum. The former option increases production costs but ensures maximum efficiency (over 20% compared with 17% in the latter variant) (see Ref. [64] for details). However, even methods lacking vacuum exposure require very strict compliance with all technological parameters of the processes to achieve a maximum efficiency and reduce the price of SCs [65, 66].

Despite long-term investigations of chalcopyrites and kesterites as materials for second-generation thin-film SCs, their high current and unpredictable future prices, as well as strict technological requirements, taken together put in question their (especially CZTS) chances of winning competitions with other SCs [20, 66].

5. Third-generation inorganic solar cells

5.1 Multijunction solar cells

Multijunction solar cells are also known as cascade or tandem SCs and, as we have already noted (see Section 1.1), they consist of layers of different photovoltaic materials with p–n junctions (Fig. 12a). Each photovoltaic layer is responsible for the absorption of a specific part of the solar spectrum (Fig. 12b), which allows converting photons in the spectral range from 0.6 to 2 eV, while, for example, CIGS or c-Si-based solar cells can convert the spectrum only in the range of 1.1–1.9 eV. However, the main feature of multijunction SCs lies in the fact that the extension of the spectrum is followed by a rise in the Shockley–Queisser limit, because photons with an energy lower than E_g in the layer are transferred to the next one.

Theoretically, the Shockley–Queisser limit can reach 90% (for solar cells with six layers), but practically it is around 60–70% (for solar cells with three–four layers). Moreover, the layers are connected in series, so the open-circuit voltage increases and the ohmic resistance remains unchanged, which leads to a higher fill factor [3, 4, 21, 67]. However, despite the advantages of multijunction SCs, their efficiency is not really close to the Shockley–Queisser limit due to two reasons [4]. First, the optical efficiency of such SCs is restricted, because low-frequency photons partially dissipate in the upper layers due to optical losses. Second, in the case of a series connection of cascades, their photocurrent maximum is determined by the least efficient cascade.

There are two main methods for manufacturing multijunction SCs: mechanical coupling of layers and monolithic fabrication — layer-by-layer growth using either molecular-beam epitaxy or chemical vapor deposition [3–5]. The latter method is known to be the better one, because it allows growing structures with fewer crystallographic defects and gives the opportunity to prepare SCs with a very large surface — solar panels. In order to fabricate such SCs, one most often uses semiconducting A_3B_5 compounds [68–70] and rarely A_2B_6 [67], organic materials [71], or even a dense grid of quantum dots [4]. The main criterion that defines the choice of compounds is the matching of crystallographic structures of adjacent layers. Even a weak (around 0.01%) crystallographic lattice mismatch between two layers can significantly lower the SC efficiency.

In the case of SCs with two photovoltaic layers, the most optimal structure is InGaP/GaAs, which has a maximal efficiency of 31% in earthly conditions without sunlight concentration, and 36% with 200 times concentration [68]. In the case of a three-layer structure, the efficiency of InGaP/GaAs/Ge-based SCs on Earth reaches 38% [69], and the SC efficiency for the five-layer structure AlGaInP/AlGaAs/GaInP/GaInAs/GaInNAs reaches 39% [70]. The amount of every chemical element in the layer can be varied in order to

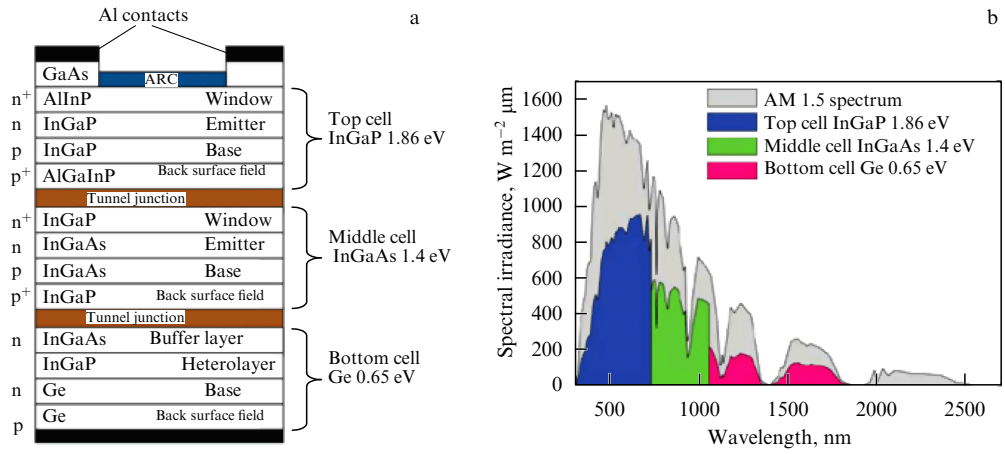

Figure 12. (Color online.) (a) Structure of a typical multijunction solar cell with three photovoltaic layers [70]. (b) Schematic illustration of different solar spectrum parts absorbed in this cell.

control the bandgap, and every layer can be doped by a large variety of elements (S, Se, Te, Sn, Si, C, Ge for n-type structures, and Zn, Be, Mg, Cd, Si, C, Ge for p-type structures). However, despite such a complicated structure, the cost of such solar cells is mostly defined by the cost of the basic element — germanium [5]. There have been several attempts to replace germanium with other materials (GaAs, InP, GaSb, Si, etc.) [69], which can lower the net cost of multijunction solar cells by approximately a factor of two. However, germanium is still the most suitable material for the bottom photovoltaic layer. In the case of three-junction solar cells, by using germanium one can achieve record high efficiencies — 45% [21] and even 46% with high light concentration [61].

The net cost of multijunction solar cells with three–four cascades is 20–50 times higher, and that of two-junction solar cells is one order of magnitude higher compared with the best first- and second-generation solar cells. As we have mentioned before, this restricts the application area of multijunction solar cells to a specific area of spacecraft. Note that multijunction solar cells can be used in space, because the parameters of the expensive materials included in their composition are highly stable under the action of solar illumination and wind, as well as cosmic gamma-rays [67–72].

Despite the fact that the idea of multijunction SCs appeared already at the end of 1950s (see, for example, classical review [72]), when the theory for such cells was not fully devised, their investigation and technological development were begun in the 1960s and were performed mainly inside technological companies or with their support. Therefore, almost all studies on this topic published during the last 40–50 years are experimental and, except for several reviews which were written by physicists (like Ref. [6]), are more related to the field of nanotechnologies than to semiconductor physics.

The leading companies in the field of research and production of commercial multijunction solar cells for spacecraft are the American companies SpectrolabBoeing and SolAero. Most such photovoltaic cells are equipped with additional optical elements, which increase their efficiency [10]. Such optical elements as flat structured lenses of the Fresnel type or parabolic mirrors can increase the amount of absorbed radiation and result in a relative efficiency increase of around 6–7% [10].

Concluding this section, it should be noted that fundamental investigations of multijunction solar cells can still make a contribution to the development of this research field. This can happen if one of the new scientific ideas can find practical realization, resulting either in a significant decrease in a solar cell cost or in an efficiency enhancement up to the theoretical limit. The cost might be decreased if a number of photovoltaic layers with different bandgap energies can be prepared based on the same material. Paper [73] considers a solar cell based on a gallium arsenide layer with a p–n–p–n doping structure and one order of magnitude difference between the doping levels of the top and bottom halves of the layer. Different doping levels obviously mean that optical absorption in two halves of the layer would be different. For high enough temperatures, the bandgap edges of photovoltaic material are smeared out due to the thermal radiation. Since different layer absorption implies the different thermal radiation spectra from two layers, the layer spectral response curves become different even at temperatures of around 200–300 °C and result in two significantly different effective values of E_g. As a result, such a SC theoretically turns out to be a two-junction solar cell [73] and allows the 30% Shockley–Queisser limit to be overcome. However, this idea has not been experimentally confirmed yet.

5.2 Solar cells with parallel spectrum splitting

As we have already mentioned in Section 1.1, such solar batteries are formed by a set of solar cells with each cell optimized for a specific spectral range. These cells are not stacked in a multilayer structure like multijunction SCs, but instead are situated in a common illuminated plane. Usually, a battery composed from such cells have common front and back contacts. Figure 13 shows a schematic diagram of a solar battery with three subcells, in which the spectrum is split into three bands by an aperiodic phase grating [74].

Phase gratings (grooves made in a transparent material) exhibit a much larger dispersion of the leading diffraction order than prisms and at the same time make it possible to avoid significant reflection losses, which are common for two- or one-dimensional gratings. For these purposes, the illuminated side is covered with a broadband antireflection coating. The ordinary transparent grooves usually have periodic spacing, and a general curvature, shown in Fig. 13, is introduced in order to achieve the focusing effect. Dispersion of periodic grooves with respect to frequency is nearly homogeneous in the visible spectrum and would correspond to a homogeneous distribution of focal spots for different colors along the surface of the solar battery (see Fig. 13). Such a regime is far from the optimal one and does not allow overcoming the Shockley–Queisser limit for each of three subcells. Therefore, the grooves in paper [74] have aperiodic spacing.

In almost all recently developed solar batteries with parallel splitting of the spectrum, transparent grooves are replaced with phase holograms (see, for example, Refs [75–80]). These structures can provide such a dispersion for the transmitted light whereat 80–90% of the energy accumulated in a specific spectral band is directed towards the corresponding solar cell, as demonstrated in Fig. 14.

Scattering losses in a hologram do not allow reaching an optical efficiency of 100%. To a greater extent it is concerned with the periodic grating where a part of the incident sunlight is reemitted towards higher diffraction orders. The researchers managed to achieve an optical efficiency of 90% for both

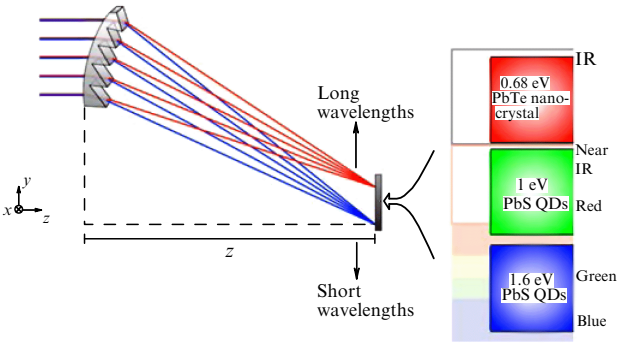

Figure 13. Solar battery made of three solar cells connected in parallel and illuminated by aperiodic phase grating (according to the description given in Ref. [74]. Authors suggest using structures based on quantum dots (QDs) as photoelectric cells (QDs in the form of lead sulfide nanocrystals with two different sizes have different bandgaps).

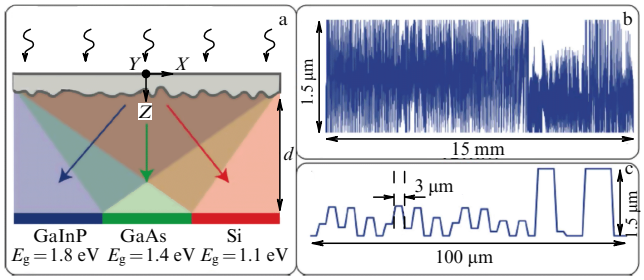

Figure 14. Solar battery composed of three first-generation solar cells connected in parallel. The spectrum is split using a flat phase hologram. (a) General setup. (b) Cross section of the hologram surface. (c) The same cross section on a larger horizontal scale. The distance $d = 1$ cm. Drawings are made as a compilation of graphical figures from paper [75].

optical systems [74, 75]. In the case of grooves from paper [74] (see Fig. 13), such high efficiency is achieved by choosing optimal deviations of thickness and tilt of every tooth from the mean values. Such aperiodic grating demonstrates many features of a hologram.

The main disadvantage of optical gratings and holograms is the dependence of their dispersion on the angle of the sunlight incidence. Therefore, they are designed for a normal incidence. The need for solar cell positioning and expensive optics, as we have mentioned before, limits the application of this solar photovoltaics outside the scientific laboratories. Space applications are not suitable for these solar cells either, because the 46% efficiency of multijunction SCs [21] is more important than the lower net cost of a solar cell with a 43% efficiency [22]. As for everyday applications, the cost of optics for solar cells with parallel spectrum splitting makes it impossible for these SCs to compete with commercial first- and second-generation solar cells. However, one should not forget that new technological solutions may lead to a significant price reduction for such optics.

6. Third-generation exciton type solar cells

6.1 General features of exciton solar cells

The operation principles of third-generation solar cells based on organic [81–94] and inorganic materials are different. As we have mentioned before (see Section 1.1), third-generation organic solar cells are photoelectrochemical in nature. The reason for that is mainly the fact that the energy carriers in organic solar cells are not the usual electrons and holes, but strongly coupled electron–hole pairs (excitons) and their binding energy is much higher in organic semiconductors than in inorganic ones.

There are two main types of excitons: Frenkel and Wannier–Mott [81]. Wannier–Mott excitons typically form in inorganic semiconductors, where effective Coulomb screening of charges weakens the bond between electron and hole in the exciton. Therefore, the binding energy turns out to be around 0.02 eV, which is less than the energy of thermal motion. This means that generated excitons quickly decay into free charges at room temperature.

If a photon is absorbed by an organic semiconductor or insulator, it usually produces a Frenkel exciton. Coulomb screening in these materials is weaker, so the exciton binding energy is one order of magnitude higher, reaching at least 0.1 eV [82]. Therefore, the Frenkel exciton dissociation is very weak at room temperature and can occur at the interface, for example, between a p-type medium, where holes are stabilized, and an n-type medium, where electrons are stabilized.

On the other hand, Frenkel excitons have a finite lifetime during which they recombine and release energy in the form of radiation or heat. Therefore, the excitons having no time to reach the interface within their lifetime do not participate in creating the photocurrent. The mean free path of Frenkel excitons in organic single crystals reaches 0.1–1 μm [81]; however, in amorphous organic semiconductors it is in the range from 2 to 30 nm [83]. Although light absorption is very high for the majority of organic materials (the absorption coefficient is of order 10^5 cm^{-1} or higher), for fully absorbing sunlight one needs a layer around 150–300 nm wide. In layers with such a thickness, most of photogenerated excitons recombine and do not reach the phase boundary.

The simplest solar cell based on organic materials consists of a thin layer of photovoltaic material placed between two electrodes, one of which is transparent to sunlight [81, 82]. In a more complicated construction, one uses a double layer instead of a single layer, the former consisting of donor and acceptor polymers [81, 84]. In both architecture variants, the excitons need to travel the distance which is much longer than their mean free path. Exciton recombination was the main reason for organic solar cell efficiency to be only a fraction of a percent [81, 94].

The first groundbreaking solution was suggested and patented in 1991 by M Grätzel and was published in the same year in paper [85]. He suggested an architecture which instantaneously lead to an efficiency of about 7% and was called the 'dye-sensitized solar cell' or the 'Grätzel cell' (GC). This cell is not a diode type photovoltaic converter, but a photoelectrochemical one. A GC consists of a thin layer of organic compound (dye), in which photons are absorbed and electrons are excited. This layer is distributed along a multiply connected boundary between two regions possessing the hole and electron conductivities (Fig. 15a).

Inorganic oxides, most often titan dioxide, are utilized as an n-type conductor, and the oxide must necessary have a large specific surface area in order to adsorb a sufficient amount of dye. This is achieved due to a mesoporous oxide structure. An electrolyte serves as a p-type material, which is usually an organic solution of a so-called redox couple, i.e., a donor molecule and its oxidized form. In Ref. [85], the authors used an electrolyte with ion pairs I^-/I_3^-. At present, there are a large number of redox couples, among which the most popular are complexes of transition metals with organic ligands [81]. An organic compound (dye) does not carry an electric current, so it does not contribute to the charge transport. However, this is not needed, because the exciton decays into an electron which is transferred to an inorganic oxide, an n-type material, and a hole which is transferred into an electrolyte, a p-type material.

In 1995, A Heeger patented another approach to creating photoelectrochemical solar cells — the so-called bulk heterojunction. The results of the first experimental investigation into bulk heterojunction solar cells (BHJSCs) were published in paper [86]. The main idea was to put p- and n-type materials together, not in layers that meet along a flat interface, but in an interpenetrative structure of nano-sized clusters (Fig. 15b). Such a structure can be realized using organic materials. The time that it takes for excitons generated inside one of the materials to get to the interface is

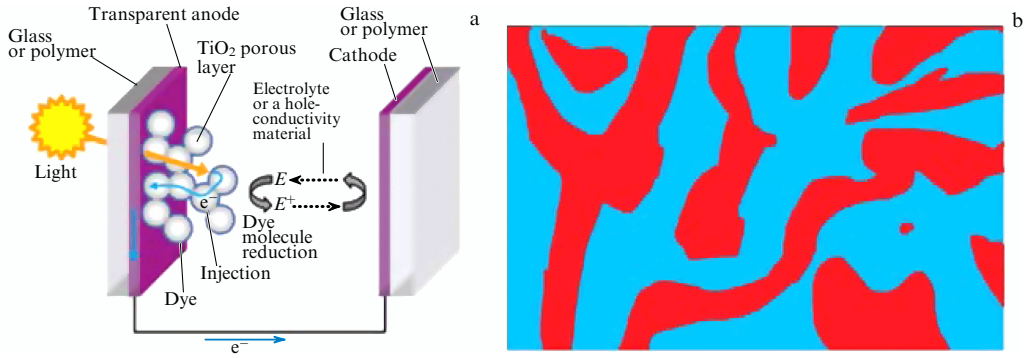

Figure 15. (Color online.) (a) Schematic of a Grätzel cell. Excitons, which are generated in a dye, dissociate and inject electrons into TiO_2, whereas holes are injected into the redox couple, which is then reduced at an anode covered with a catalytic agent. (b) Typical structure of a Heeger bulk heterojunction [86]. Different colors indicate acceptor and donor phases.

less than the exciton lifetime. Therefore, recombination losses significantly decrease [86].

Although BHJSCs could not reach the efficiency level of GCs for a long time, they were still of great interest, because this type of structure does not need a liquid electrolyte. This significantly simplifies and cheapens the solar cell fabrication, and increases the reliability and expectation of life. In the following Section 6.2, we will compare the architectures of the BHJSC and GC, analyze advantages and disadvantages of corresponding technologies, and discuss the competitiveness of exciton solar cells with respect to inorganic solar cells.

6.2 Basic operation principles of bulk heterojunction solar cells

BHJSCs consist of a bulk heterojunction placed between two electrodes (Fig. 16). The bulk heterojunction constitutes a mixture of donor and acceptor organic compounds, which form p- and n-type regions where excitons are photogenerated. Various conjugate polymers or oligomers are applied as donors, and fullerene derivatives modified in order to increase the miscibility with the donor component are usually utilized as acceptors. Fullerenes were first used in organic photovoltaics already in 1993 [88], and they became popular due to a number of unique properties, such as their exceptional ability to stabilize a negative charge, high electron mobility, and isotropic charge transport.

The material, which was used in the first work on BHJSCs, is still very popular. It is (6.6)-phenyl-C_{61}-butyric acid methyl ester, which is usually called $PC_{61}BM$ or just PCBM [83, 88]. A more effective and more expensive material — (6.6)-phenyl-C_{71}-butyric acid methyl ester ($PC_{71}BM$) — is often used in modern BHJSCs as well [89, 90]. Development is also underway of new fullerene derivatives [91]. However, fullerenes possess certain disadvantages: they have almost zero absorption in the visible range, they are hard to modify, and the modification has a weak influence on their electron levels. Therefore, there is currently a great need for search of nonfullerene acceptors. The record high efficiency of a solar cell with a nonfullerene acceptor now amounts to 6.8% [92], while a fullerene-derivative-based solar cell can have efficiencies up to 11% [91].

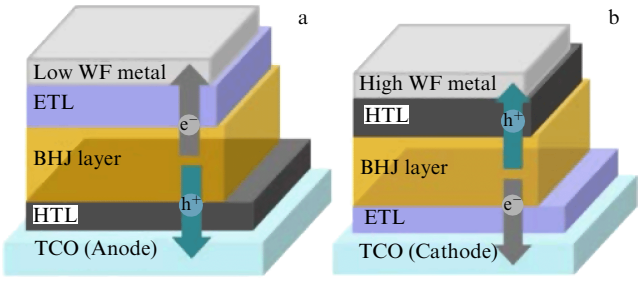

Figure 16. Schematic of conventional (a) and inverted (b) BHJSC architectures [96]: HTL — hole transporting layer, ETL — electron transporting layer, TCO — transparent conductive oxide (usually indium–titanium oxide, ITO), BHJ — bulk heterojunction, and WF — work function.

A bulk heterojunction is multiply connected and is almost symmetric with respect to the electrodes. Therefore, local static fields are directed randomly, which means that electrons and holes generated at p–n junctions can move towards both electrodes, colliding and recombining. One way to avoid high recombination losses reduces to connecting heterojunction and electrodes not directly, but through thin (3–20 nm) transport layers, which transmit charges of one type and do not transmit the other one.

The p-type layer is frequently made from an organic semiconductor consisting of a mixture of sodium salt of sulfonated polystyrene and poly-3.4-ethylenedioxythiophene, known as PEDOT-PSS, or one may at times use metal oxides (MoO_3, WO_3, V_2O_5), while an n-type layer can be formed from ZnO, TiO_x, Nb_2O_5, or LiF [93, 94]. Transport layers have different influences on the efficiencies of solar cells: it depends on the mutual adhesion of the layers, different energy level diagrams, the differences in surface energies and surface recombination [93, 94]. Notice that review [94] is focused on chemistry and mainly considers organic and hybrid solar cells with bulk and planar heterojunctions.

BHJSCs can have two types of geometry: conventional and inverted (see Fig. 16). In the conventional geometry, the p-type layer is placed between the bulk heterojunction and transparent ITO anode, while the n-type layer is placed between the bulk heterojunction and cathode made from metal with a low work function (Al, Ca) in order to avoid energy losses. In the inverted geometry, the n-type layer is located near the transparent electrode now playing the role of a cathode, and the p-type layer is next to the opaque anode which is made of silver, a metal with a large work function [95]. By replacing the usually used aluminum and calcium

with silver, solar cell stability under the action of oxygen and moisture is also improved [95].

Further, we will discuss in detail the factors influencing the stability of BHJSCs, but now we will only give one example, which demonstrates the difference between the conventional and inverted geometries. Paper [97] compares the degradation rates for unencapsulated BHJSCs with conventional and inverted geometries. A solar cell with the conventional geometry completely degraded after 5 days, while the inverted geometry lost only 20% of its initial efficiency after 40 days.

It should be noted that physically the PCBM layer (or P3HT, poly(3-hexylthiophene)) is adjacent to both transport layers, but the transitions of electrons to PEDOT-PSS and, correspondingly, holes to LiF or ZnO are energetically unfavorable. We will also note that after the transition to a more favorable energy level, the charge carrier loses energy. So, after the transition from PCBM to Al, the electron loses 0.4 eV, and if one replaces the aluminum cathode in the conventional geometry with the silver one, the losses will heighten to 1.3 eV. This is why the metals with a low work function are used in the conventional geometry. Such materials are strong reducing agents, but they undergo oxidation in air. Generally, devices with an inverted geometry have almost the same efficiency as those with a conventional geometry. For example, paper [98] reported an efficiency of 9.5% reached for the solar cell with inverted geometry. Taking into account the low costs of initial organic materials for these SCs and of their production, this is a very good result.

One of the main disadvantages of BHJSCs is the short lifetime, which lowers the industrial interest in these solar cells. A generally accepted method for the elimination of this disadvantage is encapsulation, which allows protecting the solar cell from the action of reactive gases in air, moisture, ultraviolet (UV) radiation, and mechanical damage. In doing so, the encapsulating material should be inactive, highly transparent, and mechanically strong. The best results are achieved when encapsulating with optical glass and epoxy [89]. However, optical glass is quite expensive, heavy, and inflexible and can hardly be integrated into the solar cell production technology. In order to produce thin-film BHJSCs on an industrial scale, we need to develop new encapsulation technologies, which would allow low-cost (nonvacuum and not needing an inert gas atmosphere) and efficient protection of the BHJSC from degradation. Currently, there are a number of encapsulating materials (organic, inorganic, and hybrid) which can be used for these purposes. More detailed information on thin-film encapsulation methods can be found in review [99].

A great number of recently published papers investigate the operation of BHJSCs with the conventional geometry. However, the application prospects are clearly higher for BHJSCs with the inverted geometry, because these structures are much more stable under ambient conditions [93].

6.3 Charge transport properties in bulk heterojunction solar cells

The presence of a bulk heterojunction lowers exciton recombination losses, because the excitons travel relatively small distances, but, at the same time, the complicated morphology of such heterojunctions increases the already high resistivity of organic semiconductors (it also slightly increases the recombination rate of free charge carriers). Precisely the ohmic resistance is one of the main factors which limits the efficiency of BHJSCs. Particularly, it does not allow increasing the thickness of the bulk heterojunction layer to the point where optical radiation would be fully absorbed in it. Therefore, one should either accept the low value of BHJSC efficiency or invoke highly effective and expensive light-trapping structures.

Since fullerenes and other organic acceptors have a small absorption in the visible spectral range, in most bulk heterojunctions almost all excitons are generated in the donor layer. According to selection rules, the generated excitons have zero spin and are called singlet ones. Their lifetime in organic semiconductors lasts approximately 1 ns, after which they radiatively recombine, causing photoluminescence [83]. Under specific conditions, excitons can make a transition from the singlet state to the triplet state with spin 1. Radiative recombination of triplet excitons is spin-forbidden, so their lifetime is several orders of magnitude higher than that for singlet excitons [83]. There are approaches which take advantage of singlet–triplet transitions in order to improve the exciton lifetime. For example, one can introduce fluorescent platinum complexes in the semiconductor [100].

As the exciton approaches the phase boundary, it interacts with it and forms a so-called exciplex [83]. The exciplex constitutes an electron–hole pair that has a lower potential energy than the exciton (Fig. 17). Under certain conditions, the possibility appears to directly detect the exciplex excitation. For example, the authors of paper [87] managed to extend the absorption range by 200 nm towards longer wavelengths by forming a wrinkled structure. The well-known theoretical explanation of this effect is based on the fact that such a structure allows activating direct exciplex excitation [101].

At the next stage, the exciplex transfers an electron to the molecule of the acceptor material. This process takes about 20–30 fs [83]. The hole stays in the donor material and is picked up by an electronegative molecule. The resulting complex with a charge transfer is called a polaron pair. Although the former electron and hole reside in different phases, they still experience Coulomb attraction. At the expense of kinetic energy or (less likely) the action of the local static field, the polaron pair can overcome this attraction and dissociate into polarons — quasiparticles which describe the moving charge with due regard for medium disturbance. This disturbance is significantly stronger in an amorphous organic semiconductor than in a solid-state inorganic semiconductor possessing a crystal nature. Polaron pair separation efficiency depends mainly on the difference between the potential energies of the exciton and polaron pair. This difference equals the kinetic energy of coupled polarons, which allows overcoming the Coulomb interaction [83]. Since the polaron motion and the direction of the local electric field are stochastic, the polaron pair can recombine. This process is called the geminate recombination.

The exciton potential energy approximately equals the difference between the lowest unoccupied molecular orbital (LUMO) and the highest occupied molecular orbital (HOMO) in the medium where the exciton is generated — that is, the donor material. The polaron pair potential energy equals the difference between the acceptor LUMO and donor HOMO. Thus, when an exciton is transformed into a polaron pair, an excessive energy equal to the difference between the donor LUMO and acceptor LUMO is released. The higher the donor LUMO, the higher the polaron kinetic energy and, correspondingly, the larger the contribution of dissociated

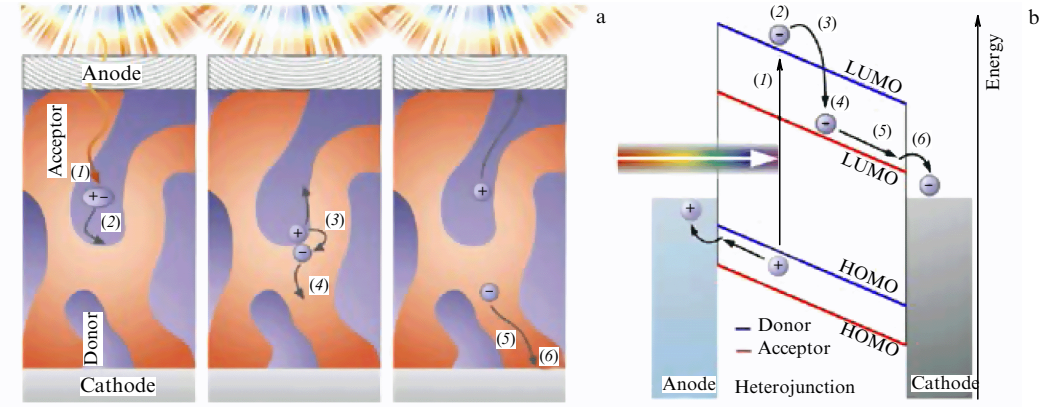

Figure 17. (Color online.) Illustration of light absorption and charge transport in BHJSCs [83]. (a) Schematic of the process kinetics. (b) Simplified energy level diagram. Here (*1*) — generation of a singlet exciton after photon absorption in the donor material; (*2*) — exciton diffusion towards the acceptor surface, where exciplex is formed; (*3*) — potential energy decrease, which corresponds to exciplex formation and electron transfer to the acceptor molecule; (*4*) — creation of a polaron pair with an excessive kinetic energy; (*5*) — polaron pair separation, i.e., free polaron generation, and (*6*) — jump charge transport towards the electrodes and charge extraction. At stages (*2–4*) losses take place through geminate recombination; at stages (*5*, *6*) they take place through nongeminate recombination. HOMO, LUMO — highest occupied and lowest unoccupied molecular orbitals.

polaron pairs to the photocurrent. On the other hand, for a fixed donor bandgap, a higher LUMO corresponds to a higher HOMO and lower open-circuit voltage (V_{oc}), which can be roughly estimated as the acceptor LUMO minus the donor HOMO. Therefore, when choosing the energy gap between donor and acceptor molecular orbitals, one should find the optimal value at which current and voltage are balanced.

Due to nonzero voltage between the electrodes, the average action of the electric field in a heterojunction supports the motion of dissociated positive and negative polarons towards the corresponding electrodes. During this motion, they cross the phase boundaries, where they can interact with molecules carrying the opposite charge and unite into new polaron pairs, which may then recombine [83]. Such a recombination is called nongeminate.

The process of charge transport is quite slow in organic semiconductors; it has a jump character and is realized mainly through tunneling and thermal activation. Moreover, charge carriers with an energy lower than a certain threshold, called transport energy, do not take part in charge transport and should be considered bound charges. Under these conditions, there are two mechanisms of nongeminate recombination: bimolecular recombination between free carriers, and band tail recombination. In the latter case, charge carriers with low energy act as electrostatic traps. So far, there has been no common opinion about the relative role of these mechanisms in BHJSCs [83, 102]. It should only be noted that nongeminate recombination enhances as the solar cell thickness decreases, because charges recombine precisely at the interfaces, while the geminate recombination, on the contrary, weakens, because excitons are more likely to reach the phase boundary.

6.4 Main development strategies for bulk heterojunction solar cells

Owing to the reasons mentioned in Section 6.3, control over the heterojunction morphology in BHJSCs comprises one of the main ways to improve the performance of such cells. In a solar cell with a sufficiently high efficiency, clusters of one phase have a size from approximately ten to a few tens of nanometers [91, 94]. Besides the combination of donor and acceptor components, the morphology is strongly influenced by annealing, solvents and additives [103–106].

In polymer–fullerene systems, the additives can heighten the efficiency by approximately one and a half times due to better exciton transport, a recombination loss decrease, and the possibility of optimizing the sizes of single-phase clusters, which are influenced by the additives. Annealing helps to improve the purity of phases in clusters, which also leads to a decrease in the recombination losses. However, heating needs additional time and energy expenditures; therefore, it is an important challenge to find a polymer–fullerene mixture which would not need annealing [94]. This research has attained some success: a solar cell possessing 8% efficiency was fabricated without annealing and even without additives [106].

Much attention has been lately paid to the development of transparent electrodes, an alternative to ITO which is highly transparent and has low resistivity, but is also quite expensive, because it contains indium and is only moderately technological. As an alternative in the literature, aluminum zinc oxide (AZO), fluorine-doped tin oxide (FTO), electrodes formed by silver nanowire arrays, graphene sheets, conducting polymers (for example, PEDOT-PSS), carbon nanotubes, etc. have been considered. This field of research has demonstrated significant progress [107, 108].

It should be noted that transparent fragile oxides are not suitable for flexible thin-film solar cells. So far, the best candidates comprise composite Ag-PEDOT-PSS electrodes, which demonstrate quite high transparency and can be imprinted by silver ink using methods compatible with roll-to-roll technologies [108].

6.5 Grätzel cells

The relatively high resistivity of amorphous organic semiconductors and the complicated morphology of the bulk heterojunction make conductivity the main factor that restricts BHJSC efficiency. Grätzel cell development has the goal to use high spectral response of organic photovoltaic materials and avoid high resistivity. Since the operation principle of GCs was already explained in Section 6.1, we

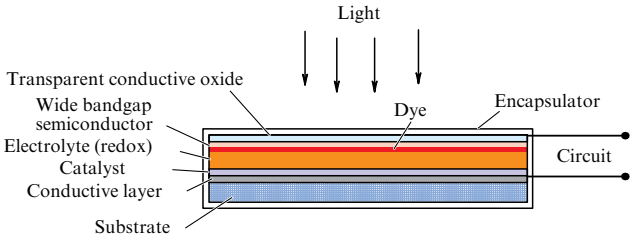

Figure 18. General setup of a Grätzel cell (according to the description given in paper [110]).

will discuss below the GC operation in more detail in order to understand the advantages and disadvantages of these devices.

Typical GC consists of a porous wide bandgap semiconductor (TiO_2, ZnO, or SnO_2) covered with a dye monolayer (ruthenium complexes, for example, N719, rhodamine, or riboflavin) and submerged in a solution of electrolyte with redox couples (usually, I^-/I_3^-). The whole system is confined between two electrodes, at least one of which should be optically transparent, while the other one can be metallic (Fig. 18). A GC schematic, shown in Fig. 18, is geometrically simplified. Actually, as is clearly seen in Fig. 15, there is no planar layering in the structure wide bandgap semiconductor–dye–electrolyte–catalyst. In order to accelerate the redox-couple regeneration process, the second electrode is covered with a catalytic agent, usually a submicrometer platinum layer.

Electron injection into TiO_2 is a very fast process, which takes about 20–50 fs [109]. Such high injection efficiency needs an overvoltage of approximately 100–150 mV, which is created by the energy difference between dye LUMO and lowest level of the TiO_2 conduction band. On their way to the anode, photoelectrons take part in the reduction of oxidized molecules of dye or electrolyte, which diffused into the titanium dioxide. This process prevents the recombination of transported negative charges: electrons become bound.

Using the I^-/I_3^- pair, one can most sufficiently suppress the recombination and achieve a significant electron lifetime [110]. Efficiency of this redox couple is, on the one hand, associated with the small size and large mobility of the iodide and triiodide ions and, on the other hand, is caused by very high overvoltage (around 600 mV), which provides fast dye reduction, but significantly lowers the output voltage. Another disadvantage of the I^-/I_3^- redox pair concerns its chemical activity, especially corrosive activity with respect to metals. This complicates encapsulation and lowers the GC lifetime due to the formation of defects in the shell and electrolyte outflow.

The most popular alternative to I^-/I_3^- is cobalt complexes (Co^{2+}/Co^{3+}), which together with porphyrin dyes allow achieving high open-circuit voltages and, consequently, higher energy conversion efficiency. Paper [111] reports a record efficiency of 13%, which is a unique result for exciton solar cells. The main problem with using cobalt complexes is their tendency to recombine with electrons from TiO_2. This process decreases the GC lifetime. Researchers try to solve this problem by introducing bulky ligands, which prevent electron capture, but the presence of such ligands deteriorates diffusion [110].

At the same time, both I^-/I_3^- and Co^{2+}/Co^{3+} can be used as organic solutions. The need to protect a solvent from evaporation and outflow causes significant problems, and the process of even filling the solar cells with electrolyte is difficult to scale [112]. Therefore, for the development of GCs one needs to replace the liquid electrolyte with no less effective solid or quasisolid electrolytes. The latter ones at room temperature include so-called ion liquids. They are distinguished by high chemical and thermal stability and good ion conductivity, but also high viscosity, which slows down ion transport [112, 113]. Gelatinizing agents (both organic and inorganic) can also be applied [113]. Gelatinizing agents stabilize the system, but do not prevent solvent outflow. Moreover, if the gelatinization proceeds with the aid of inorganic nanoparticles, the gel system can separate into layers of organic and inorganic phases [113].

In order to overcome these disadvantages, there have been many attempts to invoke polymer systems, which can be divided into three types (see, for example, Ref. [113]).

(1) Polymer electrolytes — ionic conductors that are obtained by dissolving salts and plasticizers in a polymer with high molecular mass.

(2) Polyelectrolytes — polymers with chains that contain cationic or anionic groups with mobile counterions solvated by a polar solvent.

(3) Gel-polymer electrolytes, where conductivity is provided by a salt solution, and the polymer plays the role of a gelatinizing agent forming a three-dimensional grid where ions can move freely.

Currently, taking advantage of polymer electrolytes led to a solar energy conversion efficiency of 8–10% and a quite high stability (efficiency loss of 1–10% after 700–1000 h of continuous illumination, depending on the system) [113]. Charge transport is still a problematic stage in these systems. Polymer electrolytes cannot compete with liquid ones in this parameter, so solid-state GCs have a lower efficiency than conventional GCs. However, polymer electrolytes have great development potential, because polymers can be easily integrated into the technological process.

Finally, there are GCs that do not employ the ionic conductivity. Their electrolyte is replaced with a p-type layer, as in BHJSCs. Currently, the most efficient p-type material that is used in GCs is abbreviated as spiro-OMeTAD. Chemically, it is 2,20,7,70-tetrakis (N,N0-di-p-methoxyphenylamine)-9,90-spirobifluorene. The highest efficiency, achieved using spiro-OMeTAD doped with a cobalt complex is 7.2% [114]. There are also projects on the creation of fully-printed GCs with spiro-OMeTAD, although the efficiency of these SCs is still much lower (1.7%) [115].

GCs with liquid electrolyte are more effective, but the presence of this material is their main disadvantage. First, all components of GCs except the liquid electrolyte can be formed using roll-to-roll technology [112], which is optimal for mass-production of thin-film solar cells. Production of solid-state GCs using roll-to-roll technology can become profitable starting from lower efficiency levels. Secondly, liquid electrolyte, unlike the solid one, can leak out through microcracks in encapsulating shell, which inevitably form with time due to the corrosive action of the electrolyte. Therefore, we consider solid-state GCs to be the most promising solar cells in the framework of this research line [112].

Regarding the lifetime of GCs, historically they were always in a favorable position with respect to BHJSCs. Already in the first work on GCs it was noted that after two months of continuous illumination the efficiency of the

photovoltaic module lowered by only 10% [85] (the efficiency of an unencapsulated BHJSC becomes almost zero after this time). Currently, however, this advantage of GCs over BHJSs does not seem so obvious. Generally, in order to compete with other solar cells, Grätzel cell production technologies should be further optimized.

6.6 General prospects of exciton solar cells

In order to become a commercial product, exciton solar cells need to successfully compete with, on the one hand, crystalline silicon solar cells (90% of the market) and, on the other hand, thin-film inorganic solar cells (10% of the market). Currently, exciton solar cell efficiencies are much lower than that of these other ones [116].

Efficiency is, of course, an important parameter, but one cannot judge the competitiveness leaning upon only this parameter. Kilowatt-hour cost mostly correlates with the EPBT (energy payback time) parameter — that is, the time for energy expense reimbursement. The EPBT parameter depends on the illuminance; therefore, for a comparison, we put to use data for the solar illuminance on Earth's surface of 1700 kW·h m^{-2} per year, which corresponds to countries in southern Europe. Asia, Africa, Australia, the USA, and Central and South America are, on average, illuminated more intensively. By this parameter, BHJSCs have a significant advantage over other solar cells [116]. By analyzing the life cycle [116], it was shown that already existing BHJSCs have an EPBT parameter of 90 days with an efficiency of only 3%.

Further optimization may decrease the EPBT to 17 days for a 3% efficiency, and technological improvements (including recycling and improving the lifetime) can result in an EPBT of 7 days for a 3% efficiency, and one day for a 15% efficiency. Other estimates give slightly higher EPBTs for organic solar cells (100–190 days) [117]. For comparison, the EPBT of a CdTe solar cell (the EPBT record holder among inorganic solar cells) turns out to be of order 250–750 days [117]. GCs with a rather optimistic assumption of a 20-year lifetime have an EPBT of approximately one year [118]. The EPBT is longer than a year for solar cells based on perovskites (see Section 7), obtained by chemical vapor deposition, if it is assumed that their lifetime is 15 years and efficiency is 15.4% [119].

In the literature, one can find estimates of the electricity costs for BHJSCs (see, for example, Ref. [120]), which lead to a conclusion that the dependence of electricity costs on the efficiency and lifetime is described by a curve with saturation; so, for an efficiency of 10% and 10-year lifetime, the price becomes almost minimal and reaches a plateau. For an efficiency of 3% and 3-year lifetime, organic photovoltaics will be able to compete with silicon ones; for an efficiency of 5% and 5-year lifetime — with coal, and for an efficiency of 10% and 5–10-year lifetime — with atomic energy.

Let us now discuss the prospects of BHJSCs in comparison with GCs. Currently, the main factors that cause BHJSC degradation are known: UV radiation, oxygen, and humidity, as well as bad adhesion of dye and electrolyte to the semiconductor [116]. By synthesizing new photovoltaic materials, optimizing the solar cell architecture, and, most importantly, optimizing the encapsulation [99] (let us recall that encapsulation eliminates the first three reasons for BHJSC degradation), over two decades the researchers managed to increase the BHJSC lifetime from several hours to 6–8 years [89]. Note that the lifetime is defined as the number of years after which the solar cell loses 20% of its efficiency [89]. In order to measure the lifetime, accelerated testing is performed under continuous illumination from a normal (nonconcentrated) sunlight simulator. The number of hours of continuous operation after which solar cell loses 20% of its efficiency are recalculated into real hours of sunlight illumination per given number of years. In doing so, the sunlight standard on the surface of Earth (AM1.5, Fig. 1b) assumes that the solar cell is located at a latitude of approximately 50°.

Some researchers believe that GCs can operate longer than 6–8 years, specifically 20 years, because this is the time after which the dye fades under illumination with normal sunlight [122–124]. However, when comparing GCs to BHJSCs, one should take into account such GC drawbacks as the possibility of solvent evaporation and outflow with the formation of microcracks in the shell, and, in the case of quasisolid polymer electrolytes, instability of the electrolyte itself. As an example, consider the work performed by Grätzel and co-workers [111], where GCs with a record-high efficiency of 13% lost 20% of their efficiency after 500 hours of continuous illumination due to the instability of the spiro-OMeTAD polymer electrolyte. By comparing this result with the best BHJSCs, where the efficiency decreased by only 11% after 2000 hours of continuous illumination [89], it can clearly be seen that the stability problem is urgent both for GCs and BHJSCs. In this situation, the solar cell cost comes to the forefront.

BHJSCs are very cheap due to the low cost of the basic components. An analysis of the BHJSC life cycle has shown that the most expensive part of the solar cell is the transparent ITO electrode (87% of the cost), and the next most expensive part appertains to the PET barrier film (polyethyleneterephthalate, 7% of the cost) [122]. By replacing the ITO electrode with a silver nanowire array electrode, one can achieve a multifold decrease in the BHJSC cost, get rid of the most fragile component in the solar cell structure, and make organic photovoltaics independent of the rare element indium [117, 122].

Another equally important factor is the possibility of recycling solution components, which, in turn, opens up possibilities of applying various casting and printing technologies that are compatible with continuous and easily scalable fabrication using roll-to-roll technology [122]. In order to take this advantage, one needs to simplify all fabrication stages as much as possible by excluding vacuum and inert gases and lowering the recycling temperature to the lowest possible values. For example, paper [123] describes an imprinting of a 14-layer tandem solar cell with a width of 305 mm, which was performed under normal atmospheric conditions with heating that did not exceed 140 °C and with a speed of approximately 1 m min^{-1}. Although the efficiency measured for the surface area of 52.2 cm^2 was only 1.6%, one should keep in mind that this result is only one of the first steps in the work on scaling and commercial implementation of the product.

The last BHJSC advantage which should be noted is the fact that organic semiconductors are ideal materials for flexible thin-film photovoltaics. This significantly broadens the spectrum of solar cell applications. An interesting example is solar cell integration in clothes [124].

Based on the above discussion, we can conclude that exciton solar cells can reach the stage of commercial fabrication thanks to the following advantageous features.

(1) Low-cost components. Porous titanium dioxide and organic dyes in GCs, and donor and acceptor organic semiconductors in BHJSCs, are much cheaper than purified inorganic semiconductors. Moreover, exciton solar cells refer to thin-film cells, for which the consumption of raw materials is very low.

(2) Easily scalable technology; BHJSCs and GCs can be fabricated using roll-to-roll technology.

(3) GC and BHJSC production can proceed without using rare chemical elements. This not only makes such devices cheaper, but also stabilizes their cost. However, GCs consume platinum or ruthenium, but it is possible to find alternatives to these rare elements [121, 122].

Summing up, exciton solar cells are likely to become one of the main elements of photovoltaic technologies, despite their relatively low efficiency and lifetime with respect to solar cells based on inorganic compounds (25 years). In order to achieve this, their cost must be further decreased, while maintaining the efficiency already achieved. This needs careful selection of components and recycling technologies, which would be cheap enough to provide a low cost of EPBT and at the same time would increase the efficiency and lifetime of solar cells. For BHJSCs, this goal can be achieved by finding new encapsulation methods, which would make their lifetime longer than the current 6–8 years, and by developing cheaper, but no less effective, electrodes that do not need annealing of polymer compositions. For GCs, this goal can most likely be achieved by switching to stable solid-state electrolytes, which open possibilities of scaling and developing new dyes and materials for the bottom electrode that would not need such expensive catalytic agents as platinum or ruthenium.

However, it should be noted that many years of research on BHJSC and GC efficiency enhancement have not produced the desired results. The most successful improvement was made by structuring the semiconductors in GCs, but the cost of the solar cell increased in parallel with the enhancement of its efficiency [121]. Replacing dye in GCs with quantum dots led in several cases to an efficiency increase, but this increase is insignificant and is followed by a large rise in cost during the fabrication (see, for example, Ref. [94] and the Conclusions in this review). Replacing organic electrolytes with inorganic ones lowered the cost, but also reduced the GC efficiency. BHJSC efficiency is also still below the level comparable with modern commercial photovoltaics. Accepting the existing efficiency values and concentrating on a further price reduction for commercial companies can result in expensive research without a guarantied return on investments. Therefore, conventional GCs and BHJSCs do not currently interest the investors, unlike perovskite-based solar cells, which have lately become very popular. Newly developed solar cells based on perovskites are almost two times more efficient than GCs and BHJSCs. These new solar cells are discussed in the next section.

7. Solar cells based on metal-organic materials

In this section we are going to discuss some advantages and drawbacks of new solar photovoltaic trend — conversion of sunlight into electricity using metal-organic structures. This class contains, first, polycrystalline substances called metal-organic perovskites (MOPs), and, second, so-called coordination polymers — metal-organic frameworks (MOFs). We demonstrate below historical retrospective of this field, evolution of the architecture of the MOP-based solar cells and consider development prospects of solar cells based on MOFs.

7.1 Metal-organic perovskite in Grätzel cells

Naturally occurring perovskite ($CaTiO_3$) is a rather rare mineral found in the Urals in the 19th century, and it feels like a sort of dry clay. The mineral consists of microscopic cubic crystals. The slightly distorted cubic crystal of natural perovskite is formed by titanium atoms in the lattice points, and by calcium atoms occupying the pseudocubic center. Oxygen atoms enframe titanium atoms with an almost ideal slightly turned and pitched octahedrons. Among well-known compounds possessing the crystal structure analogous to that of $CaTiO_3$ halides (synthetic perovskites). They are formed, for example, by impregnation of some porous materials with a metal-organic precursor — a solution of a heavy metal halide (for example, $PbCl_2$ or $PbBr_2$) mixed with organic halide (CH_6ClN, CH_6IN, or CH_6BrN). The presence of a halide ion (F^-, Cl^-, Br^-, I^-) in the solution has crucial importance for the formation of perovskite [125].

As was found recently in experiment, halides with the crystal structure of natural perovskite promote remarkably high conversion of sunlight into photocurrent. The estimated energy conversion efficiency of perovskite solar cells amounts to 25%, the same as of the best first-generation solar cells, and this level will be achieved in the nearest future [125]. The SCOPUS database includes more than 650 articles with the keyword 'perovskite solar cell' published in the period from 2009 till the present, and their number is growing exponentially. No fewer than 50% of these papers were published in journals with an Impact factor higher than 5. What has drawn researchers attention so much to this material?

Halides structurally analogous to natural perovskites were first used in Ref. [126] as sunlight catchers in Grätzel cells undergoing modification with the aim to enhance efficiency. In this work, the Kojima group classified metal-organic perovskite as a new type of pigment. However, after the measurement of the MOP optical absorptivity, which occasionally surpassed that for organic dyes (by 2 orders of magnitude in the visible and near-UV ranges), solar cells based on MOPs became a self-standing pillar of solar photovoltaics [125, 127–142].

7.2 Crystal features and bandgap structure of metal-organic perovskites

Figure 19a shows the crystal structure of MOPs with the general formula ABX_3. European tradition defines A and B elements as cations, and X as an anion, whereas the Russian school denotes BX cluster as an anion, and element A as a cation. Organic compounds like methylammonium (MA) ($CH_3NH_3^+$), formamidinium (FA) ($NH_2CH=NH_2^+$), and guanidinium ($(NH_2)_3C^+$) with ionic radii from 0.18 to 0.23 nm play the role of A cation in metal-organic perovskites. Some heavy metal ions like Pb, Ge, Eu, Cu, or Sn with ionic radii in the range of 0.07–0.12 nm can appear as a smaller cation B (in European notion). Ions of I, Br, Cl, and F with ionic radii from 0.13 to 0.22 nm are used in the anion X position. Figure 19b shows the energy level diagram of MOP electronic states.

Because of the wide range of cation and anion sizes, the MOP crystal structure can be cubic, orthorhombic, tetragonal, etc. However, the same crystal often possesses several

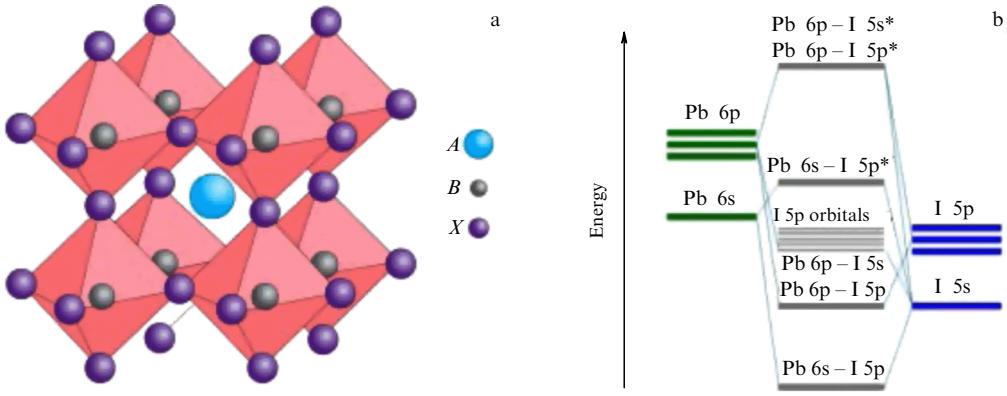

Figure 19. (a) Crystal structure of synthetic perovskites with metal-organic cations (*A*, *B*) and anions (*X*). (b) Electron energy levels in $CH_3NH_3PbI_3$ metal-organic perovskite, formed by energy levels of the anion–cation $[PbI_6]_4$ cluster (based on reviews [129, 130]).

structural modifications (which is the main drawback of this material as the basic element of solar cells); a second-order phase transition at elevated temperatures (usually $T > 60\,^{\circ}C$) occurs due to low lattice energy [127]. Among other things, MOPs can coordinate in different planes, including 3D-, 2D-, 1D-, and 0D-structures [128]. In particular, this feature induced research on the influence of the spatial restriction on the physical properties of layered inorganic perovskites in the late 1990s: exciton emission, high mobility of charges, nonlinear optics with ultrafast response, and even polariton emission [128].

MOPs are interesting not only because of exhibiting the photoelectric effect. Another advantage is their high optical absorption, which allows MOP-based thin-film solar cells to absorb most of the sunlight without using light-trapping structures [125]. The absorbance coefficient reaches a value of around 10^6 cm^{-1} for certain MOPs in the near-UV range, which corresponds to a 10-nm penetration depth at the 300-nm wavelength [129, 130]. The crystal bandgap structure is responsible for this. Inorganic BX_3 clusters make the main contribution to the band gap formation, whereas organic cation *A* stays out of the game. In particular, in the most popular $CH_3NH_3PbI_3$ perovskite, Pb 6s–I 5p σ-bonds form the valence band, while Pb 6p–I 5p π-bonds and Pb 6p–I 5s σ-bonds form the conduction band (Fig. 19b) [131, 132]. Density functional theory calculations and experimental results for the absorbance coefficient indicate the occurrence of direct interband electron transitions [133, 134]. Taking into account spin–orbital interactions lowers the effective bandgap energy [134].

The value of the MOP static permittivity and its dispersion in the frequency range lower than 1 kHz support the ionic crystal structure and low energy of the lattice [135–137]. As a result, the integral MOP absorbance coefficient in the sunlight spectrum turns out to be comparable with that in the doped multicomponent semiconductors, for example, CdTe, which is unique for the exciton solar cell.

The capabilities of contemporary chemistry allow perovskites to be synthesized at room temperature by just combining different cations and anions. This simplicity induced extensive research of the bandgap energy of different MOPs in order to find the optimal one for a solar cell. Energy levels and optical transition schemes of chemically different MOPs were examined by photoelectron spectroscopy. The MOP bandgap energy can vary from 3.1 to 1.1 eV, which is the most favorable for solar photovoltaics, especially for parallel split-spectrum multijunction cells. As was mentioned before, an increase in cation *A* size does not affect the bandgap energy but cation *B* causes an essential increase in the bandgap width (from 1.4 to 2.2 eV) due to the crystal structure change according to Goldschmidt's rules. Thus, the variation of the inorganic part of MOPs makes the biggest contribution to the bandgap energy variation: up to 0.4 eV by combining Pb and Sn cations in one and the same crystal, and up to 1.6 eV by combining anions.

7.3 Evolution of MOP-based solar cell architecture

The evolution of the MOP-based solar cell architecture (Fig. 20) reflects the contest between technologists and researchers to increase the efficiency and duration of cheap exciton solar cells, whose commercial cost was estimated as much lower than others from the beginning [129, 130, 139–141]. Let us consider every step shown in Fig. 20a–g in detail.

Research interest in organic–inorganic crystalline materials such as MOPs began to rise in 2009 after the publication by Kojima et al. [126] devoted to the Grätzel liquid photoelectrochemical cell containing MOPs as a pigment, in which a 3.8% efficiency was declared. Despite the fact that the authors of paper [126] proposed a solar cell with a similar structure in 2006 (Fig. 20a), its main drawback remained as before: the liquid polar hole-conductive electrolyte dissolved MOP ionic crystals in several minutes. In 2011, Im et al. [142] made an important step in MOP modification. A new technological approach — pre-treatment of porous titanium dioxide with liquid $Pb(NO_3)_2$ prior to the precursor (halide of organic ligand) deposition on it — yielded a photoelectrochemical solar cell with nano-sized MOP crystals that was analogous to the previous one but whose efficiency climbed to 6.5%. Nevertheless, the problem of perovskite ionic crystal dissolving in the liquid polar electrolyte remained.

One year later, in 2012, the efficiency value of the Grätzel cell pushed the limits. The Grätzel and Park groups used a submicron layer (0.6 μm) of a porous semiconductor for impregnation of a photoelectric layer (dye), and a spiro-MeOTAD solid-state organic polymer as an electrolyte (Fig. 20b). The collaboration resulted in an efficiency of 9.7% and the cell stability during 500 h of continuous performance [143].

Again in 2012, a group led by H J Snaith reported an efficiency of 11% for a Grätzel cell with a nonliquid electrolyte [144]. The main difference here was the application of a new and more stable MOP ($CH_3NH_3PbI_{3-x}Cl_x$). A

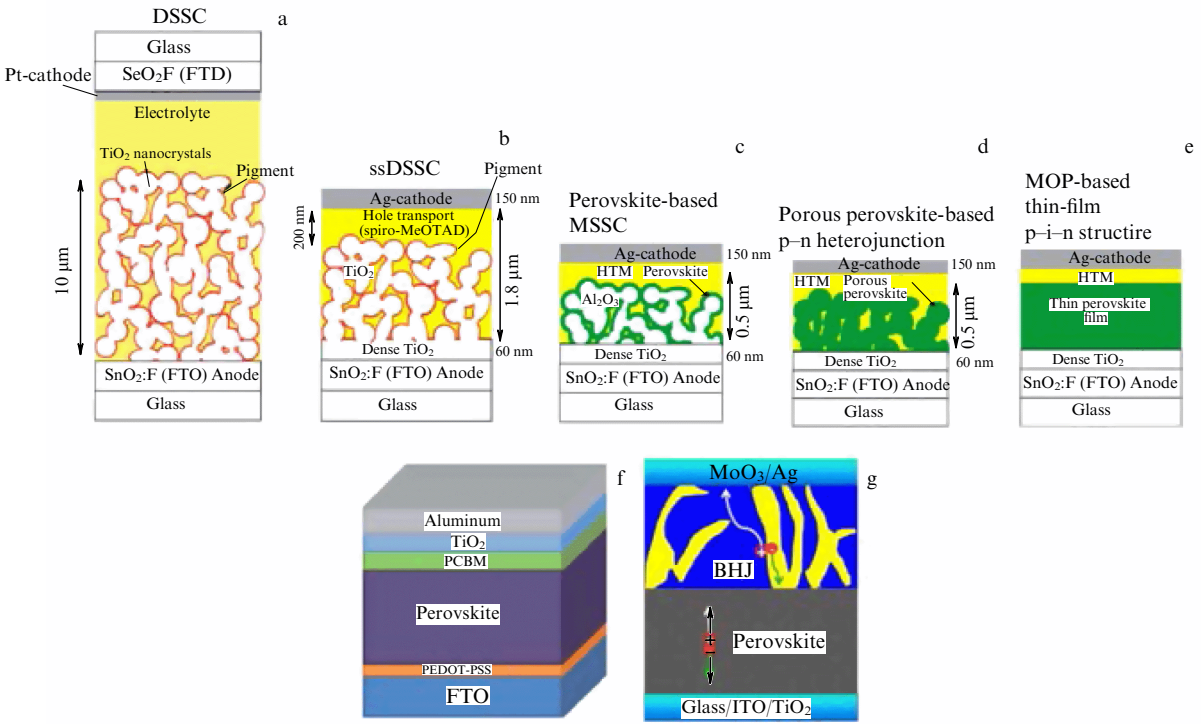

Figure 20. Architecture evolution of MOP-based solar cells starting from the first photoelectrochemical Grätzel cells (DSSC, Dye-Sensitized Solar Cell) (a) to contemporary thin-film p–i–n type (f) and p–n type (g) heterojunction structures. (Copied from Refs [139, 140].) In figures (a)–(e), notion HTM stands for Hole Transporting Material, in this case, polymer electrolyte; MSSC — Meso-Superstructured Solar Cell, and ssDSSC — solid-state DSSC. In figure (g), BHJ — Bulk Heterojunction.

nanometer-sized layer of wide bandgap insulator Al_2O_3 (Fig. 20c) obtained by atomic layer deposition (ALD) separated the MOP and porous TiO_2 from each other. This dielectric layer prevented recombination between electrons residing in the TiO_2 layer and holes residing in the electrolyte. However, it inhibited electron transport through porous TiO_2 layer to the Grätzel cell anode (electron transport through Al_2O_3 occurred due to the tunnel effect). At the same time, this solar cell possessed an unexpectedly high efficiency. This allowed the assumption that MOP is not only a GC pigment analogue but also an electron-transporting material (ETM), although less conductive than titania.

Based on the Grätzel cell structure shown in Fig. 20d, a number of research groups in 2012–2014 studied the influence of nanostructured ETM layers on solar cell efficiency. Generally, they failed to optimize the SC performance and raise the efficiency by increasing the number of electrons that reach a collector electrode with an ETM in the form of nanorods, nanofibers and whiskers, nanoplates, etc. [145–150]. A relatively low efficiency of 5–8% in some cases, obtained without using the hole transporting material (HTM), led researchers to check whether MOPs can work not only as light absorbers and ETMs, but also as HTMs, although their hole conductance is lower than that of spiro-MeOTAD, for example. Results of this type of work yielded the idea of a thin-film MOP-based solar cell at the end of 2013, in which the perovskite conjoins functions of photoelectric material and conductor (for both electrons and holes). In so doing, the efficiency was raised to 12% [151] and 12.3% [152].

In 2013, a number of studies broke through to high-efficiency MOP-based solar cells (with an efficiency of more than 15%) thanks to a changeover of photoelectrochemical Grätzel cell structure to thin-film p–i–n and p–n diode structures (Fig. 20e, f). In p–i–n structures, the MOP served as the i-layer, and the p- and n-type layers were ETM and HTM. In p–n structures, the MOP thin layer works as a light absorber and HTM, whereas the ETM constitutes the combination of thin layered solid titania and MOP-impregnated porous titania [129].

The production process of layered elements (deposition of ITO, FTO, ETM, and HTM layers, metal contacts, and an absorptive layer) circumvents extra technical obstacles and its steps were generally polished during production of second-gen thin-film solar cells. The processes comprise atomic layer deposition, one- and two-stage spin-coating — a method based on centrifugal force, liquid or vapor deposition [155], and simultaneous liquid–vapor deposition [153]. At the same time, the relatively simple MOP crystallization process takes place in an inert atmosphere near room temperature from several minutes to hours [128, 130, 153] and allows controling the layer thickness (hundreds of nm), reaching high crystallinity, lacking of domains, a low concentration of defects and traps, and, correspondingly, good electrooptical properties.

Review [153] presents the essential parameters (efficiency, I_{sc}, V_{oc}, FF) of different MOP-based solar cells with $MA = CH_3NH_3$ cation. For example, the $TiO_2/MA\,PbI_3$/spiro-configurated solar cell has $I_{sc} = 21.6$ mA cm^{-2}, $V_{oc} = 1.1$ V, $FF = 0.75$, and an efficiency of 17%. At the end of 2014, some studies reported an efficiency of 18% for p–i–n cells [156] and even 19% [157] for more complex combined crystal structure of MOP $(FAPbI_3)_{0.85}(MAPbBr_3)_{0.15}$. Defectless MOP deposition from solution on different ETM substrates granted comparable GC efficiencies [158, 159].

The practical importance of MOP-based solar cells increased due to the development of the deposition technology for pliant ETM and HTM coatings on perovskites, and as

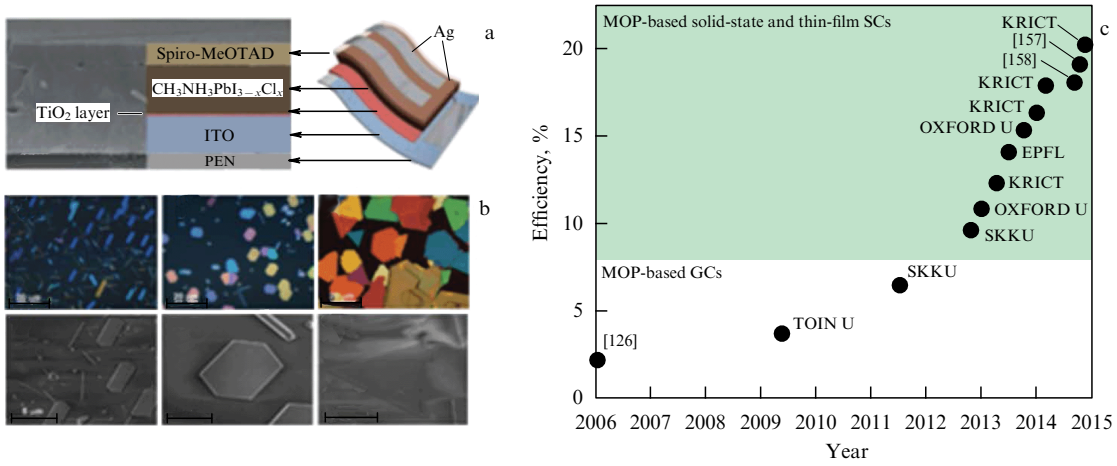

Figure 21. (a) Pliable p-i-n-junction planar solar cell [153]. (b) Images of MOP microcrystals based on different cation–anion complexes, $PbCl_2$, $PbBr_2$, PbI_2, obtained by an optical microscope (upper row, scale bar 20 μm) and by a scanning electron microscope (lower row, scale bar 5 μm) [165]. (c) Progress of MOP-based solar cells (http://www.nrel.gov/ncpv/images/efficiency_chart.jpg). Institution names: KRICT — Korea Research Institute of Chemical Technology, EPFL — École Polytechnique Federale de Lausanne, SKKU — Sungkyunkwan University, TOIN U — Toin University of Yokohama, Oxford U — Oxford University.

an example mention may be made of polyethylene naphthalate (PEN) and PEDOT-PSS, as well as bulk heterojunction layers. These technologies apply to fabricating p–i–n structures (Fig. 20f) and tandem structures (Fig. 20g), in which bandgap energies of perovskite and the heterojunction layer differ sufficiently [140, 160–164]. Because these structures support sequential spectrum splitting, they compete with two-junction multicomponent semiconductor solar cells, but are at least an order of magnitude lower in cost. On the other hand, the efficiency of the best tandem solar cell is 14.3% [140], i.e., far from the records held by diode multijunction solar cells (see Section 5).

Thin MOP layers (hundreds of nanometers), despite being polycrystalline, can withstand strong mechanical strains (bending radius up to 1 cm) for a long time, maintaining the initial efficiency and not producing detectable defects. Pliable thin-film MOP structures (Fig. 21a) have appeared only recently [153], so growth in their efficiency should be expected in the near future. Although the efficiency of MOP-based pliable solar cells is 30% lower than that of solid analogues, their field of application extends much broader [140, 153, 160–164].

Since 2013, fine-tuned thin-film technology has stimulated a great amount of research focused on searching for optimal ETM and HTM prospect for charge transport and impregnation of MOP thin layers. The efficiency value played the role of optimum criteria. Moreover, the possibility of structuring the MOP crystals themselves [165] led to preparing micron-sized single crystals with extremely smooth surfaces (roughness of less than several nanometers) (Fig. 21b), thus simplifying the application of contact materials and reducing the concentration of intrinsic defects.

The evolution of MOP-based solar cells in recent decades has resulted in an increase in the stability of their performance and their efficiency, which is the key point. Figure 21c reflects this issue.

7.4 Operation principle of metal-organic perovskite solar cells

The efficiency value of organic solar cells increased tenfold starting from first known application of MOPs as a solar light absorber in Grätzel type photoelectrochemical cells (2.2% efficiency) [126], in which 2–3-nm amorphous MOP particles were deposited onto porous ETM instead of dye molecules, up to today's contemporary technique of defectless MOP thin layer synthesis with a crystal structure fitted for p–i–n or p–n junction cells. This efficiency gain obviously relies on a gradual understanding of MOP photophysics, but not on *ad hoc* material selection and blindly choosing the cell architecture. This knowledge predestines goal-seeking technological optimization of solar cells and their architecture.

For MOP-based solar cells, trends predict efficiency values sufficiently higher than 20% (particularly for enhanced tandem structures), permitting these cells to come to the solar photovoltaics market [129, 130, 154, 156, 166]. In 2014, the estimated cost of 1 kW·h reached $1 and was obtained by the best silicon solar cell; $0.55 obtained by a thin-film CdTe-based solar cell; $0.4 obtained by a model MOP-based solar cell [129, 130]. Still, a number of problems remain unsolved, first of all, concerning the lack of a fundamental understanding in the way of MOP-based solar cell improvement.

The operation principle of MOP-based solar cell is still hidden behind curtain; we attempt to figure it out as follows. Incident light causes in such a direct gap semiconductor electron transitions to energy levels with a high density of states. Then, some excited electrons in the conduction band become free, while the rest cohere with holes and form excitons with a binding energy of 0.02–0.55-eV, depending on the MOP structure (3D, 2D, 1D, or 0D crystal dimension) and its static dielectric properties.

The exciton binding energy in $CH_3NH_3PbI_3$ MOP falls into the 0.02–0.05 eV range, which is a transient situation between Wannier–Mott and Frenkel type excitons. Solar cells with p–i–n and p–n type junctions, based on this MOP, are rather diode-like than exciton-like structures, because their photocurrent is mainly produced by free charge carriers. Excitons in the rest of MOPs have a sufficiently high binding energy, and they dominate in photocurrent composition in the MOP layer central part. A substantial fraction of excitons dissociates during migration to the ETM/MOP and HTM/MOP interfaces, because these solar cells operate at moderate

temperatures around 50 °C (28 meV), and thermal fluctuations may disrupt some of the excitons into free charges. This process takes a few picoseconds [168]. That is why only approximately a quarter of excitons reach the phase boundaries in the case of thick MOPs (350–400 nm).

The long lifetimes (around several microseconds [169]) and high mobilities (8–2320 $V^{-1}\,cm^2\,s^{-1}$ for electrons, and 8–322 $V^{-1}\,cm^2\,s^{-1}$ for holes in different crystalline MOPs [168–170]) favor the transport of free charges after the exciton dissociation. This extremely large scatter in the mobility originates from the charge effective mass variation and sophisticated MOP energy structure, which, as it has turned out, depends on the transport parameters in this medium [168–171]. Electrons and holes diffuse through the phase boundaries for several and tens of nanoseconds, accordingly [171]. As a result, the mean free paths for electrons and holes in MOPs are around 0.5 and 1 μm [172]. These long paths prescribe the optimal MOP thickness in the 350–500-nm range [173].

At first sight, a decrease in the MOP thickness to 100–200 nm would reduce photocurrent losses. Indeed, holes in MOPs have a longer mean free path compared with electrons, so the electron component drastically limits the maximal photocurrent at 350–400-nm MOP layer thickness, which is roughly equivalent to the electron mean free path. On the other hand, the MOP layer lacks persistence and flatness, consisting of submicron crystals and air interspaces. HTM and ETM molecules inherently fill these spacings from both sides during solar cell fabrication. Generally, at an MOP layer thickness of less than 300–350 nm, the gaps among separate crystals form through holes, thus allowing the HTM and ETM molecules to meet in the spacings and to form end-to-end passage-ways, resulting in the formation of MOP-shunting spurious contacts and a decrease in SC open-circuit voltage V_{oc}.

One more reason for the 300–350-nm MOP layer thickness limitation in contemporary solar cells centers around the numerous crystal structure defects that trap the charges. Charge accumulation in the light-absorbing layer leads to emergence of a capacity effect and to the solar cell current–voltage curve hysteresis, decreasing both V_{oc} and the photocurrent [174]. However, both electrons and holes fall into these traps, so statistical averaging takes place at sufficient layer thickness. Eventually, an increase in the MOP layer thickness from 100 to 400–500 nm provides a fast decrease in its effective capacity, and the hysteresis loop almost disappears. The layer capacity falls even faster than its thickness grows, because of the accompanying drop in MOP static permittivity [174, 175]. An increase in the exciton binding energy causes this mesoscopic effect: excitons in too thin an MOP layer 'feel' phase boundaries that weaken the bonds between the charges. Thus, 300–500 nm for the MOP layer thickness seems to be optimal.

Recombination processes resulting in a gain of ohmic resistance and an efficiency drop proceed much more slowly than the carrier diffusion; the application of additional 2–3-nm thick blocking dielectric layers (Al_2O_3 or Y_2O_3) remarkably elongates the recombination time and raises efficiency [173]. In this case, the well-known Auger effect plays the role of the main recombination pathway on which the electron fails to get to the ETM, falling into the MOP valence band for tens of picoseconds after excitation and spreading its own energy among other electrons [173]. A high density of states in the conduction band, mentioned earlier, provides great promise for this type of recombination. At the same time, the calculations demonstrate a low possibility of exciton collapse without considering interactions with other particles [173]. That is why the exciton recombination effect is negligible, in contrast to the thermal dissociation of excitons.

At the moment, the most effective and optimal MOP-based solar cell is the p–i–n junction with the ETM/HTM layer thickness varied from tens to two–three hundred nanometers, and the MOP layer thickness in the range of 350–500 nm. However, the lack of theory blocks further progress. The MOP bandgap structure continues to remain out of sight, because it varies depending on running processes and the ambient conditions. Moreover, the contributions from various energy carriers to the MOP photoeffect are quantitatively inaccurate, and relaxation pathways are poorly described. Available calculations mostly rely on qualitative evaluations often based on empirical data. Any theoretical models applicable to precise numerical simulations are absent, so high efficiencies reached by MOP-based solar cells are theoretically unjustified. Blind spots of solar cells in the existing theory throw the findings of their enhancement potential off course.

7.5 Metal-organic frameworks (coordination polymers)

The sudden success of MOPs in the field of solar photovoltaics in the middle of 2013 drew attention of researchers to other organic–inorganic compounds that have a potential for electric transport and for conversion of light into electricity. Metal-organic coordination polymers (MOCPs) in the general classification or metal-organic frameworks (MOFs) in a particular case (after solvent removal) belong to this group. To be a solar cell component, MOCPs have to effectively (in tandem with the rest of the elements) carry out the transfer of charges and/or absorb sunlight. Because cheap MOP-based solar cells are highly effective but are still far away from large-scale production, the novel exciton MOCP-based solar cells have to surpass them in the duration of stable operation, working surface area, efficiency values, and other parameters.

A photoelectric MOCP constitutes a semiconducting or dielectric microcrystal (Fig. 22a) with metal ions or clusters of polyvalent metals (Fe, Ru, Cu, Cd, Al, Mn, Cr, Zn_4O ...) situated at the lattice points and bounded to each other by coordination-active organic molecule ligands (for example, terephthalic acid), which can be highly polar and conductive by themselves (for example, anthracene-based carboxylic acids). Because the ligand size can reach a few nanometers, the crystal itself can possess rather high porosity (a surface area up to $10^4\,m^2\,g^{-1}$) with a pore size up to 5 nm. Component variation during synthesis, just as for MOPs, widens the class of MOCPs by producing almost any 3D- and

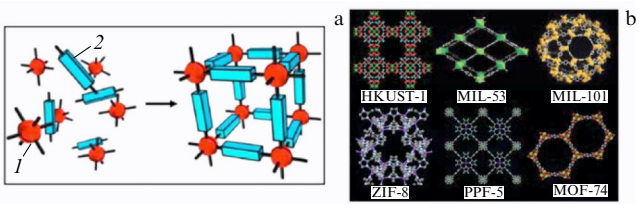

Figure 22. (Color online.) (a) MOCP formation principle: red elements (*1*) — metal ions or their clusters, and blue elements (*2*) — binding ligands. (b) Different crystal structures of MOCPs.

2D-crystal structures (Fig. 22b) and a bandgap energy from 1 to 3 eV, and sometimes higher [176, 177].

Since the beginning of the 21st century, a number of publications on MOCPs, according to SCOPUS database, exceeded 12,000, showing, as was for the case of MOPs, quasi-exponential growth in 2000–2014. A major part of this research focused on the synthesis of new crystals and investigations into their chemical and electrochemical properties. Notice that for the last 10 years, MOCPs have successfully penetrated into the commercial production area of gas and flammable sorbents due to their high porosity, great absorption properties, and high thermal stability (up to 500 °C).

Relying on the metal-organic frameworks, physical properties, and relative success of 'congenerous' MOPs in solar photovoltaics for the last 10 years, we assume the application of MOCPs for production of next-gen solar cells in the role of nano-sized photoelectric absorbers (analogous to MOPs in a Grätzel cell) or a conductive photoelectric absorber of submicron thickness (analogous to MOPs in thin-film p–n and p–i–n junctions), serving, moreover, as a host for additional dyes and/or quantum dots. Let us consider each of these opportunities.

(1) The clearest way of applying MOCPs in solar cells is to use them as a photoelectric absorber, as was done with dyes and MOP nanocrystals in a Grätzel cell (Fig. 23a). However, most of the synthesized MOCP microcrystals have a bandgap width of more than 2 eV, so the photoeffect happens in them only in the short-wavelength range of solar spectra. That is why their application as absorbers will be inefficient. Goal-seeking chemical synthesis of narrow-bandgap MOCPs can improve the situation, but it requires production of high-purity ligands.

Pioneering work in this area, published in 2013–2014 [178–180], showed that test Grätzel cells based on liquid electrolyte and MOCP nanocrystals instead of dye molecules or MOP nanocrystals demonstrated a rather good efficiency value (around 7%) and, in comparison with MOP-based solar cells, freedom from some drawbacks, such as crystal dissolving in the liquid electrolyte and low thermal stability. The MOCP crystallization scale-up at the phase boundaries is very important and useful for solving the technological problem of multilayered solar element production. However, one should expect MOCP-based Grätzel cell replacement by a more effective solar cell, probably diode-like, as was the case with MOP-based solar cell architecture evolution.

(2) Effective sunlight absorbance along with the opportunity of energy transport in the crystal, with the energy gained in the photon absorption in the bulk, corresponds to the operation principle of thin-film MOP-based p–n and p–i–n junctions solar cells. Synthesizing narrow-bandgap MOCPs and structuring their volume with dye molecules or nanocrystalline quantum dots will extend sunlight absorption spectra: the MOCP porous structure is suitable not only for gas or liquid sorption, but also for relatively large (> 1.5 nm) molecules and nanoparticles. Modern synthesis methods allow us to obtain metal (Ag, Au, Pt) or semiconducting (CdTe, Fe_3O_4, Cu/ZnO...) nanoparticles ranging in size from one to tens of nanometers inside the pores of MOCP microcrystals (Fig. 23b) [181, 182]. What is more, the MOCP crystal structure must support growth or application of ETM and HTM layers of different thicknesses and lattice periods during multilayered solar cell production. So far, the mechanisms of charge carrier transport in MOCPs remain unclear. One should expect that research on photophysical processes in MOCPs will help to define the right architecture of the cell and optimize its structure in the future, as it was in the case of MOPs.

A number of experiments [183–191] revealed an electro-optical response of some MOCPs and their arrays. UV-, visible-, and AM 1.5 (source with sunlight spectra) light illumination of the microcrystals between contacts caused a circuit current: crystal conductivity (10^{-7}–10 S m^{-1}), its character (hopping or metallic), and the type (electron or hole) depend crucially upon the experimental conditions (variation of illumination intensity, wavelength, or crystal modification).

Three types of energy transfer from absorbed photons to photocurrent electrons can probably occur in MOCP-based solar cells [192–203]: charge-free Förster resonance energy transfer (Fig. 23c) or Terenin–Dexter energy transfer, exciton energy transfer, and electron energy transfer. The first mechanism takes place due to the presence of closely (around one nm) situated molecule ligands in the crystal structure, which play the part of photoluminescent sources having overlapping absorption and luminescence spectra [201, 202]. This provides resonant energy transfer for both MOCPs and impregnated dyes or quantum dots: from molecule to molecule, from molecule to metal ion, and then from the crystal itself to the contact layers.

The second mechanism of energy transfer (exciton migration) also relies on resonant molecular interactions and is not connected with charge transport. MOCP homogeneity and high crystallinity successfully sustain this mechanism. Molecule ligands bonded by π-orbitals through metallic clusters with d-band f-levels are capable of providing effective exciton transport, even guided transport, due to molecule orientation. An additional rise in ligand acidity (bipyridine to pyridine) and the employment of metal ions

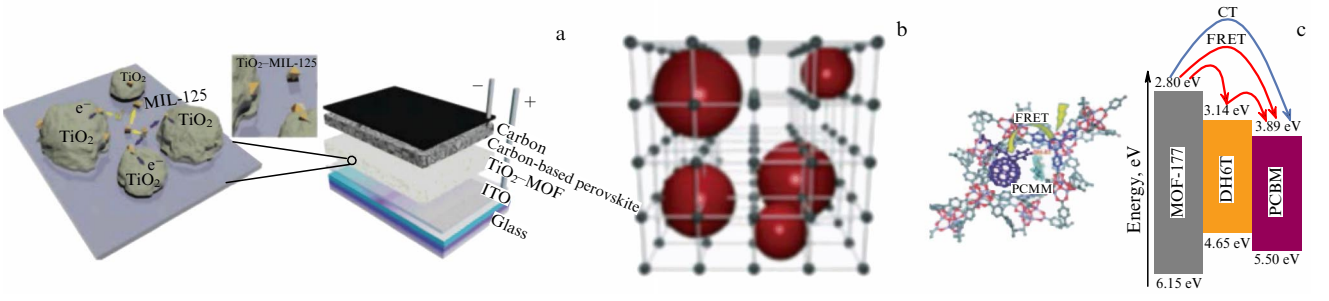

Figure 23. (a) MOCP nanocrystals on submicron porous titania (TiO_2-MOF) in the structure of a photoelectrochemical cell [180]. (b) Formation of nanoparticles inside the MOCP pores [181]. (c) Förster resonance energy transport [192]. CT — charge transport, FRET — Förster resonance energy transport, DH6T — ω-dihexyl-sexithiophene, MOF — MOCP.

(Ru, Os) strongly bounded with the ligands π-orbitals favor the formation of electron-conductive pathways in the crystal and transform it to the ETM/HTM element.

7.6 Prospects of solar cells based on metal-organic perovskites and metal-organic coordination polymers

MOP-based solar cells potentially put competitive pressure on the world market on second-gen solar cells based on multicomponent semiconductors, amorphous silicon, and hybrids of amorphous and microcrystalline silicon. There are two groups of major tasks to complete for MOP-based solar photovoltaics.

7.6.1 Technological tasks. This area contains a number of problems with in-touch solutions and one main problem critical for the commercialization of MOP-based solar cells. Side tasks include the replacement of toxic elements (Pb) with nontoxic analogues (Sn, etc.) with the respect to the European Restriction on Hazardous Substances (RoHS), a price cut on some of the materials (like spiro-MeOTAD), an increase in thermal stability and performance of MOP-based solar cells to several years, and optimization of encapsulation technology.

The main problem here is an increase in the solar cell working area to a commercial level [206]. High efficiency values of such cells excite everyone except energy market participants, because these values have been achieved for solar cells with areas less than 0.5 cm^2 (today this limit is 1 cm^2; it was reported recently by Grätzel in *Science*, DOI: 10.1126/science.aaf8060). An increase in area yields a decrease in *FF* and, hence, efficiency. The same solar cell with an area of 0.09 cm^2 has an efficiency of 12%, while those with an area of 1 cm^2 have only 8.3% [166]. The record efficiency for a 16.8-cm^2 cell amounts to 5.1% [167]. Overcoming this challenge leads to the next one — the production of pliable MOP-based solar cells.

7.6.2 Fundamental tasks. Despite high-quality research on the fundamentals of solar cell functioning (impedance and photoelectron spectroscopy, time-resolved spectroscopy, electron-induced current spectroscopy, etc.), photophysical processes taking place in organic–inorganic halides with the perovskite structure still trickle through the fingers. Several points are under question at present: (1) what, in fact, plays the role of energy carrier, with the energy obtained from photons — the exciton, as in organic solar cells, or the divided electron–hole pair; (2) what charge relaxation pathways (mono- and bimolecular recombination, Auger recombination) and which of the interfaces (MOP/ETM or MOP/HTM) exert a decisive influence on the SC charge lifetime and efficiency; (3) how does the MOP crystal structure influences the mobility of charges, and so on. Resolving these issues will blaze a trail to further improvements in solar cells and their efficiency [149, 153, 158]. If this is done, cheap thin-film perovskite photovoltaics will overcome in efficiency the best existing commercial solar cells.

Concerning MOP-based solar cells, other than Grätzel cells, in which MOCP nanocrystals replace dyes, it is too early to speak about their commercialization. At the moment, we know of only two pioneering papers (beginning in 2007) devoted to manufacturing MOCP-based solar cell analogous to MOP-based ones [203, 204]. MOCP-based solar cells are potentially better than their MOP-based analogues, especially in view of thermal stability and pliability [205]. However, it is crucial to better understand the operation principles of these solar cells for any further development. This implies that one should formulate a quantitative theory of photophysical processes that proceed in MOCP-based photoelectric layers, i.e., overcome a number of fundamental obstacles.

8. Optical systems that are constructive parts of solar cells

Optical efficiency is an important parameter defining the solar cell efficiency. 100% optical efficiency would mean that all sunlight incident on the solar cell is absorbed in its photovoltaic layer. In order to get close to this goal, one needs to avoid light energy losses in reflection from the solar cell and in the back scattering from it (diffuse reflection losses and diffraction losses), as well as losses resulting from parasitic transmission of light through the photovoltaic layer if its thickness is not enough to fully absorb the incident wave. Light losses caused by solar cell protective glass (if it is used) would not be considered a decrease in solar cell optical efficiency, since this glass is not a part of the solar cell.

All photovoltaic materials have a large refractive index (especially in the visible region) and, thus, they are highly reflective. This means that every solar cell needs sunlight reflection suppression. The structural part of the solar cell, which suppresses the reflection, including reflection associated with light scattering, is called the antireflection coating (ARC). When the thickness of the photovoltaic layer is enough for full absorption of light after two its passes (for example, for a solar cell based on amorphous silicon with the p–i–n heterojunction, this corresponds to 1 μm or more, while for crystalline silicon it is several micrometers), polished metal is often used as a bottom electrode. In such solar cells, the ARC is enough to provide maximal optical efficiency. This is especially related to solar cells, where all light that enters the photovoltaic layer is absorbed in a single pass.

A similar situation is observed in the majority of crystalline solar cells, precisely in those where the thickness of the doped layer exceeds 5–6 μm, as well as in many thin-film cells. For example, in some solar cells based on amorphous silicon, the photovoltaic layer thickness is on the order of 1 μm [11]. In this case, approximately 90% of the solar spectrum is absorbed in one pass. The majority of solar cells based on multicomponent semiconductors have photovoltaic layers with thicknesses of several micrometers, while 1 μm is already enough for them to fully absorb light in one pass.

The total thickness of photovoltaic layers in multijunction solar cells lies in the range of 1–3 μm, and by using spectrum splitting the full absorption of transmitted light can be achieved. However, a large number of solar cells, like pliable ones based on amorphous silicon with the optimal thickness of the photovoltaic layer (which, as was mentioned above, is approximately 250–400 nm), as well as the absolute majority of exciton solar cells and many solar cells based on epitaxial crystalline silicon, do not provide full absorption of light transmitted into the layer.

After passing the ARC, the light stays in the photovoltaic layer in the form of a plane wave that propagates across the layer and is absorbed according to the Bouguer law. This absorption is not high enough in the above-mentioned types of solar cells, and even the reflective bottom electrode cannot provide maximal optical efficiency. In this case, the so-called light-trapping process, in which the transmitted light wave is transformed in such a wave packet that will experience larger

absorption in the same material, needs to be carried out. At the same time, the parasitic transmission of light through the photovoltaic layer is suppressed. The structural part of the solar cell, which suppresses both parasitic transmission and light reflection, is called the light-trapping structure.

8.1 Antireflection coatings

Much experience was accumulated in glass optics in the field of multilayer ARCs (see, for example, papers [207–209]). The operation principle of such layered ARCs is common for any medium which it is applied to and is based on the destructive interference between waves reflected from the top and bottom surfaces of each layer. The larger the number of interfaces, the greater the possibilities for destructive interference between partially reflected waves. Thus, in a multi-layered structure, the reflection is effectively suppressed at various frequencies. A special feature of ARCs for solar cells is that they need to be broadband, because the solar spectrum is very wide. This task is simplified by the fact that the material, the reflection from which needs to be suppressed, has in this case large optical absorption.

Moreover, from the electrodynamic point of view, the structure of the absolute majority of solar cells is already layered. Complex dielectric constants of materials, which are included in the composition of every functional layer in a solar cell (photovoltaic layer, transparent electrode, p-type material, n-type material, etc.), have significantly different values. At the same time, heterogeneous layers in BHJSCs, GCs, and other exciton solar cells have subwavelength inhomogeneities, which, except for several cases (see lower), can be described macroscopically using averaged values of the refractive and absorption indexes.

The effective electrodynamic layered structure of a solar cell, significant optical contrast between the layers, and absorption make it possible to achieve a quite broad antireflective band by using only one dielectric film and, in some cases (for solar cells based on CdTe or CIGS), by just optimizing the thickness of a transparent electrode [208, 209]. However, such solar cells in the best case reflect around 10–20% of incident sunlight power [208, 209]. Due to this, many solar cells do not look black in sunlight, even without the protecting glass.

In some solar cells, maximal light absorption is achieved by using multilayer coatings (from 4 to 12 layers), which are fabricated with nanometer precision and allow decreasing the integrated reflection in the whole sunlight spectral range down to 1% (on the illuminated area of the solar cell — that is, outside the contact grid) [209]. Of course, such coatings are not suitable for solar cells used in everyday situations; they are used in multijunction solar cells, where their cost is a significant part of the whole structure value (see, for example, monographs [3, 4]). Moreover, nanometer layers of even the strongest dielectrics would quickly degrade on Earth due to environmental factors.

Let us note that using protective glass for multilayer coatings does not make sense, because any glass with macroscopic thickness provides significant reflection losses (about 10% and higher). Moreover, in most on-Earth applications, solar cells do not rotate with the Sun, so the sunlight incidence is almost always not normal. This means that the coating, if possible, should operate for any angle of light incidence. Practically important are the angles of incidence in the range from 0° to 60°, at which the reflection coefficient should be lower than some threshold. Multi-layered coatings should result in losses of no more than 1–2%. Flat layered ARCs can almost completely suppress the reflection in a very broad frequency range for a single light incidence angle, but they are unable to provide such low reflectivity for all significant angles of incidence [207].

Reduction of reflection losses to a few percent in the effective sunlight band of 320–1350 nm and in the incidence angle range from 0° to 60° can be achieved in three different ways. First is the formation of an optically dense (much smaller than the average wavelength of the solar spectrum) and strongly protruding texture (rods, cones, etc.) on the surface of the ARC. Second is the formation of so-called *black silicon* (for crystalline silicon-based solar cells). Third is the formation of a composite antireflection coating. Such an optical composite can be realized in the form of a dielectric film with submicrometer-sized particle inclusions, a monolayer of close-packed dielectric particles, etc.

Texturing a dielectric ARC with close-packed protrusions in a form similar to frustums with a smoothed top (Fig. 24a), according to the theory [210], leads to the formation of a plane parallel layer of the medium with a vertical gradient of the refractive index (averaged in the horizontal plane). At the level of cone tops (in Fig. 24a their average height is approximately 440 nm, and the texture period is 300 nm), this averaged refractive index is close to unity, because in the plane which goes through the cone tops the dielectric covers zero area. In every horizontal plane located lower than the one corresponding to the cone tops, the area fill factor for the dielectric increases, so the effective refractive index becomes larger than unity. Finally, the refractive index of an effective medium becomes equal to the dielectric refractive index in the plane of the cone bases.

The authors of paper [210] used silicon nitride with a refractive index of approximately two in the visible range, and this value is close to the refractive index of the photovoltaic AlInP material. By properly choosing the shape of the cones described by a cubic polynomial function, one can achieve an almost optimal refractive index gradient along the vertical axis. If the refractive index is unity on the top interface of an optically inhomogeneous medium and its value increases with the distance from the top interface with an optimal gradient, then the light reflection becomes negligible and does not depend on the layer thickness and wavelength [210, 211].

In reality, replacing a commercially available composite antireflection film with such a texture on the surface of an AlInP-based solar cell allows decreasing the integrated

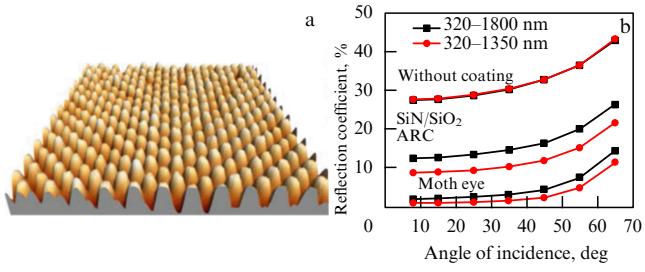

Figure 24. 'Moth-eye' textured coating (a) and the effect of this coating on AlInP-based solar cells available on the world market (b). Integrated reflection coefficient is plotted versus the angle of incidence for two ranges of the solar spectrum: on Earth (320–1350 nm), and in space (320–1800 nm). The coated solar cell is compared with the uncoated SC and with the SC covered by a commercially available antireflection film made from a silicon nitride with inclusions of silicon dioxide nanoparticles.

sunlight reflection (in earthly conditions) from 4 to 2% at normal incidence, and from 10 to 7% for a 60° angle of incidence (Fig. 24b). The increase in reflection at higher angles of incidence, shown in Fig. 24b, is the effect of spatial dispersion in the array of cones. At such large angles of incidence, the phase difference of the incident wave between two neighboring cells of the texture becomes so large that the model of an effective refractive index averaged over horizontal planes turns out inadequate.

Despite this disadvantage, such coatings (due to the similarity to the microstructure of a moth's eye, they are called *moth-eye coatings*) [210, 211] are very promising for commercial applications, because they can be fabricated using the nanoimprint lithography method. Silicon nitride is a relatively flexible material, so in order to prepare the proper profile in hundreds of samples of silicon nitride film one only needs to fabricate the quartz plate for one sample. This technology is also compatible with the roll-to-roll solar cell fabrication method. Of course, the method of refractive index gradient will work if there are no jumps in this gradient, which means that the film refractive index needs to be approximately equal to the refractive index of the layer beneath it. Therefore, moth-eye coatings will not be so effective for crystalline silicon-based solar cells with a mesh electrode, in which case one can obtain maximal efficiency by using a semiconductor with the refractive index in the range of 2–3 in the sunlight spectral band together with an ITO or AZO top electrode (refractive index of ITO and AZO is close to 2).

In paper [212], various types of textures are compared (nanowires, nanocones, nanopyramids) in respect to the uniformity of the effective refractive-index gradient in the horizontally homogeneous texture model. The results for different shapes of protrusions theoretically turn out to be almost the same as they were close-packed in the lattice and had optimized values of height and period.

Textured antireflection films are not used for crystalline silicon solar cells, because the silicon refractive index has a large dispersion in the solar spectral range and the reflection from the interface between the film coating and silicon can be suppressed only in a narrow range of frequencies and angles of incidence. Instead, silicon itself is textured [36, 37, 43]. This is possible due to the fact that its surface corresponds to the $\langle 111 \rangle$ crystallographic plane. Usually, various single-crystal growth techniques are applied to form a submicrometer transition layer on the top boundary with the effective refractive index lying between the silicon refractive index and the refractive index of the adjacent medium lying above the layer. The transition layer acts as an ARC and is formed by closely spaced and strongly protruding random roughnesses with characteristic lateral sizes on the order of 100 nm (Fig. 25).

The upper medium can be made of silicon dioxide or nitride layer, which can be deposited on the rough silicon upper boundary (at the same time, this layer passivates silicon and acts as an additional ARC, while having a flat upper boundary [43, 213]). However, the best antireflection is achieved when the upper medium is absent. In paper [214], the roughnesses themselves are covered with an extremely thin layer (2–5 nm) of passivative corundum Al_2O_3, deposited layer-by-layer using the atomic layer deposition (ALD) method. Due to such small thickness, the corundum does not influence the optical properties of the structure. Then, reflection losses at normal incidence do not exceed 2% [214]. At oblique incidence of sunlight, the reflection increases, and

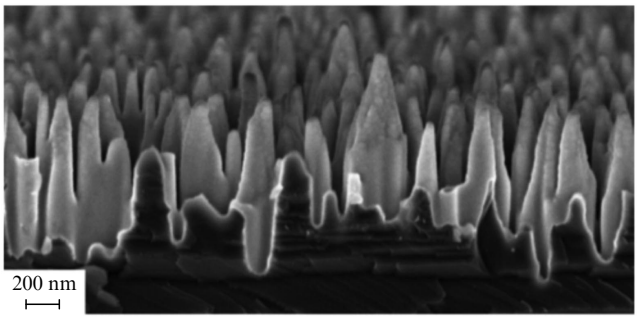

Figure 25. Black silicon with random inhomogeneities (image obtained in paper [214] using a transmission electron microscope).

at 60° reaches value close to 10%. After averaging over all possible incidence angles of sunlight, the reflection losses in this structure turn out to be lower than in Refs [43, 213] and several times smaller than in the case of flat layered coatings. Let us note, however, that atomic layer deposition of corundum is an expensive nanotechnology.

An alternative method for obtaining black silicon is a regular texturing of silicon with nanocones, including frustums, or nanowires, including hollow ones (nanotubes). Corresponding nanotechnologies are based on plasma etching [36, 37, 43, 214, 215]. If texturing is performed with an optically small period — around 200 nm — the incident light power is not scattered through diffraction lobes and the textured region can be described in the same way as in the case of a polymer coating — that is, in terms of the averaged refractive index gradient. Regularity of the structure prevents diffusive reflection of light, which allows decreasing the reflection losses to 1% for normal incidence [215]. Examples of some of these structures are given in Fig. 26. The surface of black silicon is passivated with deposited silicon dioxide. Regular texturing of silicon is more efficient, but is also much more expensive than mask-free etching, which results in a random relief.

In some of the papers, it is suggested that silicon be textured through chemical etching, resulting in a honeycomb structure with the size of the cell being larger than 10 μm (Fig. 27a). A silicon solar cell with such texturing would be obviously cheaper in commercial applications than ones obtained in Refs [36, 37, 43, 214, 215]. However, due to the parasitic effect of diffraction grating, which is significant for such large structure periods, the reflection losses, including back scattering, turn out to be on the order of 10% even at normal incidence [216]. Thus, such textured silicon can hardly be ascribed to black material.

Another cheap method for suppressing the light reflection losses in diode solar cells consists in using such composite coatings as, for example, a close-packed lattice of dielectric spheres a micrometer in diameter (Fig. 27b). Such coatings were developed for GaAs solar cells, because the GaAs crystallographic plane is $\langle 001 \rangle$, and it is not possible to make a coating similar to black silicon on gallium arsenide [217]. It turns out that a structured coating consisting of touching latex spheres 1 μm in diameter acts at normal incidence as a dielectric layer with a 1.27 refractive index, which lowers the sunlight reflection from the surface of a GaAs single crystal by approximately a factor of two (on average, down to approximately 20%). At the same time, useful absorption and, accordingly, the photocurrent grow by 25%.

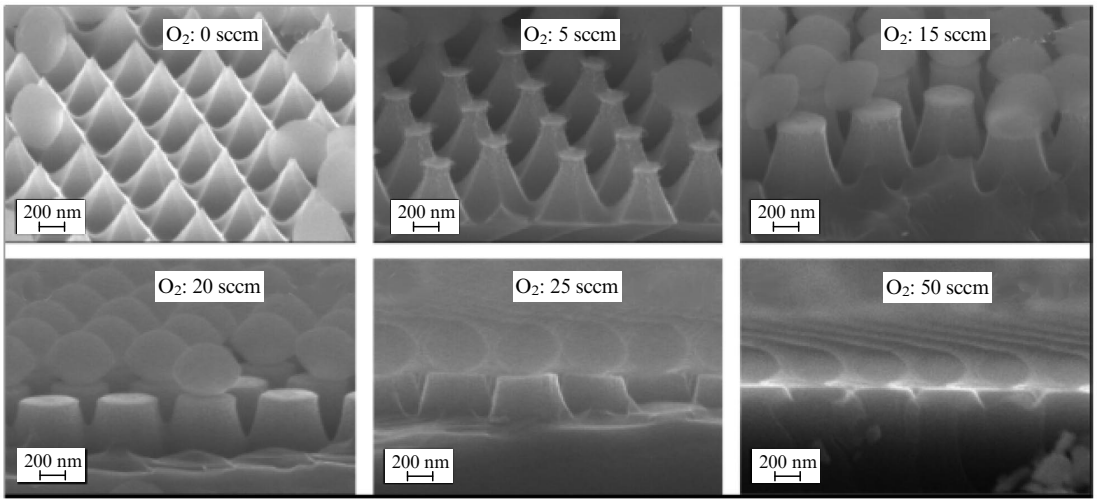

Figure 26. Examples of textures which manifest the black silicon effect in paper [215]; sccm — standard cubic centimeter per minute, the unit of mass consumption under standard conditions, $cm^3\ min^{-1}$.

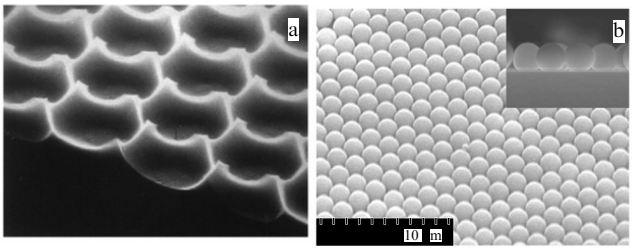

Figure 27. Relatively cheap antireflection coatings: (a) honeycomb structure on silicon (cell diameter is approximately 14 μm; the image was obtained with a scanning electron microscope [216]), (b) close-packed lattice of latex spheres [217].

At normal incidence, the dielectric layer with an optimal refractive index would result in even lower reflection, but at oblique incidence the spheres' coating operates much better than the flat layer. In addition, flat dielectric layers do not hold onto the surface of GaAs single crystals any better than micrometer or submicrometer spheres, especially with the addition of an adhesive layer 100–200-nm thick. Such a coating can be cheaply fabricated on a macroscopic area by either spin-coating [218] or adhesion method [219] which is one of the cheapest self-organization methods. The reason is that as the sample moves in a colloidal solution with an optimal speed, dielectric nanospheres from the solution stick to the surface of the sample and form a close-packed monolayer.

It is important to note that, due to the all-angle antireflection effect, such a composite coating is promising not only for GaAs solar cells, but also for solar cells based on other semiconductors. Various optical properties of the semiconductors require the optimal choice of a nanosphere size. The optimal diameter of silicon dioxide spheres ranges from 300 nm to 1 μm, depending on the type of a solar cell [217–221].

A theory of composite ARCs consisting of an array of submicrometer dielectric inclusions into a flat dielectric layer with another refractive index was developed in papers [222–227]. The inclusions can be realized as spherical air cavities or just pits. Such nanostructured layers can be used as antireflection coatings for almost any transparent material, and they can be matched to the specific medium by changing the geometrical parameters. The spectral region, in which this surface antireflection effect shows itself, is much broader than in the case of applying a homogeneous ARC, and there is no need to match the materials of the substrate and the blooming agent.

Of special interest is a broadband all-angle antireflection with the aid of a lattice of submicrometer pits in a polymer coating [227]. Despite strict requirements on the structure periodicity and geometry of this sub-micrometer texture, these coatings, just like the moth-eye coatings, can be obtained by a nanoimprinting method, which is cheap for mass production. The operation principle is, however, different from the refractive index gradient effect and is based on the phase adjustment effect, when the wave reflected from the layer acquires a phase shift which depends on the wavelength, and the condition of interferometric blooming can be realized in a relatively broad spectral region and not for a single wavelength, as in other cases [222–227]. It is of particular interest how this idea can be realized in the fabrication of ARCs for thin-film solar cells based on multicomponent semiconductors. Currently, these cells are usually covered with flat-layered coatings that do not provide all-angle antireflection. Therefore, all values of efficiencies for such solar cells reported in the literature are measured for a normal incidence of sunlight.

One of the most efficient antireflection coatings, although expensive, is the black-silicon structure from paper [228], where the authors suggested and experimentally investigated HIT nanostructured solar cell (see Fig. 5). The photovoltaic layer in this cell is prepared from an ordinary plane single-crystal doped silicon (thickness of about 10 μm and with n-type conductivity) using physical (plasma etching) and chemical (self-organization) methods. The structure consists of vertically oriented silicon microneedles with a thickness of about 100 nm, length of about 10 μm, and average lattice period near 200 nm.

The morphology of this structure is illustrated in Fig. 28. Silicon microneedles are covered with a passivative material, polyaniline, which forms a large number of nano-sized needles on silicon. Due to the high adhesion of the needles,

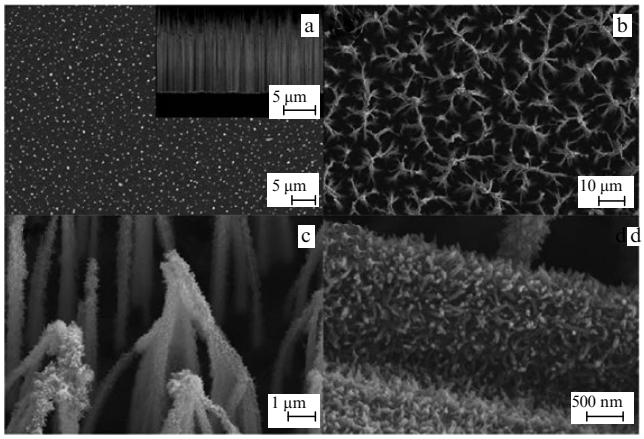

Figure 28. Scanning electron microscopy images of a microneedle structure and a black-silicon self-organizing hierarchical structure. (a) View from the top (the inset shows a side view of a cross section, and the lower interface of the microneedle region is the p-n junction). (b) Top view at a larger scale. (c) Zoomed image of connecting silicon microneedles in a hierarchic structure. (d) Further zoomed image of nano-sized needles grown on silicon microneedles. (Images are taken from paper [228].)

Table 2. Well-known best results on silicon solar cell ARCs (taken from paper [228]).

	Flat surface of single-crystal silicon	Black silicon surface
Reflection losses at normal incidence of light, averaged over the corresponding range, %		
UV (300-400 nm)	54.0439	0.0046
Visible light	35.2259	0.0031
Near-IR (1200-2000 nm)	31.3626	0.0102
Reflection losses averaged over all angles of light incidence and the corresponding range, %		
UV (300-400 nm)	61.5751	0.6414
Visible light	39.0719	0.4633
Near-IR (1200-2000 nm)	48.0257	0.5215

the upper parts of silicon microneedles connect with each other and form a complicated hierarchical structure similar to cones. Since the microneedle lattice is optically dense in the region where the microneedles are parallel to each other, the lattice can be described by a uniaxial tensor of complex dielectric constant with a giant anisotropy. In the region where needles meet, this structure can be described by a gradient profile of a refractive index. Such a combination of refractive index gradient and anisotropy results in the most efficient antireflection effect in the visible, UV, and near-IR ranges. Corresponding data are presented in Table 2.

8.2 Light-trapping textures and diffraction gratings

In solar cells with an absorbing bottom electrode, one needs light-trapping structures if the light is not fully absorbed in the photovoltaic layer after one pass. In the case of solar cells with a reflective bottom electrode, light-trapping structures are used if the incident light (plane wave) is not fully absorbed in the photovoltaic layer after two passes.

The highest efficiency in microcrystalline silicon solar cells is achieved for a photovoltaic layer of thickness about 1 μm (see Section 3) and a reflective bottom electrode. The doubled thickness of the layer appears to be slightly less than the effective attenuation length for long-wavelength light in silicon, so the vertically propagating light is not absorbed. However, for oblique propagation — at angles near 45° — the optical path of light in silicon becomes sufficient for full absorption after two passes (at least in the UV and visible ranges). In this section, we discuss light-trapping structures like micrometer-scale textures. Texturing can be applied either to the upper surface of the solar cell or to the bottom electrode surface. Light-trapping in such structures is realized, first, by suppressing reflection from the upper textured surface and, second, by achieving oblique propagation of waves in silicon.

The application area of these textures is limited by the minimal thickness of the photovoltaic layer, which is connected with the so-called Yablonovitch limit that we will discuss later. This limit has no practical significance for polycrystalline and microcrystalline silicon solar cells, but it is important for epitaxial silicon solar cells with the photovoltaic layer thickness of less than 5 μm, for solar cells based on amorphous silicon, and for all exciton solar cells.

Oblique propagation of the sunlight in μc-Si is realized by saw-like texturing of the surface, with the size of the protrusions being large enough for describing the light trapping by means of geometrical optics and for the silicon surface to be covered with a silicon nitride antireflection coating [229] or two-layer ARC, as in paper [52]. This corresponds to the length of the tilted facets being on the order of 1 μm or longer. Texture can have various geometries. For example, microcrystals can be grown asymmetrically, as shown in Fig. 29a. This principle was realized in paper [230], where the μc-Si solar cell has a minimal thickness of 1 μm and the optical path of the light wave in silicon is enough for full absorption, as shown in Fig. 29b.

A disadvantage of this light-trapping method is the scattering losses, because the size of the texture protrusions is only 0.5–1 μm, and the poorly ray mechanism in Fig. 29b does not fully describe the wave processes inside the structure. At an oblique incidence on this texture from the right-hand side, as is clear from the same figure, adjacent protrusions screen each other, leading to high scattering losses. In order to overcome this problem, single-crystalline silicon is not grown on a flat reflective substrate, but instead on a substrate textured with micrometer-high pyramids, as was performed in the paper mentioned above [53]. The corresponding light-trapping mechanism works well for all practically important angles of light incidence [231].

Since the optical losses on the bottom (reflective) electrode of a microcrystalline silicon solar cell are negligible, the light-trapping effect in the structures is fully described in terms of reflection losses integrated over the solar spectrum, which are in the range of 10–20% for the structure studied in Ref. [230] (Fig. 29a), depending on the incidence angle, and 5–15% for the structure reported in Refs [53, 231] (Fig. 29c).

In order to achieve light trapping in single-crystalline silicon solar cells with a photovoltaic layer thicknesses of several micrometers, one can use more complicated textures — inverted pyramids [39, 232, 233], as well as saw-like surfaces combined with microlenses, so that every microlens lies between the adjacent protrusions [234]. Other texture geometries can also be found in the literature. They all meet a common condition that the size of the tilted facets be on the order of 1 μm or more. The light transmitted to the

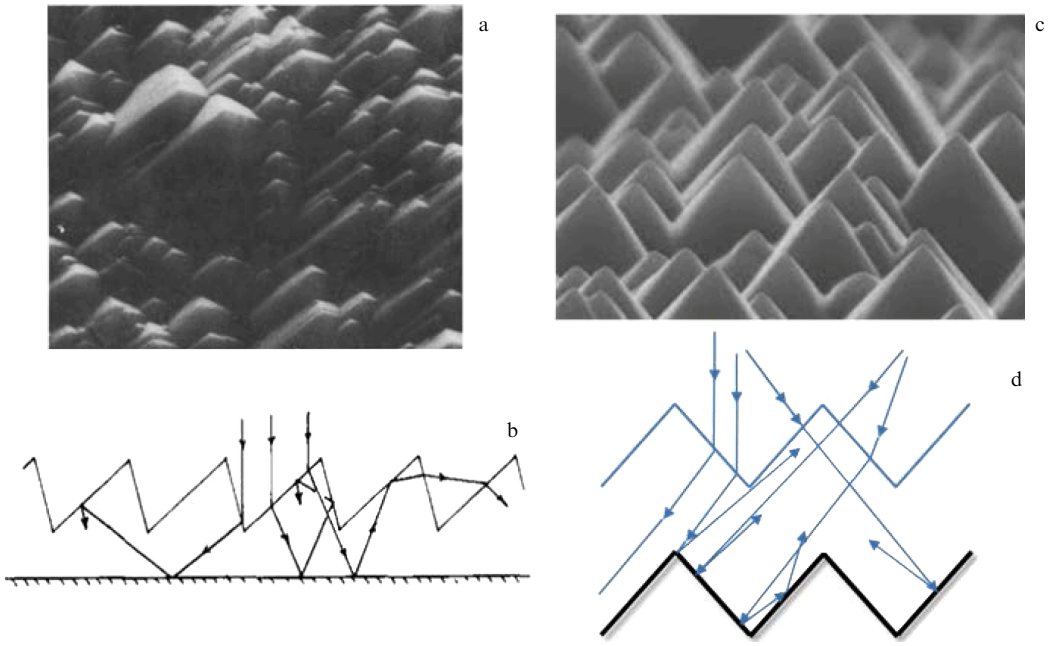

Figure 29. Light trapping in a textured crystalline silicon. (a) Asymmetric texture with protrusions of micrometer length (scanning electron microscopy image [230]). (b) Light-trapping illustration by means of geometrical optics in such a texture with a reflective substrate (bottom electrode from polished metal). (c) Pyramidal microtexture of silicon [231], grown on the glass substrate with the same microtexture and covered with a polished metal. (d) Illustration of light trapping in such a texture by means of geometrical optics.

photovoltaic layer remains a packet of locally plane waves, and it can be described in terms of geometrical optics.

We should pay special attention to textures which cannot be described by means of geometrical optics. The period of such a texture equals several wavelengths in the middle part of the solar spectrum, which is practically 2–3 μm. A surface with such grooves is the well-known phase diffraction grating. Such gratings are effective not only for solar spectrum splitting (see Section 5.2), but also for excitation of integral optical waveguides by a normally incident plane wave [229]. However, tooth-like grooves with a large period are not optimal, when the light should be trapped in the layers of microcrystalline or epitaxial single-crystalline silicon (see Section 3) with the same thickness as the height of the tooths themselves or smaller.

For a solar cell based on epitaxial crystalline silicon with a thickness less than 5 μm, the optimal light-trapping effect is achieved by phase grating with rectangular protrusions, structurally matched with the lower silicon layer and the electrode. It is optimal to take advantage of a two-component grating, where a dielectric phase grating with a 1-μm period is followed by a metallic grating with a 5-μm period. Such a double grating does not practically reflect a plane wave (at least in the visible range) in the direction of its incidence and transforms it into waveguide modes of the silicon layer (the main diffraction maxima of the grating coincide with the directions of the Brillouin waves that form these modes). A review of such inner textures is given in paper [235].

8.3 Light-trapping structures beyond the Yablonovitch limit

The ability of textured surfaces to redirect incident light into a continuous layer of material is limited by the minimal thickness of this layer. This thickness should not be too small with respect to the height of the tooths (or any other roughness) and must be on the order of the light wavelength in the medium or larger. This fundamental limitation was obtained by the Yablonovitch group in 1982–1984 [236–238] and applies not only to textures, which obliquely refract or reflect light rays by means of geometrical optics, but also to phase gratings and any structures at all for which the wave optics approximation holds true. In other words, it applies to all structures where light waves remain wave beams and no evanescent waves are produced [239].

By the Yablonovitch limit is sometimes meant the limiting gain in energy absorbed from a light plane wave at a certain frequency incident on a layer of a medium with refractive index n and damping coefficient k (for $k \ll n$) that can be provided by some passive periodic structures located either inside the layer or outside it and not producing evanescent waves. This gain can be achieved by redistributing the light flux, and for a large enough thickness of the layer at normal incidence it is equal to $4n^2$ [236].

For most photovoltaic materials, the Yablonovitch limiting gain means that useful absorption of sunlight can be enhanced by at least a factor of 20 (and about 50 for amorphous silicon) by using some periodical structure. A twenty-fold enhancement may not be enough only for organic solar cells with a flat heterojunction, where the photovoltaic layer is so thin that it absorbs less than 5% of the incident light. However, one can effectively use the light flux energy redistribution mechanism and approach this limiting gain only in a layer with a thickness close to the light wavelength in the medium [237]. This condition is not fulfilled for many exciton solar cells, resulting in their very low optical efficiency. Finally, if the thickness of the textured or structured part of the photovoltaic layer significantly exceeds the thickness of its continuous part, then the light flux mostly redistributes in the textured (structured) part. In this case, the light-trapping is not useful, because this region contains electrodes which are made to some extent of optically absorbing material.

As a result, useful absorption does not reach the limit $4n^2$ [238] in textured solar sells with protrusions or depressions larger than the thickness of a continuous part of the photovoltaic layer. Periodical structures or diffraction gratings operate properly when the characteristic size of the protrusion or depression is not less than 1 μm. Thus, the results of Yablonovitch's research imply that such texturing or structuring is useless for thin-film solar cells thinner than 1 μm [237–241].

Among thin-film solar cells of sub-micrometer thickness, one can distinguish diode solar cells based on multicomponent semiconductors like CdTe (see Section 4), multijunction solar cells with submicrometer thickness (see Section 5), and pervoskite solar cells (see Section 7). All of these have an optimal thickness of the photovoltaic layer of less than 1 μm but, as was mentioned before, they do not need light-trapping devices. All other exciton solar cells and amorphous silicon solar cells have such an optimal photovoltaic layer thickness (with respect to quantum efficiency and the fill factor) which is not enough for light to be absorbed in one pass or, in some cases, in two passes. These solar cells need light-trapping structures operating beyond the Yablonovitch limit.

In a number of papers, including Refs [240, 241], thin-film solar cells based on epitaxial crystalline silicon with a thickness of 0.5–1 μm are also considered to be promising for the commercial production. As we have mentioned before, for solar cells of this design, the optimal with respect to the photocurrent thickness of the photovoltaic layer equals 5 μm. As this value is decreased to 500 nm, quantum efficiency and the fill factor fall. However, this reduction is not catastrophic. Under the condition of full absorption of the incident light, the efficiency of such a solar cell would decrease by a factor of only two [240], while the consumption of crystalline silicon would be decreased by a factor of ten when compared with the optimal solar cell. Therefore, the development of such solar cells can be really useful and they also need efficient light trapping.

In order to fully absorb light in a solar cell based on epitaxial silicon with a layer thickness ranging 0.5–1 μm, a physical mechanism, discussed in papers [240, 241] and known from the optics of so-called photonic crystals, was triggered. Photonic crystals are bulk periodical gratings in a transparent medium with periods on the order of half the wavelength of light in the medium λ_m and larger [242]. These crystals possess a very wide bandgap — a range of wavelengths that cannot propagate in the medium. However, the bandgap of a photonic crystal is more or less densely filled with frequencies of so-called polaritons — eigenmodes of the lattice which are damped upon receding from its boundary. Thus, if the sunlight spectral range approximately coincides with the bandgap of a photonic crystal with finite thickness, polaritons would be generated in the crystal.

Polaritons constitute evanescent waves; therefore, the Yablonovitch limit does not apply to a solar cell with a photonic crystal inside the photovoltaic layer. Actually, in order to overcome the Yablonovitch limit, it is not necessary for the solar spectrum range to be equal to the bandgap. It is sufficient for the solar spectrum just corresponding to the opaque band of a photonic crystal for a single vertical direction, since the excitation of a photonic crystal eigenmode, which propagates in the horizontal plane, is substantially a light-trapping event which is similar to that achieved by texturing thicker solar cells. In other words, if a photonic crystal has an opacity band for a vertical direction approximately equal to the solar spectrum width, then this structure can redirect incident light into the eigenmodes of the photovoltaic layer beyond the Yablonovitch limit.

In order to excite polaritons in a photonic crystal, the following condition needs to be fulfilled: the photovoltaic layer thickness has to be equal to the size of only two unit cells of the photonic crystal [240]. Moreover, if the flat bottom electrode is made of polished metal, one layer of inclusions would be enough [240, 241]. This can be done, because the plane, which reflects light, allows the mirror image principle to be applied. This means that the SC bottom electrode can replace the second layer of inclusions. A single-layer grating of air cavities with a complicated form in crystalline silicon, suggested in Ref. [241], constructively looks like some unusual phase grating. However, in the presence of a silver reflective electrode, this grating works completely differently and provides light-trapping in only a 400-nm thick layer of epitaxial silicon.

Let us now consider amorphous silicon SCs. The main advantage of these solar cells is their low cost and flexibility. The light-trapping mechanism using photonic crystals is expensive and can be realized only in rigid structures; therefore, it is not suitable for amorphous silicon solar cells. A variety of light-trapping structures designed for this type of solar cells are based on the effect of sub-wavelength light concentration through microscopic resonances [243]. A sub-wavelength concentration of light (in a spatial region with dimensions much less than the light wavelength λ_m in the medium) is different from a macroscopic light concentration (focusing), when light can be described as a wave beam. In the case of focusing, the minimal attainable focal spot size is limited. As known from optics (see, for example, manual [244]), this limit is called the diffraction limit and it equals the diameter of the so-called Airy disc, $1.22\lambda_m/NA$, where NA is the numerical aperture of the focusing system. An incident plane wave can be concentrated in a volume with a smaller size, if evanescent waves are produced in the medium [243, 245, 246].

Summing up, in order to trap light beyond the Yablonovitch limit, light should be concentrated in a region with a sufficiently smaller size than $1.22\lambda_m/NA$ by producing evanescent waves in this region. In nanooptics, such a region is called the hot spot. The transformation of a spatially homogeneous field of a plane wave incident on the solar cell surface into a system of hot spots [243] is usually realized through so-called plasmon resonances [245, 246].

Plasmon resonances in optics are associated with collective oscillations of electron gas in metals. The collective effects of electron plasma significantly prevail over the conduction effects in metals like silver or gold at frequencies of the solar spectrum. This means that their complex dielectric constant ε_m is close to a negative real number (the imaginary part of ε_m is small). Such a feature leads to the ability of light to resonantly excite metallic nanoparticles of various forms, as well as nano-sized irregularities or holes on a metallic surface. In order to excite a plasmon resonance in a periodic structure, it is important that the size of the irregularity not be too large (otherwise, the phase matching condition may not be fulfilled) and not too small (otherwise, electron scattering by the surface will become significant) [246]. Practically, plasmon resonances at frequencies of the visible spectrum can be excited in gold or silver inclusions or irregularities with sizes in the range from 10 nm to 1–2 μm.

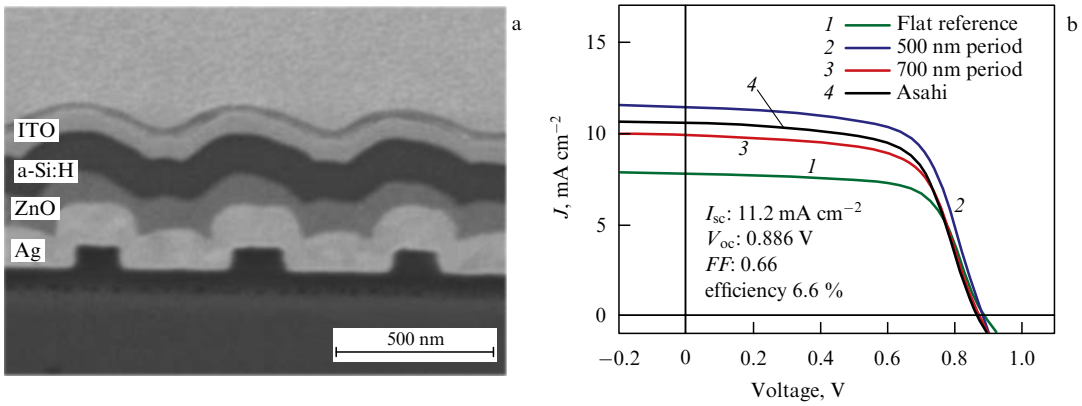

Figure 30. (Color online.) Solar cell based on amorphous silicon with the overall thickness of the p–i–n structure being 220 nm. The bottom silver electrode supports excitation of SPP on its surface due to texturing with nanodisks 150–160 nm in diameter and 70–80 nm in height. (a) Vertical cross section of the structure obtained with a scanning electron microscope. (b) Current–voltage characteristic of a solar cell (blue line *2*). For comparison, current–voltage characteristics of other solar cells are given: a similar solar cell with a nonoptimal period of 700 nm (*3*), solar cell with a flat bottom electrode without antireflection coating (flat reference *1*) and the same solar cell with an ARC (Asahi U glass *4*).

Plasmon resonance in silver or gold periodical structures can be collective. A plane wave at the frequency of a collective plasmon resonance can excite the plasmonic grating and lead to a Wood anomaly, known from diffraction theory [247]. This effect consists in the suppression of diffraction maxima and even reflection from the grating with a period larger than the light wavelength, and the energy of the incident wave is then transferred to the eigenmodes. These eigenmodes are nonradiative, because they correspond to high-order Flocke harmonics of a diffraction grating. Such a wave is called the surface plasmon polariton (SPP). It offers properties similar to a surface wave at a flat interface between plasma or a continuous plasmonic metal and a free space. The only difference is in the fact that, due to the periodicity of the structure, this mode can be excited by a plane wave.

Since there are an infinite number of Flocke harmonics, the plane wave excites not only one such eigenmode in the plasmonic grating, but the SPP wave packet. While propagating along the grating, which is located on a nonabsorbing substrate, all harmonics of this wave packet rapidly decay due to their dissipation in the grating. If a plasmonic grating is located on the boundary of the photovoltaic layer, the incident plane wave with a frequency corresponding to the Wood anomaly will excite the SPP wave packet (the presence of an absorptive layer will only shift the frequency, but not cancel the effect), and some of the SPP wave packet harmonics will be phase-matched with the waveguide modes of the photovoltaic layer. In this case, the light dissipation in the plasmonic grating elements is mostly replaced by a useful absorption in the layer. In the experiment, this mechanism allows trapping light in amorphous silicon layers with a thickness of 240–400 nm [248–250].

Light trapping takes place in several frequency ranges, with the overall width being quite small with respect to the solar spectrum width. The light with frequency outside these bands is reflected by the metallic grating. Therefore, if the grating is located on the upper boundary of the solar cell, it will generally have a bad effect on the operation of the device. If one wants to increase the light-trapping efficiency without increasing the reflection losses, the plasmonic grating should be placed on the lower boundary of the amorphous silicon layer. It is usually realized as a grating of nano-sized protrusions on the surface of a silver or gold bottom electrode, as shown in Fig. 30a. A zinc oxide layer is applied for a better ohmic contact with silicon. Since the refractive index of zinc oxide is close to 2 in the visible range, the light wavelength in this medium is half as long. Thus, the grating period of 500 nm is enough for excitation of three or even four (depending on the incidence angle) Wood anomalies at frequencies of the solar spectrum [250]. One can see in Fig. 30a that the texture of the bottom electrode leads to the texturing of the whole solar cell, including its surface.

The effect of the Wood anomaly, like any other plasmon resonance, implies the excitation of the evanescent wave packet and, in this case, the hot spot spreads along the thickness of the photovoltaic layer, also covering metallic protrusions themselves. This leads to parasitic absorption, and the overall operation of the cell is not strongly improved by using such a bottom electrode texture. According to Fig. 30b, the photocurrent is approximately 45% higher in the case of a texture with a 700-nm period than in a similar flat solar cell without an antireflection coating (flat reference), but is smaller than in a solar cell with a textured ARC (Asahi). For an optimal texture period (500 nm), the photocurrent of the solar cell considered exceeds the photocurrent of the solar cell with the antireflection coating by approximately 10%. This gain, obviously, is not high enough to justify the fabrication of such complicated solar cells. The problem does not lie in the fact that SPP excitation needs structure regularity, but in the requirements imposed on the spread of geometrical parameters of the texture, which cannot be fulfilled when using cheap chemical nanotechnologies in the texture fabrication. Nanoimprinting technology is not applicable in this case, either, and the fabrication of solar cells becomes very expensive and we have found no data on the commercial integration of such light-trapping structures.

In paper [251], it was suggested that light be trapped in thin-film amorphous silicon solar cells using the individual resonance of plasmonic nanoparticles. Appropriate plasma oscillation is called the localized surface plasmon [245]. If a single nanoparticle of plasmonic metal is excited at this oscillation frequency, it creates a hot spot with effective sizes from several dozen nanometers up to 100 nm, with intensity maxima located on the particle surface. In these maxima, the strength of the local electric field can exceed the strength of the incident field by 10–20 (gold particle) or even by 40–

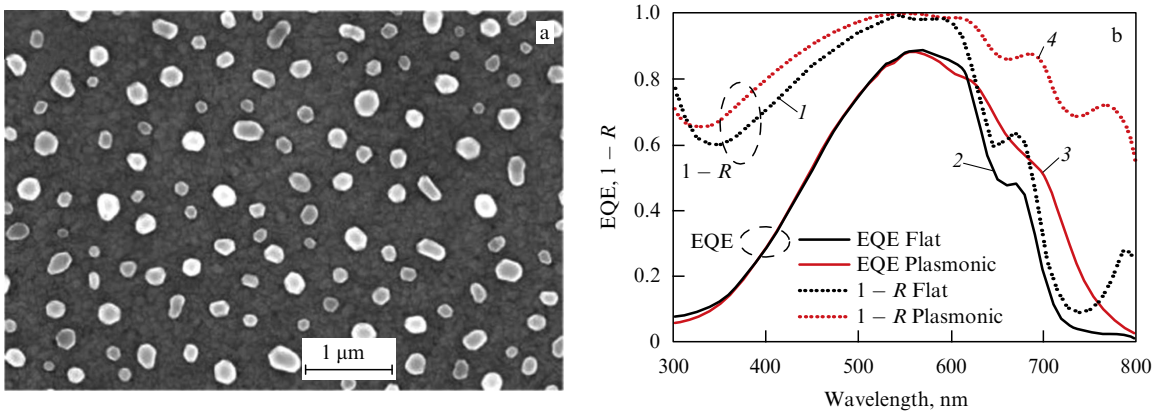

Figure 31. (Color online.) (a) Image of an irregular structure of silver islet nanoparticles obtained in paper [253]. (b) Spectra of external quantum efficiency (EQE) and the absorption coefficient, equal to $1 - R$, where R is the power reflection coefficient, because the transparent electrode of the solar cell is located above a polished silver reflector. Black curves (*1*, *2*) correspond to the same solar cell without silver nanoparticles, and red curves (*3*, *4*) correspond to the solar cell with nanoparticles. Integral gain in absorption equals about 40% and is achieved due to the plasmon resonance region (600–1100 nm, image shows range of 600–800 nm). This gain corresponds to EQE enhancement by 10%. Such disproportion is connected with the fact that part of the trapped light is absorbed in the nanoparticles themselves.

50 times (silver particle). If such a particle is located in a homogeneous medium, the huge local electric field inside the particle will lead to resonant absorption in the metal. However, if there is a sufficiently contrasting substrate, the main part of the spot shifts inside the substrate. If this substrate is a semiconductor, most of the light absorption at plasmon resonance frequencies takes place just inside the substrate.

As a result, by placing arrays of silver or gold nanoparticles near the surface of the SC photovoltaic layer, the useful absorption in the solar cell can be increased. This mechanism does not require regularity of the array. The particle size spread is even useful, because it allows extending the overall plasmon resonance band. This method can be realized using cheap chemical self-organization method [251] (with consequent annealing at 400 °C), so the idea of local light trapping with single nanoparticles became a separate research field (see, for example, Refs [252–255] and references cited in review [255]).

The self-organization method refers to chemical methods and, regarding islet films, this method was developed already in the 1970s to fabricate nanostructures for giant surface-enhanced Raman scattering. Optimization in such structures can be applied only to the averaged parameters of the plasmonic coating, such as average size of the islet particles and their surface density. This method was used in paper [253] to prepare a layer of silver nanoparticles on glass with a nearly disc shape, 100–200 nm in diameter, and 30–50 nm in thickness (Fig. 31a).

Glass (with the upper surface covered with a layer of nanoparticles, and the bottom layer fully metalized) was employed as a reflector in a thin-film solar cell based on 300-nm thick amorphous silicon with the n–i–p structure. The bottom electrode (ZnO:Al) of the solar cell was transparent and thin enough (50 nm), so that the hot spots produced by every particle would be partially located in a silicon layer. It was shown that silver nanoparticles allow getting a gain in quantum efficiency (Fig. 31b) and photocurrent density by approximately 10% (without loss in fill factor) with respect to a similar solar cell with a flat bottom reflector. Thus, a comparison to the solar cell without nanoparticles revealed improvement. However, a comparison with a randomly textured antireflection coating has shown almost the same efficiency [253].

In other work related to the same field, we could not find any comparison of a light-trapping structure with an antireflection coating. This is not surprising. If an irregular tenuous array of metallic nanoparticles is placed at the upper boundary of the photovoltaic layer, then, at frequencies outside the plasmon resonance, it increases the diffusive reflection losses, and this parasitic effect approximately compensates for the useful trapping of light in the range of plasmon resonances. If the layer is placed on the bottom boundary, as in paper [253], a second parasitic effect remains: the nanoparticle array creates hot spots at plasmon resonance frequencies with the maxima always located on the metal surface, so the electric field inside the nanoparticles is also locally enhanced with respect to the incident field. As a result, a significant part of the sunlight power is absorbed in the metal. Specialists have long known that this effect inevitably accompanies plasmon resonance (see, for example, monograph [246]). Therefore, even the best architectures of light-trapping structures, which use plasmon resonances of a random nanoparticle array, as the one in Ref. [253], for example, cannot operate better than antireflection coatings.

Attempts to displace the localized plasmon hot spots from the nanoparticles led to the understanding that a regular structure is necessary. By exciting collective oscillations in a regular grating, light concentration can be achieved outside the plasmonic particles. Such regular plasmonic gratings are often called nanoantenna arrays, because they create light hot spots outside their volume, similarly to lens antennas that focus a plane wave in like manner.

Particularly, paper [256] theoretically investigates light trapping by a regular grating of silver strips with a 50×80-nm rectangular cross section, located on the surface of a 10-nm thick glass layer deposited on top of an amorphous silicon layer (Fig. 32a). The glass layer ohmically isolates silver elements from the semiconductor, preventing the parasitic flow of photocurrent through them. The current-collecting electrodes were made in the form of more massive wires than nanostrips and were placed with a large spacing.

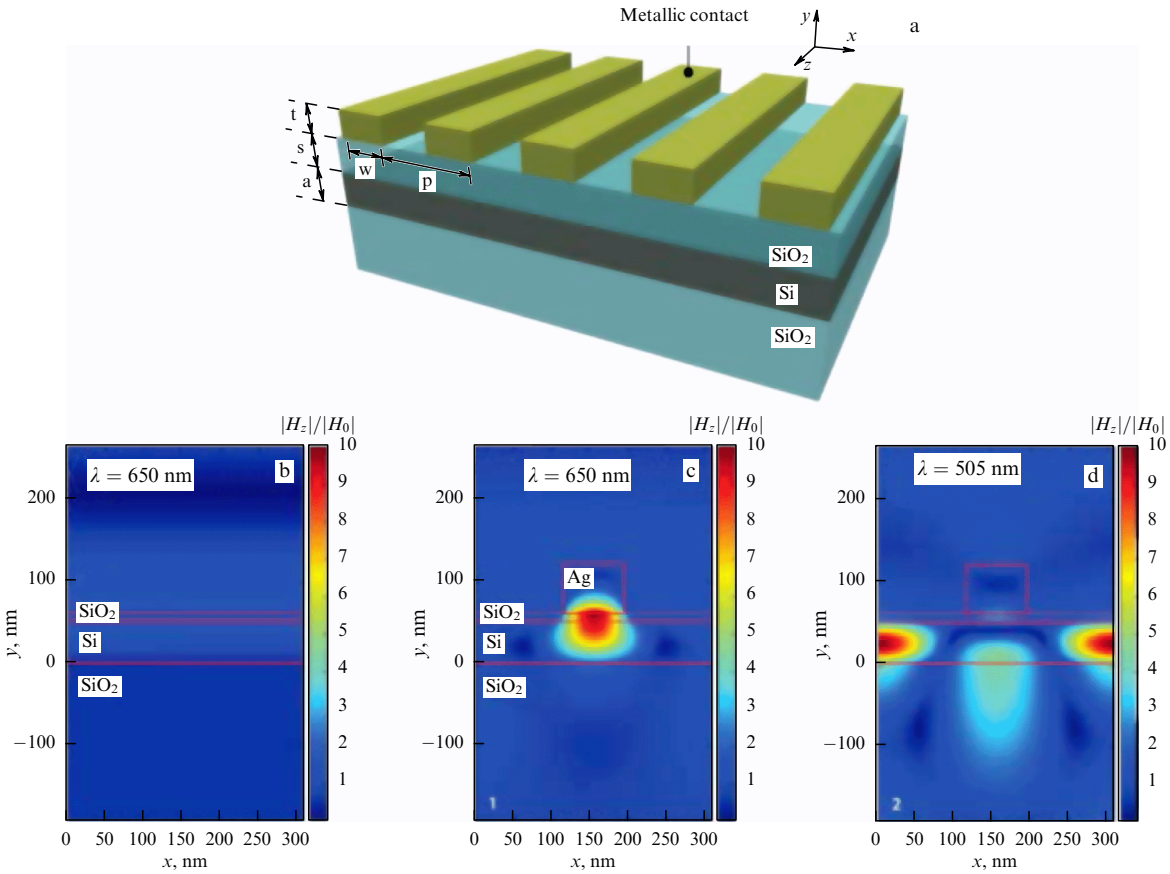

Figure 32. (Color online.) (a) Geometry of a light-trapping structure consisting of long silver strips with a nano-sized cross section and used in a thin-film silicon solar cell with a 50-nm thick photovoltaic layer. Local magnetic field distribution in a system without strips (b) and in a system with strips at two resonant frequencies (c, d) [256].

The authors assumed that the spacing was large enough, so the electrodes did not influence the results of the numerical simulation of light absorption. Silver nanostrips effectively concentrate light on hot spots at frequencies from three quite narrow ranges of collective plasmon resonances.

Figure 32b plots the local magnetic field distribution for the reference object — a structure without strips — while Fig. 32c, d shows this distribution over a structure with strips at two eigenfrequencies. It is clear that the field can be concentrated close to the strips and even quite far from them. It was revealed that the presence of a silver strip grating results in the integrated increase of absorption up to 43% in the case of a 50-nm thick photovoltaic layer. This gain turns out to be slightly larger than the one achieved by the antireflection coating. However, this effect was demonstrated only for normal incidence of light and only for one polarization, when the vector of the light electric field **E** was perpendicular to the strips.

The 45% gain in absorption in the photovoltaic layer independent of polarization was theoretically demonstrated in paper [257], using a horizontally isotropic light-trapping coating in the form of square array of silver nanodisks with the thickness of 70 nm (Fig. 33). It was shown that self-absorption in silver nanoparticles takes place in the wavelength region of $\lambda = 400-450$ nm, corresponding to the plasmon resonance of a disc on the substrate. This parasitic effect is overlaid by an almost three-fold absorption enhancement in the wavelength region of 490–525 nm, where collective modes of the antenna grating are excited. As a result, when the silicon layer thickness is 80 nm, the integrated gain in the useful absorption becomes almost 45%. The gain in useful absorption is larger at smaller thicknesses, and smaller at larger thicknesses.

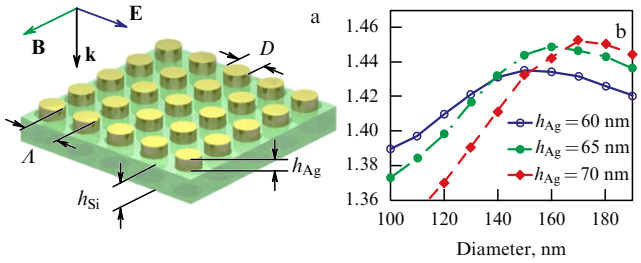

Figure 33. (Color online.) (a) Light-trapping coating based on a regular array of silver nanodisks on a silicon layer. **E** and **B** vectors correspond to the electric and magnetic field vectors of the wave incident on the structure in the direction of **k**. (b) Ratio of absorption in silicon integrated over the solar spectrum in the presence of a light-trapping coating and the integrated absorption without the coating for various diameters (D) and heights (h) of disks [257]. Grating period is $1.5D$.

An even larger absorption growth was theoretically predicted in paper [258], where the authors suggested an array of silver nanoantennas with a complicated form, part of which (in the corner of the wire grid) is shown in Fig. 34. In order to reduce the reflection, the nanoantenna array needs to be covered with a layer of polymer material, such as PMMA (polymethylmethacrylate). It is proposed that the bottom

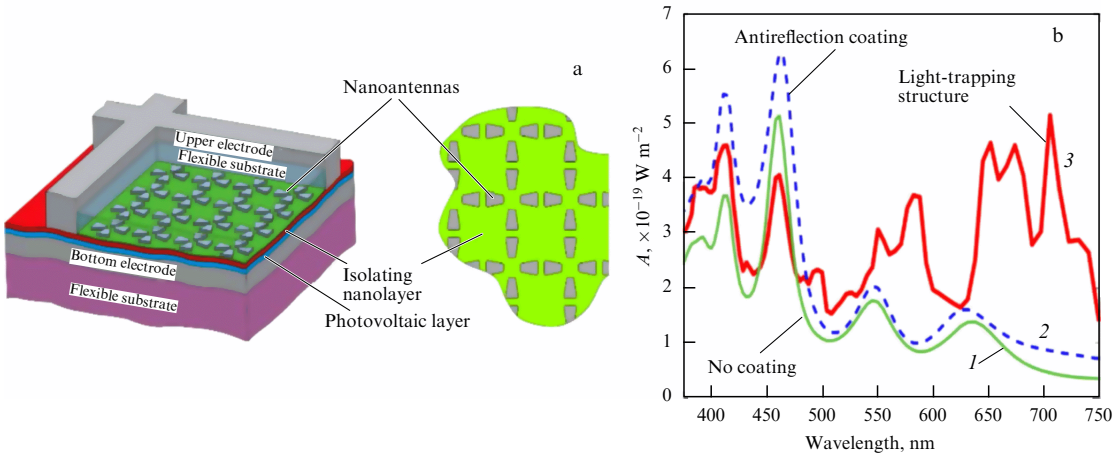

Figure 34. (Color online.) (a) Geometry of a thin-film solar cell based on either Si or CIGS and a schematic illustration of a nanoantenna array. (b) Absorption spectrum of a silicon solar cell without a coating (green line *1*), with a silicon nitride flat antireflection coating (blue dashed line *2*), and with an array of nanoantennas (red line *3*).

electrode be made of conductive oxide (AZO). For a 150-nm thick silicon layer in the structure presented in Fig. 34, the absorption in the presence of a nanoantenna grating grows by approximately 50% and turns out to be 17% higher than when the nanoantenna array and polymer coating are replaced with a conventional antireflection coating. This effect is achieved by exciting collective modes of the grating, which cover two wavelength ranges, 540–600 and 640–750 nm. The parasitic effect of local plasmon resonances in trapezoid elements (410 and 460 nm) is concealed due to large absorption in silicon exactly at these wavelengths (see Fig. 34). Of course, such an operation regime is the result of perfect grating optimization, so there are relatively high requirements on its regularity (the parameter spread should be not more than 10 nm).

Despite the large number of publications on this topic, it is currently clear that metallic nanoantenna arrays, as well as plasmonic textures in the bottom electrode region (especially random plasmonic structures), do not provide a radical solution to the problem of light absorption in amorphous silicon solar cells. It is no surprise that the record high 10.2% efficiency of a single-junction solar cell based on amorphous silicon with a 310-nm thick photovoltaic layer was obtained in papers [52, 259], where antireflection coatings were used (moth eye coating in Ref. [52], and flat layered coating in Ref. [259]) instead of a light-trapping structure.

In research on plasmonic light trapping in diode (not only silicon-based) solar cells, the following trend can be noticed: the photovoltaic layer thickness is chosen to be less than the optimal value with respect to solar cell quantum efficiency and fill factor. Due to a smaller thickness, the light losses caused by parasitic transmission through the semiconductor become much larger than reflection losses. No wonder that in this case the plasmonic light-trapping structure will lead to a larger gain than the antireflection coating. But the resulting efficiency for such semiconductor thicknesses turns out to be lower than the record high values and is usually 6–7 % (see, for example, Refs [260, 261]).

As an exception, we can consider paper [262], where an efficiency of 10% is demonstrated for an amorphous silicon p–i–n structure solar cell with an overall thickness of 200 nm. This value would have been the record for this type of solar cell at the time of publication (2011). Such a high efficiency corresponds in this paper to an optical efficiency of approximately 70% and is achieved by broadband resonances of an antenna array (which is covered by a layer of transparent polymer, as in paper [258]). The array is constructed as a chessboard made of silver nanoplates connected at the corners, with plasmon resonances with their large losses in the metal being shifted towards the IR range of the solar spectrum by optimizing the structure parameters.

However, the idea of this research did not find any experimental verification after four years. We believe that the problem of technical realization of structure [262] lies in the fact that the collective modes of the array are highly sensitive to the geometry of the nanoplates forming the 'chessboard'. In numerical simulations [262], all nanoplates were connected with each other at the corners, with the contact regions being 3 nm wide and the nanoplate thickness being 50 nm. Most probably, if the spread of geometrical parameters exceeds 3 nm (which is inevitable even if the structure is fabricated using the most expensive electron-beam lithography method) and the contact between adjacent plates can be damaged, then the broadband light-trapping regime may not take place.

Here, we come to a discussion of the main disadvantage of nanoantenna arrays applied to light-trapping structures in amorphous silicon solar cells — the high fabrication costs, which can hardly be compatible with the idea of a large surface solar cell with a low cost justifying low efficiency. Although the authors of paper [258] believe that the nanoantenna array can be fabricated on a large surface using the method of nanoimprinting on a polymer substrate which then is held up against the SC surface, this idea has not been experimentally confirmed yet. Such an array was practically realized only on a surface of less than 1 mm^2, and it was fabricated using electron-beam lithography [263]. However, even the realization using the nanoimprinting method would hardly justify the structure fabrication costs, if the solar cell optical efficiency would not reach 100%. Unfortunately, no known metallic nanoantenna arrays provide useful light absorption higher than 60–70%, because these structures are resonant. Useful absorption can be

enhanced in the solar cell by collective resonances of such gratings, including Wood anomalies, but even in the best case [258, 259, 261] this enhancement is observed in the frequency band with a 40% relative width.

Since regular arrays of plasmonic nanoparticles are too expensive to fabricate (with an efficiency well below 100%) and arrays fabricated using self-organization methods are inefficient, it was suggested in Ref. [264] to perform light trapping using dielectric nanoparticles. We have already mentioned the light-trapping features of composite antireflection coatings consisting of close-packed spherical dielectric nanoparticles with the diameter comparable to the wavelength of light in air. Thus, in a number of papers (see, for example, Refs [220, 221, 265, 266]) it is suggested to use such nanostructured layers not only for SC blooming but also for light trapping in thin-film solar cells based on amorphous silicon. These papers consider using so-called whispering gallery modes. Corresponding modes inside the sphere are standing waves with the electric field concentrated on spots with diameters of approximately $\lambda_m/2$. Outside the spots, the whispering gallery field exponentially decays, so it transforms to a packet of evanescent waves. Thus, when placing such a sphere on a semiconductor layer surface, the Yablonovitch limit can be disregarded. Close packing of spheres, which is needed for the antireflection effect, weakly influences this resonance (it only shifts its frequency). For an optimal diameter of nanospheres, two whispering mode resonances are found in the region of the solar spectrum. Maximal gain of useful absorption achieved by using such nanospheres was 11% at normal light incidence. As simple calculations show, such a light-trapping structure cannot compete with a conventional flat antireflection coating (due to a narrow bandwidth of a whispering mode resonance).

A similar structure was suggested and investigated in paper [267], applied to a GaAs solar cell with photovoltaic layer thicknesses of 100, 500, and 1000 nm. In order to additionally enhance the optical efficiency, a bottom metal reflector was used together with a two-layer antireflection coating made of TiO_2 and SiO_2. Maximal enhancement of useful absorption was obtained, obviously, for a GaAs layer with minimal thickness (at a thickness of 100 nm, the parasitic transmission losses become twice as high as the reflection losses), and at normal light incidence it was equal to 11% as compared to the solar cell with an antireflection coating. However, as we have already mentioned, thin-film gallium arsenide solar cells are not very interesting for practical applications.

Papers [268, 269] and some others considered amorphous silicon solar cells, and it was suggested to switch from whispering gallery modes to Mie resonances, and from dielectric spheres to spheroids and disks. The latter scheme turned out to be very promising from the prospects of resonance bandwidth. The grating period should be low enough for the scattering losses to be insufficient, so the authors of Ref. [269] suggested silicon disks 250 nm in diameter and 150 nm thick, forming a square array with a 450-nm period. The structure was additionally covered with a silicon nitride antireflection layer.

In paper [270], smaller diameters and periods were recommended for silicon nanodisks. At the same time, the band where light-trapping in the substrate is observed broadens due to the excitation of not only the Mie magnetic dipole resonance but also electric dipole resonance. However, these adjustments did not lead to a significant improvement. The effect still had a narrow bandwidth. Besides, structures from papers [267, 269, 270] are expensive to fabricate. It is desirable to achieve the antireflection effect from the dielectric nanoparticle monolayer itself and, at the same time, operate in the framework of cheap technologies based on self-organization and adhesion effects.

A very simple light-trapping structure for an amorphous silicon solar cell was suggested in Ref. [271] and experimentally realized in Ref. [272]. These studies fundamentally reject the use of any sort of resonance for light trapping. The usage of evanescent waves is rejected as well. Indeed, it is noted in Ref. [273] that the Yablonovitch limit is often falsely interpreted in the literature on light-trapping structures. It is true that a structure in the form of large tooths (protrusions) does not allow concentrating light on the layer with a thickness less than the height of these protrusions. But it does not mean that any structure that does not involve evanescent waves cannot concentrate light on a layer with a thickness of less than that of the concentrating structure itself. The focal spot of the lens can be much smaller than the lens itself. Of course, in order to fully absorb light after one pass, the thickness of the photovoltaic layer should not be less than

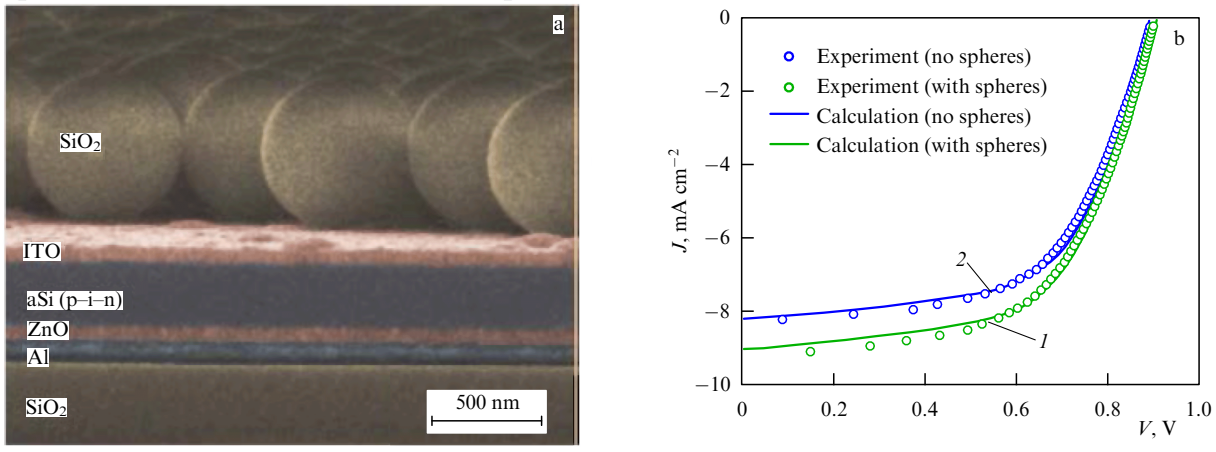

Figure 35. (a) Structure of glass resonators 500 nm in diameter, located on an amorphous silicon solar cell with a 220-nm thick photovoltaic layer. (b) Current–voltage characteristics of the solar cell — experiment and numerical calculations for the structure with spheres (*1*) and without them (*2*). (Taken from paper [221].)

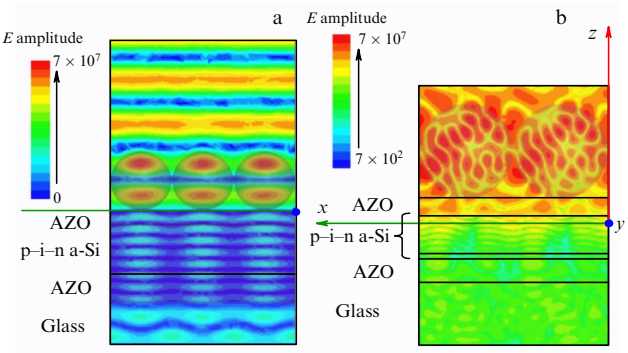

Figure 36. Numerical calculations of electric field distribution in an amorphous silicon solar cell [272] with light at wavelength $\lambda = 500$ nm being incident normally (a) and at a 60° angle (b). For normal incidence, reflection losses at this wavelength equal 36%, and transmission losses equal 11%, so the optical efficiency is 53%. At oblique incidence, these losses significantly decrease and optical efficiency exceeds 90%. These calculations are in full agreement with the measurements of external quantum efficiency. The insets to figures show the color scale for the **E**-component of the electromagnetic field.

the focal spot size ($1.22\lambda_m/NA$), but this condition is fulfilled for a 350-nm thick layer of amorphous silicon in the whole visible frequency range. This means that it is theoretically and practically possible to fully absorb transmitted light in such a photovoltaic layer in one pass by using simple lens focusing and not involving evanescent waves and resonances.

Lens focusing and the antireflection effect can be combined and provide light trapping in a structure of close-packed glass spheres, similar to the one shown in Fig. 35a. However, in order to focus the transmitted light, one needs spheres with a diameter larger than 750 nm, which was the value chosen in Ref. [221] as the optimal one for the sphere array to act as an antireflection coating in a solar cell. As the diameter increases, the period of an effective semispherical texture of the upper surface increases, and diffraction lobes appear in the region of the reflected field, which means that scattering losses increase. On the other hand, the numerical aperture of the spherical lens gets larger, which means that the focal spot size decreases and the light trapping in the layer improves. Thus, there is an optimal diameter of a glass sphere with respect to a light-trapping effect. The solar cell based on p–i–n structure 580- nm thick (480-nm thick i-layer) and AZO layer electrodes with 220- and 250-nm thicknesses was experimentally and theoretically studied in Ref [272], and the optimal diameter of the spheres turned out to be 1 μm.

At normal light incidence (Fig. 36a), the structure is slightly inferior to the antireflection coating, but it has significant superiority at oblique incidence. At a light incidence under 60°, the gain in useful absorption reaches 70%, and the optical efficiency of the solar cell exceeds 90%. Such a large effect is achieved by cascade focusing, when the light is focused on the layer interior after passing two adjacent spheres (Fig. 36b). An integrated increase in quantum efficiency (averaged over the spectrum and angles of light incidence), which is almost equal to the gain in photocurrent and efficiency in a solar cell with a light-trapping structure [272], turned out to be 16% with respect to the same solar cell but with microspheres replaced with an antireflection coating. In comparison with the solar cell without an ARC, the gain in efficiency due to spheres was 32%. This result was reported for three sets of samples of every type.

A light-trapping effect was predicted in paper [274] for an amorphous silicon solar cell covered with a polymer layer, which is structured by a periodical grating of submicrometer pits in the form of frustums. This light-trapping structure was already discussed as an antireflection coating which can be applied to various transparent and semitransparent substrates (see, for example, Ref. [227]). Light focusing in such a structure is linked to the excitation of collective oscillations and has a diffractive nature. Useful absorption enhancement in this structure turned out to be twice as large as in the case of conventional antireflection coating. If the Yablonovitch limit is falsely interpreted, which is common for articles on light-trapping structures, then the result of work [274] seems to be incorrect.

However, as was explained in Ref. [273], the absorption enhancement up to $4n^2$ (and even larger at oblique incidence of light) is quite achievable by using diffraction effects even for a layer with a thickness of less than λ_m. This was experimentally confirmed in paper [275], where the 240-nm thick amorphous silicon p–i–n structure itself was structured in the horizontal plane by creating pores with a complicated shape, so that the energy would be optimally redistributed in higher diffraction orders. The structure of such porous silicon is created on a glass substrate, which is then etched down to the desired thickness and plays the role of an antireflection coating (Fig. 37). Integrated enhancement of the absorption with respect to the nonstructured case was 45% (notice that the thickness of the ARC on the reference cell was optimized separately). Also, if a perfect (Lambert) diffuser is imaginatively placed on the surface of the lower electrode (not shown in Fig. 37), then, according to the calculations, the absorption enhancement would become 55%. One of the disadvantages of these solar cells is the difficulty in fabricating the layer of porous silicon with the needed pore structure [275].

Based on the literature analysis, one can make a conclusion that antireflection coatings for thin-film flexible solar cells based on amorphous silicon should be replaced or supplemented with light-trapping devices based on nano- or microstructured dielectrics. This allows increasing the efficiency of flexible solar cells by 15–20% — that is, from 8–9% to approximately 10–11%, achieved for rigid solar cells. Although the concept of light trapping in amorphous silicon solar cells itself is questioned in paper [276], this doubt is more likely to be attributed to scientific curiosity than to conclusions which follow from scientific investigations. The authors of Ref. [276] assume that ARCs will always be better than any light-trapping structures for layers with thicknesses higher than 200 nm. They justify this assumption by the fact that in their calculations and experiments the close-packed nano-

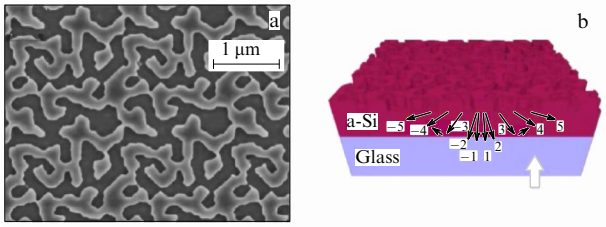

Figure 37. Nanostructured amorphous silicon [275]. Top view (a) and general view with a glass antireflection substrate (b). Light is incident from the bottom. The bottom grid electrode and upper continuous electrode are not shown.

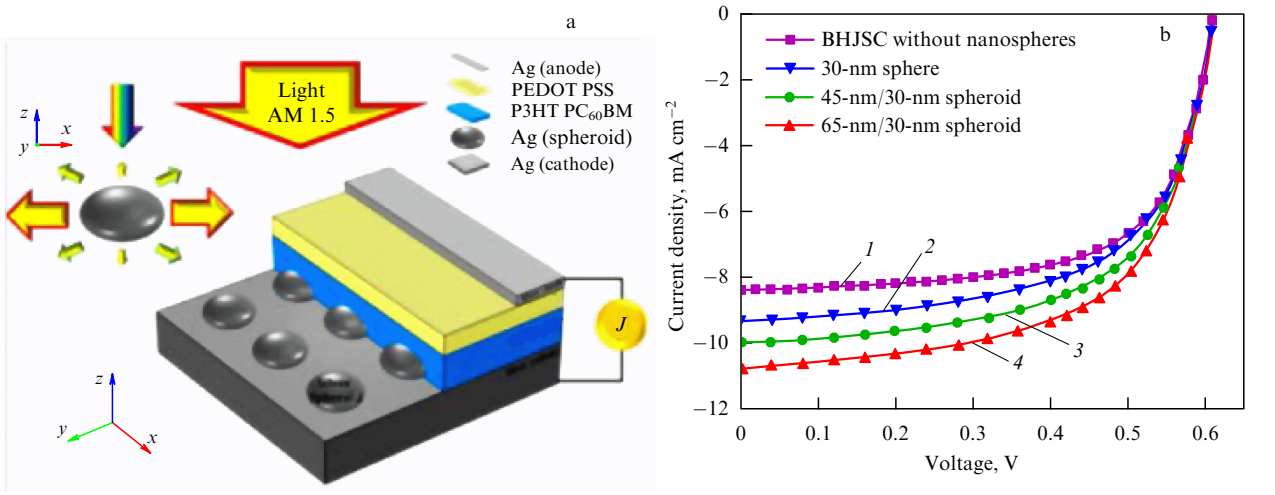

Figure 38. (a) BHJSC structure with a plasmonic texture and a reflective electrode from polished silver [278]. Upper electrode is made of a continuous silver layer, but it is semitransparent due to its small thickness (10 nm). (b) Current–voltage characteristics for various geometrical parameters of the texture protrusions — as a semisphere with a 30-nm radius (curve *2*) and semispheroids of two different sizes (curves *3*, *4*, semiaxis lengths are shown in figure). Periods of these three textures are 200, 210, and 230 nm, respectively. The efficiency of the BHJSC is increased due to an optimal texture from 3.5 to 4%. Curve *1* corresponds to the reference sample.

sphere arrays, which provide light trapping through Mie resonances (SiC and TiO_2 spheres were considered), operated less effectively than flat antireflection coatings. However, as is clear from the above discussion, the light trapping in such structures is a resonant effect with a narrow bandwidth, and parasitic transmission is suppressed in a small frequency range. Moreover, replacement of an ARC with such gratings is followed by a reflection increase, because SiC and TiO_2 are materials with a high refractive index. Thus, it is always necessary to cover such light-trapping structures with antireflection coatings, as demonstrated in paper [270], but not in Ref. [276].

Mechanisms based on the scattering of the wave transmitted inside the solar cell, similar to ones used in Refs [274, 275], are also promising for light-trapping effect in exciton solar cells. For example, it is suggested in paper [277] to fill GCs with a porous ETM material as nonhomogeneously as possible, so the light would feel the morphology of the porous material (see the flat layered structure in Fig. 18 and the structure with submicrometer morphology in Fig. 20a). This can be achieved by using anatase — the rarest polymorphic modification of TiO_2. Natural anatase demonstrates a suitable submicrometer morphology. Alternatively, one can increase the inner scattering by adding gold or silver nanoparticles into the titanium dioxide pores or by forming an artificial relief on its surface. All these methods are compared with each other in Ref. [277] and anatase gives the best result. With the overall thickness of the GC structure being 4 μm, the transition to anatase increased the efficiency from 4 to 7%.

In BHJSCs, the photovoltaic layer is very thin and exhibits low absorption; therefore, the transmission losses in them are always larger than the reflection losses if the bottom electrode is not reflective. If the bottom electrode is made as reflective, then no antireflection coating would be able to suppress the light reflection [278–280]. In this case, it turned out to be useful to return to plasmonic light-trapping mechanisms, which, as we remember, found no practical application to amorphous silicon. Paper [278] gives a review of plasmonic textures using Wood anomalies (optimal texture is shown in Fig. 38). In this case there are losses in the plasmonic particles as well, but they are fully compensated for by a twofold reflection suppression. Useful absorption is, on average, increased by 60%, and efficiency by 15%.

An alternative method for absorption enhancement is the integration of plasmonic nanoparticles inside an ETM BHJSC [279]. Locating the nanoparticles directly inside the photovoltaic material leads to the degradation of this material due to parasitic tunneling of electrons from the metal, so the nanoparticles should be located deep inside the titanium dioxide pores. In order for part of the plasmonic hot spot to reach the photovoltaic material (dye), silver nanoparticles are grouped into oligomers producing larger hot spots than single nanoparticles [279]. The integrated gain in absorption obtained in Ref. [279] turns out to be approximately the same as in paper [278], with the efficiency increasing from 2.8 to 3.2%.

In the case of exciton solar cells with a flat heterojunction, nanoantenna arrays turn out to be effective [280, 281]. A remarkably sufficient, almost three-fold increase in useful absorption was numerically obtained in paper [281], where the light trapping was performed using the nanoantennas similar to those shown in Fig. 26. The idea of study [281] is to cover window glass with a thin-film solar cell, which would absorb IR radiation from the Sun and transmit the visible light (Fig. 39). However, there has not yet been any experimental confirmation of the results reported in Ref. [281].

The general conclusion of this section can be formulated in the following way. While for some antireflection coatings the applied research has quite a routine character (which does not lower its importance) and in practice it is a question of another tenth of a percent improvement in efficiency, the development of light-trapping structures remains a very important field of research, which can bring new life to thin-film solar cells. This mainly refers to solar cells on a flexible substrate and to many organic solar cells, including BHJSCs and GCs.

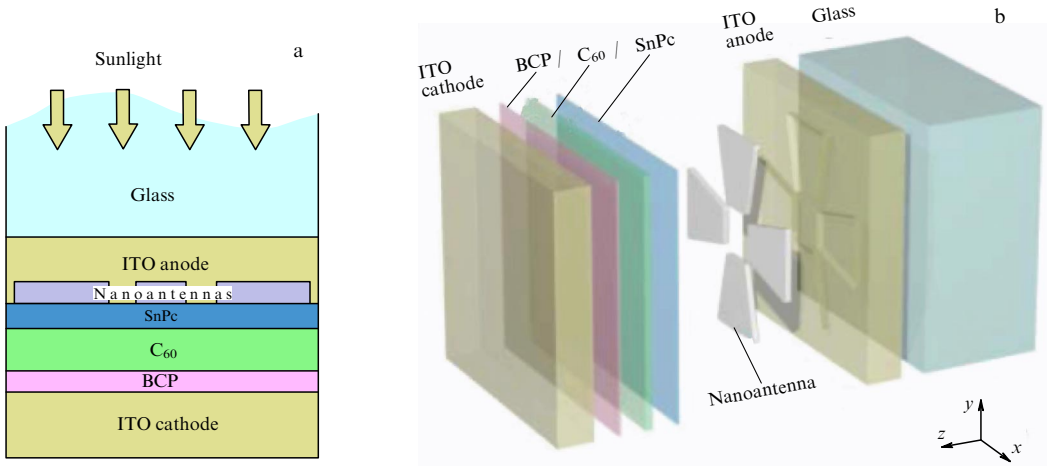

Figure 39. Light-trapping structure as a grid of silver nanoantennas for an organic solar cell with a flat heterojunction, designed for the conversion of the IR region of the solar spectrum. (a) View of the cross section. (b) Unit cell of the nanoantenna array. The structure is integrated with a window glass and transmits visible sunlight, while producing electricity by converting the invisible light [281]. In figure (a), the BCP layer stands for 2.9-dimethyl-4.7-diphenyl-1.10-phenanthroline.

9. Conclusions

Although our review is an attempt to cover the material as broadly as possible, some issues of solar photovoltaics have escaped our consideration. First, this review was written by physicists and for physicists, and many important aspects like marketing, manufacturing applications, electricity costs, and market prospects were hardly dealt with. Nor were the engineering aspects of uniting SCs in large-scale panels (batteries), issues of their mechanical structure, connection to different loads, or other problems of their service considered in our review. Furthermore, we did not review several kinds of SCs that either have no standalone product line (for instance, microscopic and nanodimensional SCs) or are inconsistently covered in the literature.

The latter applies to SCs utilizing quantum dots, on which great hopes were pinned only 10 years ago (see, for instance, Refs [3, 4]). It was believed that such SCs could become a relatively cheap alternative to multijunction SCs, because quantum dots would make it possible to substantially heighten the 30% Shockley–Queisser limit. Despite the narrow bandgaps of many quantum dots, their room-temperature excitonic photoelectric response is rather strong, and their essentially discrete energy spectrum results in a rather slow exciton relaxation. Furthermore, many quantum dots exhibit the so-called inverse Auger effect [282]. Since the bandgap is narrow, the majority of absorbed photons of the solar spectrum exceed $2E_g$ in energy, i.e., may, in principle, be expended on two excitons. The inverse Auger effect suits this scenario. It consists of the excess energy of a photogenerated exciton being expended on the excitation of the second exciton with a higher probability than on relaxation, which, in quantum dots, signifies primarily the excitation of phonons. Eventually, two excitons emerge with energies rather close to E_g, which significantly raises the Shockley–Queisser limit (according to the theory devised by Nozik [282], it may rise to 66%).

A similar mechanism of overcoming the 30% limit was already discussed in Section 1.1, as applied to Mott dielectrics [26], and we noted the high probability of the practical implementation of this idea. For quantum dots, however, the inverse Auger effect turned out to be less efficient than expected; despite the encouraging results of the first experiments with InAs nanocrystals [282], the spectra of the corresponding quantum dots — InAs, PbSe, or PbS nanocrystals — demonstrated insufficient stability [283]. As pointed out in Ref. [283], the data of the experiments reviewed in Ref. [282] were most likely misinterpreted. The efficiency growth supposedly took place due to the increase in open-circuit voltage and not because the inverse Auger effect prevailed over phonon dissipation of an exciton.

Another review on this subject, Ref. [284], named the most promising SCs utilizing quantum dots: first, the analogues of multijunction SCs utilizing layers of a different kind of quantum dots; second, Grätzel cells in which quantum dots replace natural pigment, and, lastly, SCs utilizing the rapid dissociation of a hot quantum-dot exciton with the simultaneous tunneling of charge carriers into the electrodes (more precisely, into ETM and HTM layers). In our opinion, multilayered SCs with quantum dots will hardly make mass production cheaper than multijunction SCs based on bulk-heterojunetions, whereas the highest attainable efficiency of multilayer SCs with quantum dots amounts to only 10% [284]. Nor do we believe that Grätzel type SCs, in which the dye is replaced with quantum dots, show good promise. This replacement will obviously entail an increase in SC production cost, while there are no studies demonstrating a gain in efficiency due to this replacement (this issue was analyzed in Ref. [124]). The GCs with quantum dots show no gain in lifetime, either: the natural pigment is more stable with respect to UV burn-out than quantum dots [112, 117, 121, 124].

As for the quantum dots in which a rapid hot-exciton dissociation occurs with the simultaneous electron and/or hole tunneling from a quantum dot directly into an ETM and HTM, such SCs are still considered to be highly promising for manufacturing applications, and experiments on them are proceeding vigorously (see, for instance, Ref. [285]). Since the exciton dissipation in a quantum dot itself is prevented by a fast tunneling of the charges, and the ETM and HTM may have a low ohmic loss, the additional exciton energy does not go into heat and is spent on the photocurrent.

However, quantum-dot SCs operating in this mode are a special case of hot-electron SCs. Different implementations of this approach are known [285–287], with the advantages of using precisely quantum dots to realize the idea of hot-electron SCs being not obvious. On the other hand, the drawbacks are obvious: in the first place, the exceptional toxicity of quantum dots and its related technological problems. The basic limitations of the mechanism of hot-carrier tunneling from the excitonic photoelectron material to the HTM and ETM were analyzed in Ref. [288]. These limitations, highly significant from the practical standpoint, also apply to quantum-dot SCs.

We nevertheless cannot state that hot-carrier SCs show no promise. There are mechanisms of using the excess energy of hot carriers whereto the limitations of Ref. [288] do not apply. In some solar cells, the excess energy of hot electrons may be employed to ionize plasmonic nanoparticles, because the metal-to-semiconductor work function is much smaller than the metal work function in a vacuum [289]. Moreover, the interaction of such plasmonic nanostructures with the semiconductor may prevent dissipation, when the energy of an electric field concentrated on the metal is spent on its ionization rather than heating [290]. Furthermore, the plasmonic structure may serve as an IR resonator, which is efficiently excited by hot carriers, with their generated IR radiation also being absorbed by the semiconductor and serving to enhance the photocurrent [291]. In this case (according to the theory of Ref. [291]), the phonon dissipation of excess hot-carrier energy lowers by an order of magnitude, and the Shockley–Queisser limit rises twofold. Such efficiency gain mechanisms deserve mentioning in our review. However, owing to the generally contradictory nature of the literature data on the practical prospects of hot-carrier SCs, we did not include this line of research as a special section in our review.

In this review, the bulk of attention was focused on SCs intended for terrestrial applications, and only multijunction SCs intended primarily for space applications were discussed at length owing to the important role they play in solar photovoltaics. It is worthy of mention here that space solar photovoltaics are different from terrestrial ones not only in the choice in favor of much more expensive and, in return, more efficient SCs, but also in the different engineering, since solar batteries unfold in space. Furthermore, the solar radiation spectrum beyond the terrestrial atmosphere (Fig. 12b) is markedly different from the 'terrestrial' spectrum shown in Fig. 1b. This difference determines the different result of parameter optimization of space SCs. This applies, for instance, to silicon SCs, which were developed for space applications prior to the commercialization of multijunction SCs [292].

The history of SC development for Earth satellites may be traced in monograph [293], which also concerns the idea of large-scale power generation on satellites — solar power stations. To reduce the mass and increase the area of the SCs, in the design of such power plants it was decided to reject multijunction SCs in favor of thin-film GaAs SCs [294, 295]. In Section 4, concerned with multicomponent semiconductor diode-type SCs, we restricted ourselves to the discussion of CdTe SCs, CIGS, and CZTS due to precisely the 'terrestrial' orientation of our review. However, for thin-film space SCs, it is precisely the gallium arsenide that is the material of choice (see also Ref. [47]). We note that satellite solar power plants are described at length in monograph [296].

It is not unlikely that the choice of those SCs which have received the bulk of our attention is not entirely free from subjectivism. However, we have endeavored to describe everything which we think is important for a physicist working in the area of solar photovoltaics, and we hope that our review is sufficiently objective and complete. In our view, we have managed to show that solar photovoltaics is now going through a remarkable period, when the interests of scientists and industry converge. While at issue for first- and second-generation SCs is the practical necessity of applied research (this applies especially to light-trapping structures for amorphous silicon), of vital importance for third-generation SCs is basic research. It would suffice to recall that at present there is no complete theory of SCs utilizing highly promising photoelectric materials like synthetic perovskites. There are only particular models which describe separate processes. The deficiency of basic knowledge does not permit developing such SCs more successfully; for instance, the stability problem remains unsolved. As regards SCs with highly promising photoelectric materials like metal-organic frameworks, so far such SCs exist only in theory.

As to industrial prospects, solar photovoltaics will experience either a continuation of routine and yet very significant growth, which is noted above and relies on applied research, or a breakthrough, which will most likely stem from basic research. We are inclined to believe in the latter course of events. Furthermore, we do not rule out the possibility of a technological breakthrough based on applied research if it permits achieving the optimal combination of a high efficiency and a low cost, as well as stable operation under realistic terrestrial conditions. Since, in our opinion, the likelihood of revolutionary development of solar photovoltaics is rather high, we consider it to be one of the most topical areas for physical research in the several years to come.

Acknowledgments

This work was supported by the Russian Foundation for Basic Research (grant Nos 16-37-60073 mol_a_dk and 15-57-45141 IND_a), Skolkovo Foundation (Grant Agreement No. 4 dd.25.12.2014), and the Governmental Task for Institutions of Higher Education (No. 3.561.2014/K). The work of I S Mukhin was supported by the President grant 14.W01.15.7736-MK, and the work of A S Shalin was supported by a stipend from the President of the Russian Federation.

References

1. Stoletow A "Suite des recherches actino-électriques" *Comptes Rendus* **107** 91 (1888); Abstract: *Beibl. Ann. Physik* **12** 723 (1888)
2. Einstein A *Ann. Physik* **17** 132 (1905)
3. Green M A *Third Generation Photovoltaics* (Berlin: Springer, 2003)
4. Marti A, Luque A (Eds) *Next Generation Photovoltaics* (Bristol: Institute of Physics Publ., 2004)
5. Ginley D S, Cahen D (Eds) *Fundamentals of Materials for Energy and Environmental Sustainability* (Cambridge: Cambridge Univ. Press, 2012)
6. Alferov Zh I, Andreev V M, Rumyantsev V D *Semicond.* **38** 899 (2004); *Fiz. Tekh. Poluprovodn.* **38** 937 (2004)
7. Ryvkin S M *Photoelectric Effects in Semiconductors* (New York: Consultants Bureau, 1964); Translated from Russian: *Fotoelektricheskie Yavleniya v Poluprovodnikakh* (Moscow: Fizmatgiz, 1963)
8. Dzhafarov T D *Fotostimulirovannye Atomnye Protsessy v Poluprovodnikakh* (Photoinduced Atomic Processes in Semiconductors) (Moscow: Energoatomizdat, 1984)

9. Fahrenbruch A L, Bube R H *Fundamentals of Solar Cells*: *Photovoltaic Solar Energy Conversion* (New York: Academic Press, 1983); Translated into Russian: *Solnechnye Elementy*: *Teoriya i Eksperiment* (Moscow: Energoatomizdat, 1987)
10. Andreev V M, Grilikhes V A, Rumyantsev V D *Photovoltaic Conversion of Concentrated Sunlight* (Chichester: John Wiley, 1997); Translated from Russian: *Fotoelektricheskoe Preobrazovanie Kontsentrirovannogo Solnechnogo Izlucheniya* (Leningrad: Nauka, 1989)
11. Afanas'ev V P, Terukov E I, Sherchenkov A A *Tonkoplenochnye Solnechnye Elementy na Osnove Kremniya* (Thin-Film Silicon Solar Cells) (St. Petersburg: Izd. SPbGETU 'LETI', 2011)
12. Yamaguchi M et al. *Solar Energy* **79** 78 (2005)
13. Green M A *Prog. Photovolt. Res. Appl.* **17** 183 (2009)
14. Peters M et al. *Energies* **8** 171 (2010)
15. McCann M J et al. *Solar Energy Mater. Solar Cells* **68** 135 (2001)
16. Chapin D M, Fuller C S, Pearson G L *J. Appl. Phys.* **25** 676 (1954)
17. Chopra K L, Das S R *Thin Film Solar Cells* (New York: Plenum Press, 1983); Translated into Russian: *Tonkoplenochnye Solnechnye Elementy* (Moscow: Mir, 1986)
18. Reinhard P, Buecheler S, Tiwari A N *Solar Energy Mater. Solar Cells* **119** 287 (2013)
19. Chirilă A et al. *Nature Mater.* **10** 857 (2011)
20. Polizzotti A et al. *Energy Environ. Sci.* **6** 3171 (2013)
21. Dimroth F et al. *Prog. Photovolt. Res. Appl.* **22** 277 (2014)
22. Huang Q et al. *Appl. Opt.* **52** 2312 (2013)
23. Mojiri A et al. *Renewable Sustainable Energy Rev.* **28** 654 (2013)
24. Song T B et al. *J. Mater. Chem. A* **3** 9032 (2015)
25. Eckstein M, Oka T, Werner P *Phys. Rev. Lett.* **105** 146404 (2010)
26. Coulter J E, Manousakis E, Gali A *Phys. Rev. B* **90** 165142 (2014)
27. Bauer T *Thermophotovoltaics*: *Basic Principles and Critical Aspects of System Design* (Berlin: Springer-Verlag, 2011)
28. Wu C et al. *J. Opt.* **14** 024005 (2012)
29. Lenert D et al. *Nature Nanotechnol.* **9** 126 (2014)
30. Fraunhofer Institute for Solar Energy Systems ISE: Photovoltaics Report, http://spotidoc.com/doc/364768/photovoltaics-report (2014)
31. Saga T *NPG Asia Mater.* **2** 96 (2010)
32. Allison J E, Arndt R A, Meulenberg H A *10th IEEE Photovolt. Spec. Conf.* 1038 (1974)
33. Bordina N M et al. *Geliotekhnika* (3) 6 (1982)
34. Rau U, Meyer T, Goldbach M *25th Photovolt. Solar Conf.* 469 (1996)
35. Brendel R *13th Eur. Photovolt. Solar Energy Conf.* 436 (1995)
36. Yamamoto K et al. *Jpn. J. Appl. Phys.* **36** L569 (1997)
37. Nakajima A et al. *Solar Energy Mater. Solar Cells* **48** 287 (1997)
38. Stalmans L et al., in *Proc. of the 2nd World Conf. and Exhibition on Photovoltaic Solar Energy Conversion, Vienna, Austria, 6 – 10 July 1998*, p. 124
39. Zhao J, Wang A, Green M A *Prog. Photovolt. Res. Appl.* **7** 471 (1999)
40. Slade A G, in *15th Intern. Photovoltaic Science and Engineering Conf., PVSEC -15, 10 – 15 October 2005, Shanghai, China*, p. 701
41. Mingirulli N et al. *Phys. Status Solidi Rapid Res. Lett.* **5** 159 (2011)
42. van Sark W, Korte L, Roca F (Eds) *Physics and Technology of Amorphous-Crystalline Heterostructure Silicon Solar Cells* (Berlin: Springer, 2012)
43. Masuko K et al. *IEEE J. Photovolt.* **4** 1433 (2014)
44. Wei C-Y et al. *Materials* **6** 5440 (2013)
45. Jayarama Reddy P *Solar Power Generation*: *Technology, New Concepts and Policy* (Leiden: CRC Press, 2012)
46. Thaidigsmann B et al. *Phys. Status Solidi Rapid Res. Lett.* **5** 286 (2011)
47. Hamakawa Y (Ed.) *Thin-Film Solar Cells*: *Next Generation Photovoltaics and Its Applications* (Berlin: Springer, 2004)
48. Ultra-Low-Cost Solar Electricity Cells — An Overview of Nanosolars Cell Technology Platform, http://www.catharinafonds.nl/wp-content/uploads/2010/03/NanosolarCellWhitePaper.pdf
49. Staebler D L, Wronski C R *Appl. Phys. Lett.* **31** 292 (1977)
50. Wesoff E "Nanosolar, thin-film solar hype firm, officially dead", http://www.greentechmedia.com/articles/read/Nanosolar-Thin-Film-Solar-Hype-Firm-Officially-Dead
51. Fehr M et al. *Phys. Rev. Lett.* **112** 066403 (2014)
52. Matsui T et al., in *28th European Photovoltaic Solar Energy Conf. and Exhibition, 30 September – 4 October 2013, Paris, France*, p. 2213
53. Sai H et al. *IEEE J. Photovolt.* **4** 1349 (2014)
54. Kadota N et al., in *21st Intern. Photovoltaic Science and Engineering Conf., 28 November – 2 December 2011, Kanagawa, Japan*, p. 2A-20-05
55. Kim S et al. *Solar Energy Mater. Solar Cells* **119** 26 (2013)
56. Green M A et al. *Prog. Photovolt. Res. Appl.* **23** 1 (2015)
57. Adirovich E I *Fiz. Tekh. Poluprovodn.* **4** 745 (1970)
58. Major J D et al. *Nature* **511** 334 (2014)
59. Bonnet D, Meyers P *J. Mater. Res.* **13** 2740 (1998)
60. Topič M *J. Acad. Sci. Arts Republic Srpska. Contemp. Mater. Renewable Energy Sources* **II – 2** 94 (2011)
61. Green M A et al. *Prog. Photovolt. Res. Appl.* **22** 1 (2014)
62. Moss R et al., JRC Scientific and Technical Reports Series (Luxembourg: Publ. Office of the European Union, 2011)
63. Siebentritt S *Thin Solid Films* **535** 1 (2013)
64. Zhou H et al. *Energy Environ. Sci.* **6** 2779 (2013)
65. Suryawanshi M P et al. *Mater. Technol.* **28** 98 (2013)
66. Azimi H, Hou Y, Brabec C J *Energy Environ. Sci.* **7** 1829 (2014)
67. Garland J W et al. *J. Appl. Phys.* **109** 102423 (2011)
68. Yamaguchi M, Takamoto T, Araki K *Solar Energy Mater. Solar Cells* **90** 3068 (2006)
69. Tanabe K *Energies* **2** 504 (2009)
70. Cotal H et al. *Energy Environ. Sci.* **2** 174 (2009)
71. Siddiki M K *Energy Environ. Sci.* **3** 867 (2010)
72. Wolf M *Proc. Inst. Radio Eng.* **48** 1246 (1960)
73. Yu Z, Sandhu S, Fan S *Nano Lett.* **14** 66 (2014)
74. Maragliano C, Chiesa M, Stefancich M *J. Opt.* **17** 105901 (2015)
75. Mohammad N et al. *Opt. Express* **22** A1519 (2014)
76. Polman A, Atwater H A *Nature Mater.* **11** 174 (2012)
77. Imenes A G, Mills D R *Solar Energy Mater. Solar Cells* **84** 19 (2004)
78. Peters M et al. *Energies* **3** 171 (2010)
79. Green M A, Ho-Baillie A *Prog. Photovolt. Res. Appl.* **18** 42 (2010)
80. Huang Q et al. *Appl. Opt.* **52** 2312 (2013)
81. Sohail A, Efstathiadis H, Salahuddin Q (Eds) *Handbook of Research on Solar Energy Systems and Technologies* (Hershey, PA: Engineering Science Reference, 2013)
82. Gregg B A, Hanna M C *J. Appl. Phys.* **93** 3606 (2003)
83. Deibel C, Dyakonov V *Rep. Prog. Phys.* **73** 096401 (2010)
84. Tang C W *Appl. Phys. Lett.* **48** 183 (1986)
85. O'Regan B, Grätzel M *Nature* **353** 737 (1991)
86. Yu G et al. *Science* **270** 1789 (1995)
87. Kim J B et al. *Nature Photon.* **6** 327 (2012)
88. Sariciftci N S et al. *Appl. Phys. Lett.* **62** 585 (1993)
89. Adams J et al. *Energy Environ. Sci.* **8** 169 (2015)
90. Choy W C H (Ed.) *Organic Solar Cells*: *Materials and Device Physics* (London: Springer, 2013)
91. Liu Y et al. *Nature Commun.* **5** 5293 (2014)
92. Lin Y et al. *Adv. Mater.* **18** 1170 (2015)
93. Lattante S *Electronics* **3** 132 (2014)
94. Parashchuk D Yu, Kokorin A I *Ross. Khim. Zh.* **52** (6) 107 (2008)
95. Ameri T *J. Appl. Phys.* **103** 084506 (2008)
96. Lai T H et al. *Mater. Today* **16** 424 (2013)
97. Hau S K et al. *Appl. Phys. Lett.* **92** 253301 (2008)
98. Huang W et al. *Adv. Energy Mater.* **5** 1401259 (2015)
99. Ahmad J et al. *Renewable Sustainable Energy Rev.* **27** 104 (2013)
100. Rand B P et al. *Organic Electron.* **10** 1015 (2009)
101. Gregg B A, van de Lagemaat J *Nature Photon.* **6** 278 (2012)
102. Hawks B S A et al. *J. Appl. Phys.* **116** 074503 (2014)
103. Hansson R et al. *J. Mater. Chem. A* **3** 6970 (2015)
104. Liu C M et al. *J. Mater. Chem. A* **2** 20760 (2014)
105. Cheng P et al. *J. Mater. Chem. A* **2** 19542 (2014)
106. Nielsen C B et al. *Adv. Mater.* **27** 948 (2014)
107. Angmo D, Espinosa N, Krebs F, in *Low-Cost Nanomaterials* (London: Springer, 2014) p. 189
108. Ellmer K *Nature Photon.* **6** 809 (2012)
109. Kuang D et al. *J. Am. Chem. Soc.* **128** 4146 (2007)
110. Hardin B E, Snaith H J, McGehee M D *Nature Photon.* **6** 162 (2012)
111. Mathew S et al. *Nature Chem.* **6** 242 (2014)
112. Hashmi G et al. *Renewable Sustainable Energy Rev.* **15** 3717 (2011)
113. Qiu L et al. *Angew. Chem. Int. Ed.* **53** 1 (2014)
114. Burschka J et al. *J. Am. Chem. Soc.* **133** 18042 (2011)

115. Yang Y et al. *Phys. Chem. Chem. Phys.* **16** 17743 (2014)
116. Espinosa N et al. *Solar Energy Mater. Solar Cells* **97** 3 (2012)
117. Lizin S et al. *Energy Environ. Sci.* **6** 3136 (2013)
118. Parisi M L, Maranghi S, Basosi R *Renewable Sustainable Energy Rev.* **39** 124 (2014)
119. Espinosa N et al. *Solar Energy Mater. Solar Cells* **137** 303 (2015)
120. Mulligan C J et al. *Solar Energy Mater. Solar Cells* **133** 26 (2015)
121. Grätzel M *Accounts Chem. Res.* **42** 1788 (2009)
122. Krebs F C (Ed.) *Stability and Degradation of Organic and Polymer Solar Cells* (Hoboken, NJ: Wiley, 2012)
123. Andersen H R et al. *Energy Environ. Sci.* **7** 2925 (2014)
124. Lee S et al. *Nano Energy* **9** 88 (2014)
125. Song T B et al. *J. Mater. Chem. A* **3** 9032 (2015)
126. Kojima A et al. *J. Am. Chem. Soc.* **131** 6050 (2009)
127. Baikie T et al. *J. Mat. Chem. A* **1** 5628 (2013)
128. Sum T C, Mathews N *Energy Environ Sci.* **7** 2518 (2014)
129. Green M A, Ho-Baillie A, Snaith H J *Nature Photon.* **8** 506 (2014)
130. Wang B, Xiao X, Chen T *Nanoscale* **6** 12287 (2014)
131. Umebayashi T et al. *Phys. Rev. B* **67** 155405 (2003)
132. Mosconi E, Amat A, Nazeerutdin M K *J. Phys. Chem. C* **117** 13902 (2013)
133. Umari P, Mosconi E, De-Angelis F *Sci. Rep.* **4** 4467 (2014)
134. Even J et al. *J. Phys. Chem. Lett.* **4** 2999 (2013)
135. Onoda-Yamamuro Y *J. Phys. Chem. Solids* **53** 935 (1992)
136. Poglitsch A, Weber D *J. Chem. Phys.* **8**7 6373 (1987)
137. Lin Q et al. *Nature Photon.* **9** 106 (2015)
138. Boix P P et al. *Mater. Today* **17** 16 (2014)
139. Snaith H J *J. Phys. Chem. Lett.* **4** 3623 (2013)
140. Liu Y et al. *Nano Lett.* **15** 662 (2015)
141. Kojima A et al. *J. Am. Chem. Soc.* **131** 6050 (2009)
142. Im J H et al. *Nanoscale* **3** 4088 (2011)
143. Kim H S et al. *Sci. Rep.* **2** 591 (2012)
144. Lee M M et al. *Science* **338** 643 (2012)
145. Etgar L et al. *J. Am. Chem. Soc.* **134** 17396 (2012)
146. Laban W A, Etqar L *Energy Environ. Sci.* **6** 3249 (2013)
147. Qiu J et al. *Nanoscale* **5** 3245 (2013)
148. Kim H S et al. *Nano Lett.* **13** 2412 (2013)
149. Dharani S et al. *Nanoscale* **6** 1675 (2014)
150. Yu Y et al. *ACS Nano* **9** 564 (2015)
151. Heo J H et al. *Nature Photon.* **7** 486 (2013)
152. Noh J H et al. *Nano Lett.* **13** 1764 (2013)
153. Jung H S, Park N G *Small* **11** 10 (2015)
154. Burschka J et al. *Nature* **499** 316 (2013)
155. Liu M, Johnston M B, Snaith H J *Nature* **501** 395 (2013)
156. Jeon N J et al. *Nature Mater.* **13** 897 (2014)
157. Service R F *Science* **344** 458 (2014)
158. Nie W et al. *Science* **347** 522 (2015)
159. Jeon N J et al. *Nature* **517** 476 (2015)
160. di Giacomo F et al. *Adv. Energy Mater.* **5** 1401808 (2015)
161. Docampo P et al. *Nature Commun.* **4** 2761 (2013)
162. You J et al. *ACS Nano* **8** 1674 (2014)
163. Roldan-Carmona C et al. *Energy Environ. Sci.* **7** 994 (2014)
164. Kim B J et al. *Energy Environ. Sci.* **8** 916 (2015)
165. Ha S T et al. *Adv. Opt. Mater.* **2** 838 (2014)
166. Malinkiewicz O et al. *Nature Photon.* **8** 128 (2014)
167. Mateocci F et al. *Phys. Chem. Chem. Phys.* **16** 3918 (2014)
168. Ponseca C et al. *J. Am. Chem. Soc.* **136** 5189 (2014)
169. Stoumpos C C, Maliakas C D, Kanatzidis M G *Inorg. Chem.* **52** 9019 (2013)
170. Giorgi G et al. *J. Phys. Chem. Lett.* **4** 4213 (2013)
171. Shen Q et al. *Eur. J. Chem. Phys. Phys. Chem.* **15** 1062 (2014)
172. Stranks S D et al. *Science* **342** 344 (2013)
173. Wehrenfennig C et al. *Adv. Mater.* **26** 1584 (2013)
174. Leijtens T et al. *J. Phys. Chem. Lett.* **5** 1511 (2014)
175. Snaith H J et al. *J. Phys. Chem. Lett.* **5** 2927 (2014)
176. Pham H et al. *J. Phys. Chem. C* **118** 4567 (2014)
177. Yang L M et al. *Inorg. Chem.* **49** 10283 (2010)
178. Lee D Y et al. *J. Phys. Chem. C* **118** 16328 (2013)
179. Bella F et al. *J. Mater. Chem. A* **1** 9033 (2013)
180. Vinogradov A V et al. *Chem. Commun.* **50** 10210 (2014)
181. Rösler C, Fischer R A *CrystEngComm.* **17** 199 (2015)
182. Yu J et al. *Nature Commun.* **4** 2719 (2013)
183. Gao J et al. *Chem. Commun.* **50** 3786 (2014)
184. Kampmeier J et al. *Cryst. Growth Design* **15** 268-277 (2015)
185. Feng X et al. *Angew. Chem.* **124** 2672 (2012)
186. Feng X et al. *Adv. Mater.* **24** 3026 (2012)
187. Lifshitz E et al. *J. Phys. Chem. C* **118** 25356 (2014)
188. Feldblyum J I et al. *J. Phys. Chem. C* **116** 3112 (2012)
189. Ding X et al. *Angew. Chem.* **50** 1289 (2011)
190. Talin A A et al. *Science* **343** 66 (2014)
191. Pan L et al. *J. Am. Chem. Soc.* **136** 17477 (2014)
192. So M C et al. *Chem. Commun.* **51** 3501 (2015)
193. Zhang X et al. *Coordin. Chem. Rev.* **284** 206 (2015)
194. Kent C A et al. *J. Am. Chem. Soc.* **133** 12940 (2011)
195. Leong K et al. *J. Mater. Chem. A* **2** 3389 (2014)
196. Narayan T et al. *J. Am. Chem. Soc.* **134** 12932 (2012)
197. Son H J et al. *J. Am. Chem. Soc.* **135** 862 (2013)
198. McCarthy B D et al. *J. Phys. Chem. Lett.* **4** 453 (2013)
199. Lee C Y et al. *J. Am. Chem. Soc.* **133** 15858 (2011)
200. Lin J et al. *J. Phys. Chem. C* **117** 22250 (2013)
201. Cui Y et al. *Chem. Rev.* **112** 1126 (2012)
202. Ordonez C et al. *Cryst. Growth Design* **14** 5452 (2014)
203. Silva C G, Corma A, Garcia H *J. Mater. Chem.* **20** 3141 (2010)
204. Llabres-i-Xamena F X, Corma A, Garcia H *J. Phys. Chem. C* **111** 80 (2007)
205. Cai W, Katrusiak A *Nature Commun.* **5** 4337 (2014)
206. Kaltenbrunner M et al. *Nature Mater.* **14** 1032 (2015)
207. Macleod H A *Thin Film Optical Filters* 3rd ed. (Bristol: IOP Publ., 2001)
208. Zhao J, Green M A *IEEE Trans. Electron. Dev.* **38** 1925 (1991)
209. Kats M A et al. *Nature Mater.* **12** 20 (2013)
210. Boden S A, Bagnall D M *Prog. Photovolt. Res. Appl.* **18** 195 (2010)
211. Tommila J et al. *Prog. Photovolt. Res. Appl.* **21** 1158 (2012)
212. Raut H K et al. *Energy Environ. Sci.* **4** 3779 (2011)
213. Liu X et al. *Energy Environ. Sci.* **7** 3223 (2014)
214. Repo P et al. *IEEE J. Photovolt.* **3** 90 (2012)
215. Lee Y C, Chang C C, Chou Y Y *Photon. Nanostruct. Fund. Appl.* **12** 16 (2014)
216. Tao M et al. *Appl. Phys. Lett.* **91** 081118 (2007)
217. Chang T H et al. *Opt. Express* **17** 6519 (2009)
218. Das S et al. *J. Phys. D* **46** 415102 (2013)
219. Grandidier J, Callahan D M, Atwater H A *38th IEEE Photovoltaic Specialists Conf.* 3325 (2012)
220. Grandidier J et al. *Adv. Mater.* **23** 1272 (2011)
221. Grandidier J et al. *Phys. Status Solidi A* **210** 255 (2013)
222. Shalin A S *JETP Lett.* **91** 636 (2010); *Pis'ma Zh. Eksp. Teor. Fiz.* **91** 705 (2010)
223. Shalin A S *J. Commun. Technol. Electron.* **91** 636 (2011); *Radiotekh. Elektron.* **56** 20 (2011)
224. Shalin A S *Quantum Electron.* **41** 163 (2011); *Kvantovaya Elektron.* **41** 163 (2011)
225. Shalin A S *Prog. Electromag. Res. B* **31** 45 (2011)
226. Shalin A S, Nikitov S A *Prog. Electromag. Res. B* **47** 127 (2013)
227. Baranov D A et al. *Appl. Phys. Lett.* **106** 171913 (2015)
228. Cho S J, An T, Lim G *Chem. Commun.* **50** 15710 (2014)
229. Tamir T *Integral Optics* (Berlin: Springer-Verlag, 1975); Translated into Russian: *Integral'naya Optika* (Moscow: Mir, 1978)
230. Campbell P *Solar Energy Mater.* **21** 165 (1990)
231. Marques F C *IEEE Trans. Electron. Dev.* **45** 1619 (1998)
232. Green M A *Prog. Photovolt. Res. Appl.* **7** 317 (1999)
233. Campbell P, Green M A *J. Appl. Phys.* **62** 243 (1987)
234. Rotich S K et al. *J. Micromech. Microeng.* **8** 134 (1998)
235. Tucher N et al. *Energy Procedia* **77** 253 (2015)
236. Yablonovitch E, Cody G D *IEEE Trans. Electron. Dev.* **29** 300 (1982)
237. Yablonovitch E *J. Opt. Soc. Am. A* **72** 899 (1982)
238. Tiedje T et al. *IEEE Trans. Electron. Dev.* **31** 711 (1984)
239. Yu Z, Raman A, Fan S *Opt. Express* **18** A366 (2010)
240. Bermel P et al. *Opt. Express* **15** 16986 (2007)
241. Mallick S B, Agrawal M, Peumans P *Opt. Express* **18** 5691 (2007)
242. Sakoda K *Optical Properties of Photonic Crystals* (Berlin: Springer, 2005)
243. Atwater H A, Polman A *Nature Mater.* **9** 205 (2010)
244. Butikov E I *Optika* (Optics) (Moscow: Vysshaya Shkola, 1986)

245. Novotny L, Hecht B *Principles of Nano-Optics* 2nd ed. (Cambridge: Cambridge Univ. Press, 2012); Translated into Russian (from 1st ed.): *Osnovy Nanooptiki* (Moscow: Fizmatlit, 2009)
246. Klimov V *Nanoplasmonics* (Boca Raton, FL: CRC Press, Taylor and Francis Group, 2014); Translated from Russian: *Nanoplazmonika* (Moscow: Fizmatlit, 2010)
247. Agranovich V M, Mills D L (Eds) *Surface Polaritons. Electromagnetic Waves at Surfaces and Interfaces* (Amsterdam: North-Holland, 1982)
248. Panoiu N C, Osgood R M *Opt. Lett.* **32** 2825 (2007)
249. Ferry M E et al. *Nano Lett.* **8** 4391 (2008)
250. Spinelli P et al. *J. Opt.* **14** 024002 (2012)
251. Pillai S et al. *J. Appl. Phys.* **101** 093105 (2007)
252. Catchpole K R, Polman A *Appl. Phys. Lett.* **93** 191113 (2008)
253. Tan H et al. *Nano Lett.* **12** 4070 (2012)
254. Akimov Y A, Ostrikov K, Li E P *Plasmonics* **4** 107 (2009)
255. Pfeiffer T V et al. *Energy Procedia* **60** 3 (2014)
256. Brongersma M L et al. *Adv. Mater.* **21** 1 (2009)
257. Rockstuhl C, Lederer F *Appl. Phys. Lett.* **94** 213102 (2009)
258. Simovski C et al. *Opt. Express* **21** A714 (2013)
259. Matsui T et al. *Jpn. J. Appl. Phys.* **54** 08KB10 (2015)
260. Catchpole K R, Polman A *Opt. Express* **16** 21793 (2008)
261. Ferry V E et al. *Opt. Express* **18** A237 (2010)
262. Wang Y et al. *Nano Lett.* **12** 440 (2012)
263. Sinev I et al. *Nanoscale* **7** 765 (2015)
264. Akimov Y A et al. *Appl. Phys. Lett.* **96** 073111 (2010)
265. Grandidier J et al. *J. Photon. Energy* **2** 024502 (2012)
266. Yao Y et al. *Nature Commun.* **3** 664 (2012)
267. Grandidier J et al. *IEEE J. Photovolt.* **2** 123 (2012)
268. Mendes M J et al. *Opt. Express* **19** 16207 (2011)
269. Spinelli P, Verschuuren M A, Polman A *Nature Commun.* **3** 692 (2012)
270. van Groep J, Polman A *Opt. Express* **21** 26285 (2013)
271. Simovski C R et al. *J. Appl. Phys.* **114** 103104 (2013)
272. Omelyanovich M, Ovchinnikov V, Simovski C *J. Opt.* **17** 025102 (2015)
273. Yu Z, Raman A, Fan S *Proc. Natl. Acad. Sci. USA* **107** 17491 (2010)
274. Voroshilov P M et al. *J. Appl. Phys.* **117** 203101 (2015)
275. Schuster C S et al. *Optica* **2** 194 (2015)
276. Zhao Y et al. *Appl. Opt.* **53** 5222 (2014)
277. Galvez F E et al. *Energy Environ. Sci.* **7** 689 (2014)
278. In S et al. *ACS Photon.* **2** 78 (2015)
279. Pastorelli F et al. *Adv. Opt. Mater.* **2** 171 (2014)
280. Chou S, Ding W *Opt. Express* **21** A60 (2012)
281. Voroshilov P M, Simovski C R, Belov P A *J. Mod. Opt.* **61** 1743 (2014)
282. Nozik A J *Physica E* **14** 115 (2002)
283. Nair G et al. *Nano Lett.* **11** 2145 (2011)
284. Rühle S, Shalom M, Zaban A *Chem. Phys. Phys. Chem.* **11** 2290 (2011)
285. Tisdale W A et al. *Science* **328** 1543 (2010)
286. Conibeer G J et al. *Thin Solid Films* **516** 6968 (2008)
287. Hirori H et al. *Nature Commun.* **2** 594 (2011)
288. Kirk A P, Fischetti M V *Phys. Rev. B* **86** 165206 (2012)
289. Chalabi H, Brongersma M L *Nature Nanotechnol.* **8** 229 (2013)
290. Clavero C *Nature Photon.* **8** 95 (2014)
291. Kong J et al. *Opt. Express* **23** A1087 (2015)
292. Vavilov V S et al. *Usp. Fiz. Nauk* **63** 123 (1957)
293. Perlin J *From Space to Earth: the Story on Solar Electricity* (Ann Arbor, MI: Aatec Publ., 1999)
294. Vanke V A, Lopukhin V M, Savvin V L *Sov. Phys. Usp.* **20** 989 (1977); *Usp. Fiz. Nauk* **123** 633 (1977)
295. Nagatomo M et al. *Phys. Usp.* **37** 589 (1994);*Usp. Fiz. Nauk* **164** 631 (1994)
296. Grilikhes V A *Solnechnye Kosmicheskie Energostantsii* (Solar Cosmic Power Plant) (Leningrad: Nauka, 1986)